



Proceedings of the 2019 National Toxicology Program Satellite Symposium

Susan A. Elmore¹ , Mark F. Cesta¹ , Torrie A. Crabbs²,
Kyathanahalli S. Janardhan³ , Gregory A. Krane¹,
Debabrata Mahapatra³, Erin M. Quist², Matthias Rinke⁴,
George W. Schaaf⁵, Gregory S. Travlos¹, Haoan Wang⁶,
Cynthia J. Willson³, and Jeffrey C. Wolf⁷

Abstract

The 2019 annual National Toxicology Program Satellite Symposium, entitled “Pathology Potpourri,” was held in Raleigh, North Carolina, at the Society of Toxicologic Pathology’s 38th annual meeting. The goal of this symposium was to present and discuss challenging diagnostic pathology and/or nomenclature issues. This article presents summaries of the speakers’ talks along with select images that were used by the audience for voting and discussion. Various lesions and topics covered during the symposium included aging mouse lesions from various strains, as well as the following lesions from various rat strains: rete testis sperm granuloma/fibrosis, ovarian cystadenocarcinoma, retro-orbital schwannoma, periductal cholangiofibrosis of the liver and pancreas, pars distalis hypertrophy, chronic progressive nephropathy, and renal tubule regeneration. Other cases included polyovular follicles in young beagle dogs and a fungal blood smear contaminant. One series of cases challenged the audience to consider how immunohistochemistry may improve the diagnosis of some tumors. Interesting retinal lesions from a rhesus macaque emphasized the difficulty in determining the etiology of any particular retinal lesion due to the retina’s similar response to vascular injury. Finally, a series of lesions from the International Harmonization of Nomenclature and Diagnostic Criteria Non-Rodent Fish Working Group were presented.

Keywords

NTP satellite symposium, INHAND, aging mouse lesions, sperm granuloma, ovarian cystadenoma, periductal cholangiofibrosis, polyovular follicles

Select Lesions From an Aging Mouse Study

Drs Erin M. Quist (Experimental Pathology Laboratories, Inc [EPL], Research Triangle Park, North Carolina), Debabrata Mahapatra (Integrated Laboratory Systems, Inc [ILS], Research Triangle Park, North Carolina), and Torrie A. Crabbs (EPL) presented a collection of cases from the Aging Mouse Study conducted by the National Toxicology Program at the National Institute of Environmental Health Sciences (NTP/NIEHS). Drs Quist, Mahapatra, and Crabbs were the 3 quality assurance (QA) pathologists for the study, which was designed as a chronic (2-year) study in which 10 different mouse strains (A/J, C57BL/6J, 129S1/SvImJ, C3H/HeJ, B6C3F1/J, PWK/PhJ, NZO/HILtJ, WSB/EiJ, NOD.B10Sn-H2^b/J, CAST/EiJ) were selected to determine any strain differences in incidence and/or predilection of age-related background changes; animals on this study received no treatment and died naturally during the 2-year period or were humanely euthanized as a moribund or terminal sacrifice. During the introduction for the

case series, Dr Quist emphasized that the QA pathologists had been instructed to review all lesions with a zero threshold in order to meet the study objectives. She also informed the

¹ Cellular and Molecular Pathology Branch, National Toxicology Program, National Institute of Environmental Health Sciences, National Institutes of Health, Research Triangle Park, NC, USA

² Experimental Pathology Laboratories, Inc, Research Triangle Park, NC, USA

³ Integrated Laboratory Systems, Inc, Research Triangle Park, NC, USA

⁴ Wuelfrath, North Rhine–Westphalia, Germany

⁵ Wake Forest University School of Medicine, Winston Salem, NC, USA

⁶ West China-Frontier Pharma Tech Co, Ltd, Chengdu, Sichuan, China

⁷ Experimental Pathology Laboratories, Inc, Sterling, VA, USA

Corresponding Author:

Susan A. Elmore, Cellular and Molecular Pathology Branch, National Toxicology Program, National Institute of Environmental Health Sciences, National Institutes of Health, 111 T. W. Alexander Drive, Research Triangle Park, NC 27709, USA.

Email: elmore@niehs.nih.gov

audience that the selected lesions represented preliminary findings and had not yet been reviewed by a pathology working group (PWG).

Dr Quist: Cases 1 and 2

For case 1, a series of photomicrographs were presented to the audience that included both low and high magnifications of an adrenal gland from an adult male C3H/HeJ mouse (Figure 1A-C). The adrenal gland was diffusely enlarged and infiltrated by a nonencapsulated neoplasm that effaced and replaced the normal tissue architecture (Figure 1A). Neoplastic cells had a varied appearance in which some were more basophilic with fusiform morphology, arranged in discrete nests and packets (Figure 1B), and others were polygonal, contained abundant eosinophilic cytoplasm, and were arranged in islands or sheets (Figure 1C). The voting choices and results were as follows: cortex hyperplasia (11%), cortex adenoma (7%), cortex subcapsular adenoma (7%), cortex cortical carcinoma (23%), cortex subcapsular carcinoma (8%), medulla hyperplasia (7%), medulla pheochromocytoma, benign (20%), medulla pheochromocytoma, malignant (17%), and other (0%). Dr Quist agreed with the audience that the diagnosis was not straightforward and showed a few tyrosine hydroxylase (TH) immunohistochemistry (IHC) images of the adrenal neoplasm to illustrate this point. Tyrosine hydroxylase is involved in the synthesis of catecholamines and is localized in adrenal medullary chromaffin cells. Tyrosine hydroxylase IHC staining revealed that the medulla was completely effaced and replaced by the infiltrating neoplasm in which only a single cluster, composed of a few medullary cells, remained. Dr Quist also shared some IHC images of the contralateral adrenal gland from this animal which confirmed the diagnosis of a second, infiltrative subcapsular carcinoma.

Dr Quist briefly reviewed the criteria available on goRENI (<https://www.goreni.org/>) for distinguishing between “cortical” versus “subcapsular” carcinoma within the adrenal gland. These criteria are listed in Table 1. She explained to the audience that the term “subcapsular carcinoma” was selected as the best diagnosis for this lesion given that (1) the neoplasm appeared to arise from the subcapsular surface, (2) neoplastic cells exhibited marked cytoplasmic basophilia, and (3) the neoplastic cells appeared to be a mixture of fusiform (type A) and polygonal (type B) cells.

The slides that followed revealed that all the male adrenal glands examined ($n = 115$) in the C3H/HeJ strain were abnormal, with marked subcapsular hyperplasia, adenoma, or carcinoma diagnosed in every animal. In the females ($n = 115$), however, only minimal or mild subcapsular hyperplasia was present. Dr Quist also mentioned to the audience that the males had a high (>60%) incidence of penile prolapse during the course of this study and wondered if there may be a correlation between the penile prolapse and adrenal gland changes.

During the audience discussion, none of the audience members were able to confirm that they had encountered a similar lesion in the adrenal glands of male C3H/HeJ mice.

Dr Quist postulated that this lesion may represent a novel finding due to the fact that this particular strain is not often used in chronic studies.

For case 2, the audience was presented with a series of photomicrographs from the seminal vesicle of an adult NOD.B10Sn-*H2^b/J* male mouse (Figure 1D-F). The voting choices and results were as follows: inflammation (0%), fibrosis (2%), sarcoma (3%), carcinoma (60%), carcinosarcoma (32%), and other (3%). Dr Quist explained that the preferred diagnosis was “carcinosarcoma” given that the neoplasm contained areas that appeared more epithelial in origin (Figure 1E), whereas others exhibited features more typical of a mesenchymal tumor (Figure 1F). After audience discussion, Dr Quist emphasized that this was a preliminary finding that would be taken to a PWG; IHC would also be used to assist with the diagnosis.

In this study, greater than 90% of NOD.B10Sn-*H2^b/J* male mice ($n = 115$) exhibited dilation and fibrosis of the seminal vesicle and >50% contained variable numbers of inflammatory infiltrates. In addition, the incidence of seminal vesicle neoplasia was relatively high (16%), suggesting a unique predilection for age-related seminal vesicle changes in this particular strain.

The author would like to thank Dr Ron Herbert, Dr Kyathahalli Janardhan, and the IHC Core at the NTP for their assistance, as well as Ms Emily Singletary for photographic editing and support.

Dr Mahapatra: Cases 3 and 4

The theme of Aging Mouse Studies was continued with Dr Debabrata Mahapatra presenting cases 3 and 4 from the 129S1/SvImj strain of aging mice. These cases were selected for background/spontaneous histopathological lesions for historical control purposes. In addition, based on preliminary findings, selected lesions had relatively high incidence rates in both sexes and hence believed to be strain-specific features. Dr Mahapatra would like to acknowledge members of the Aging Mouse Project team and ILS pathology team members for their support and assistance.

Case 3 was from a >2-year-old 129S1/SvImj female mouse. A series of 5 images of a pituitary lesion (Figure 2A-C) were presented to the audience. The voting choices and results were as follows: pars distalis adenoma (5%), diffuse pars intermedia hypertrophy (0%), diffuse pars intermedia hyperplasia (2%), pars intermedia adenoma (36%), diffuse pars intermedia hypertrophy and hyperplasia (22%), pars intermedia carcinoma (35%), and other (0%). The majority of the audience opted for pars intermedia adenoma, which was the author’s preferred diagnosis.

Adenomas of the pars intermedia are uncommon in both rats and mice. Neoplastic cells usually exhibit pleomorphism with clear compression of the adjacent pars distalis. Extension of neoplastic cells into the pars nervosa is also a characteristic feature of these adenomas; however, hyperplastic lesions may also exhibit this feature.² Table 2 illustrates the diagnostic features of pars intermedia that are helpful in distinguishing

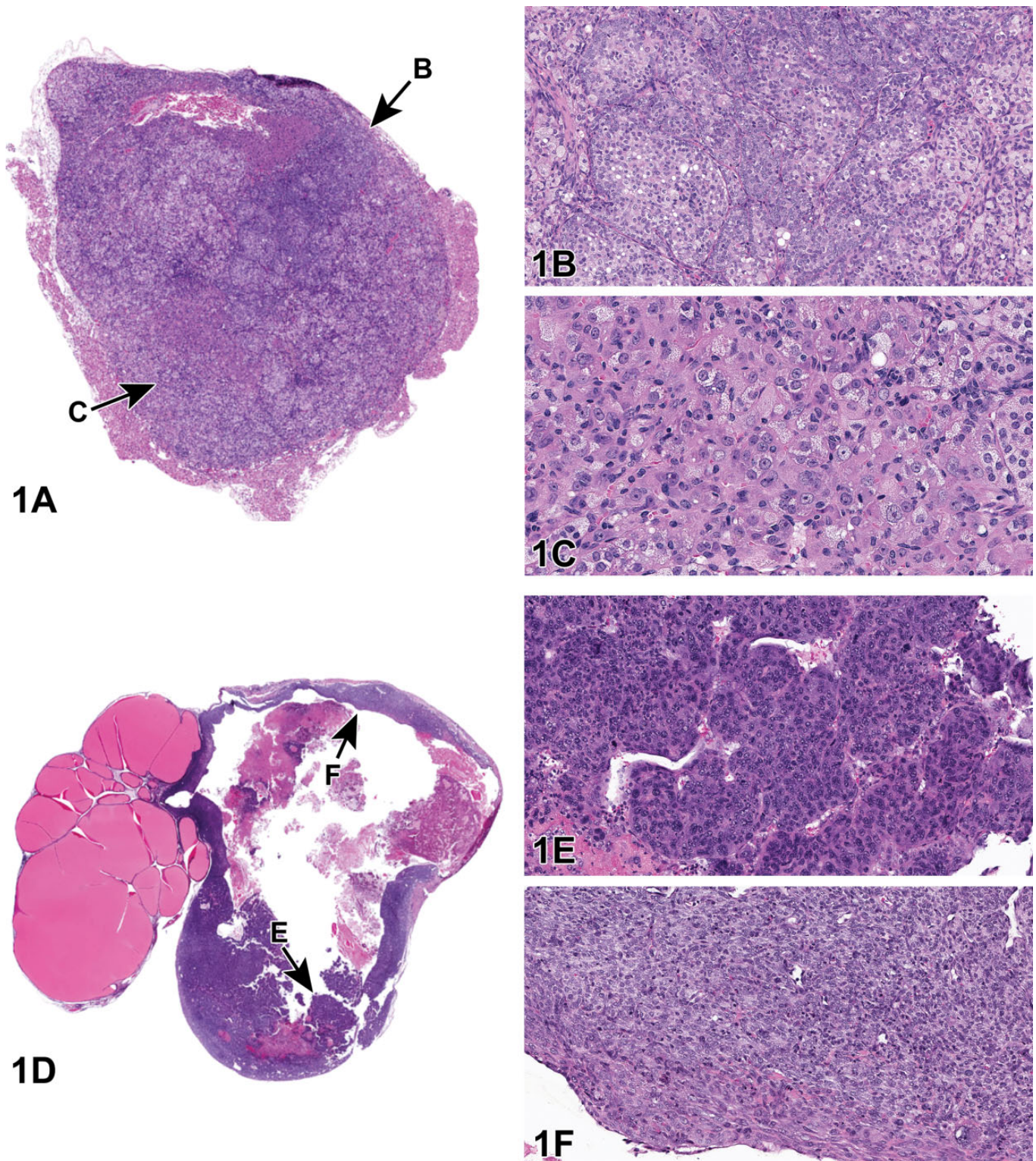


Figure 1. Adrenal gland from an adult C3H/HeJ male mouse (A-C) and seminal vesicle from an adult NOD.B10Sn-H2^b/J male mouse, both from the National Toxicology Program Aging Mouse Study (D-F). A, The adrenal gland is diffusely enlarged and infiltrated by a nonencapsulated neoplasm that is effacing and replacing the normal tissue architecture. Note that the neoplasm appears to be arising from the subcapsular surface. B, Neoplastic cells arranged in nests and packets are characterized by basophilic cytoplasm and fusiform (type A) morphology (“arrow B” region in Figure A). C, In a different area of the neoplasm (“arrow C” region in Figure A), neoplastic cells are polygonal (type B) with abundant eosinophilic cytoplasm and are arranged in islands or sheets. D, The seminal vesicle is markedly dilated and infiltrated by an unencapsulated neoplasm. E, In

Table I. Diagnostic Criteria for Cortical and Subcapsular Adrenal Gland Carcinoma.¹

Cortical	
•	Invasive growth into surrounding adrenal tissue
•	Neoplastic cells are organized in thickened trabeculae, sheets, or solid clusters with disruption of normal architecture
•	Cytoplasm is usually eosinophilic or amphophilic
•	Cellular atypia and pleomorphism are usually present
•	Mitotic figures may be numerous
•	Vacuolation, cystic degeneration, necrosis, angiectasis, or hemorrhage may be present
Subcapsular	
•	Presence of distinct invasion into surrounding tissues or vessels
•	Tumor cell atypia, pleomorphism, and mitotic figures are present
•	Cells are organized in nests, ribbons, or cords
•	The modifiers are used according to the predominant A (fusiform) or B (polygonal) cell type (>70%)
•	Mixed type: No predominant cell type is present

hyperplastic lesions from those of adenomas and carcinomas. Although the incidence of pars intermedia adenomas was relatively low in both sexes (2.6%), the relatively high incidence of hyperplastic lesions in males (22.6%) and females (10.4%) was considered potentially strain related. As part of the discussion, a question was asked if invasion by neoplastic cells into the pars nervosa would differentiate an adenoma from a carcinoma. It was explained that there were several instances where hyperplastic lesions in this strain of mouse were observed to have extended into the pars nervosa. Hence, invasion into adjacent brain structures was the only criterion used to distinguish adenomas from carcinomas of the pars intermedia. It was also mentioned that no additional immunohistochemical analyses (ie, immunostaining for ACTH) or biomarker assays were performed.

Case 4 was from a ~2-year-old 129S1/SvImj female mouse. A series of images of a pancreatic lesion (Figure 2D) was presented to the audience. The voting choices and results were as follows: islet hyperplasia (1%), diffuse acinus hypertrophy (7%), diffuse acinus hyperplasia (5%), peri-insular acinus hypertrophy (58%), peri-insular hepatocytes (7%), peri-insular acinus hyperplasia (15%), acinus adenoma (1%), and other (7%). A majority of the audience opted for peri-insular acinus hypertrophy, which was the author's preferred diagnosis.

Hypertrophy of pancreatic acinar cells is a relatively common finding in both rats and mice. Hypertrophic cells have abundant intracytoplasmic zymogen granules and are more prominent in the peri-insular regions compared to the tele-insular regions that are distally located from the islets of Langerhans.³ Because of the high incidence of peri-insular hyperplastic lesions in males (49.5%) and females (72%) based

on our preliminary findings, this lesion was considered strain-specific. For this case, it was asked whether tubular lesions were observed in the pancreas alongside hypertrophic lesions in 129S1/SvImj strain of mice. The author mentioned that there was no evidence of such tubular lesions.

Overall, the goal of this presentation was to highlight the incidences of spontaneous/background lesions in a transgenic strain of aging mice (129S1/SvImj). Accumulated data would serve as a valuable addition to the historical database for future reference.

Dr Crabbs: Cases 5 to 7

The final aging mouse cases were presented by Dr Torrie A. Crabbs. Case 5 was from an adult female B6C3F1/J mouse. The audience was shown several photomicrographs of bone marrow from the femur (Figure 3A and B). For comparison purposes, the audience was also provided representative photomicrographs of normal bone marrow (Figure 3C and D) at each magnification. The voting choices and results for this case were as follows: within normal limits (11%), increased adipocytes (33%), decreased hematopoietic cells/hypocellularity (35%), lipomatosis (16%), lipoma (2%), liposarcoma (2%), and other (0%).

There was a relatively even split in the audience's opinion between the diagnoses of increased adipocytes and decreased hematopoietic cells/hypocellularity; this split was expected. While it is stated on goRENI (<https://www.goreni.org/>) that "[i]t is generally more physiologically relevant to express changes in the relative proportions of adipocytes and hematopoietic cells in terms of hyperplasia or atrophy of the hematopoietic cells,"¹ Dr Crabbs informed the audience that the preferred diagnosis in this study was "increased adipocytes"; however, it was reiterated that these findings are preliminary and that the results from this poll would be taken into consideration during the PWG. It was subsequently stated that the choice for this diagnosis was influenced by the fact that this strain also exhibited increased infiltration of adipocytes within the medullary sinuses of the mesenteric (17%) and mandibular (22%) lymph nodes (Figure 3E and F, respectively). No direct correlation between the presence of adipocyte infiltration and body weight obesity could be made for these animals. The mean average weight of the males in this strain was similar, albeit slightly lower than the females (45.3 vs 49.0 g, respectively) at terminal sacrifice. In addition, males and females from other strains had similar mean body weights but lacked this finding.

Increased adipocytes had been recorded when there was a localized region in the bone marrow characterized by an almost complete loss of hematopoietic cells and infiltration by an abundant number of adipocytes. This finding had only been noted in females (43%) and had not been recorded in any other

Figure 1. (Continued). some areas (arrow "E" in figure D), the neoplasm appears epithelial in origin, with neoplastic cells arranged in nests, islands, and trabeculae. F, In other areas of the neoplasm (arrow "F" in Figure D), the neoplastic cells are more elongated and spindle shaped with pale, eosinophilic cytoplasm and are arranged in bundles and streams.

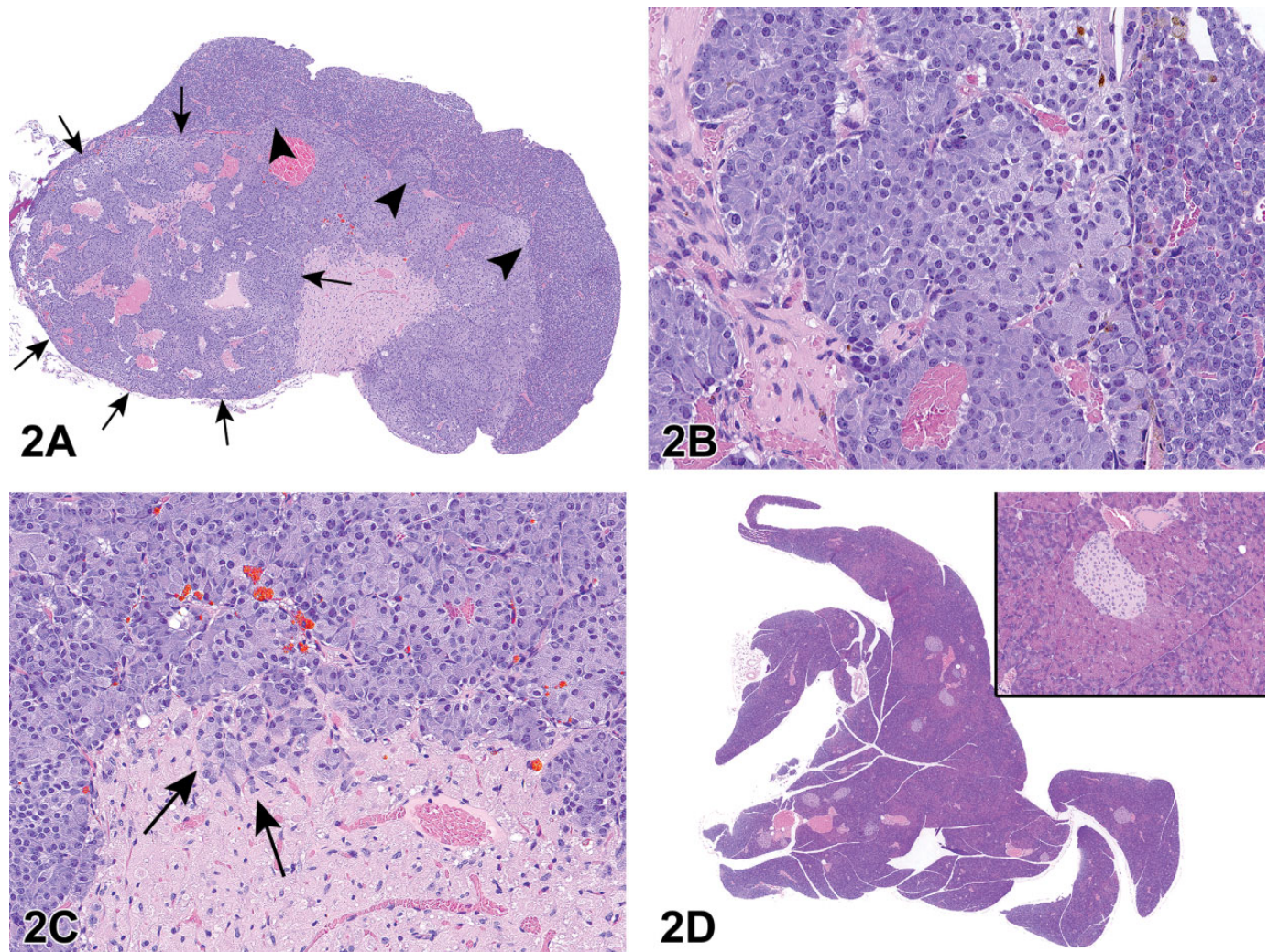


Figure 2. Pituitary (A-C) and pancreatic (D) lesions from adult 129S1/SvImj mice from the National Toxicology Program Aging Mouse Study. A, Photomicrograph of the pituitary gland showing a poorly circumscribed mass (arrows) expanding the pars intermedia and compressing the adjacent pars distalis in more than 1 quadrant (arrowheads). B, Photomicrograph of the pars intermedia showing characteristic nests of pleomorphic cells (center). C, Photomicrograph showing neoplastic cells extending into the pars nervosa (arrows). D, Photomicrograph of the pancreas. Inset shows higher magnification image of the peri-insular acinar hypertrophy characterized by intracytoplasmic accumulation of abundant zymogen granules within acinar cells surrounding the islets of Langerhans.

Table 2. Diagnostic Features of Pars Intermedia Lesions.²

Diagnostic features (Pars Intermedia)	Hyperplasia	Adenoma	Carcinoma
Pleomorphism	–	Yes	Yes
Compression (>1 quadrant)	–	Yes	Yes
Extension into pars nervosa	May be present	Yes	Yes
Invasion of adjacent brain/meninges/sphenoid bone	–	–	Yes

strain from this study. When present in this strain, the finding was relatively localized to the metaphyseal region, with the mid-diaphysis being normal to hypercellular; hypercellularity was the most common diagnosis in the other 9 strains.

Fat content of bone marrow varies with species, strain, sex, age, anatomic site, and activity of the hematopoietic tissue.¹ In

general, rodents have reduced amounts of fat and increased hematopoietic elements as compared to other mammals, with mice having even less than that of rats of the same age.¹ As animals age, bone marrow cellularity tends to decrease, with a relative increase in adipocytes.⁴ During the presentation, Dr Crabbs discussed the diagnostic dilemma of the “chicken or

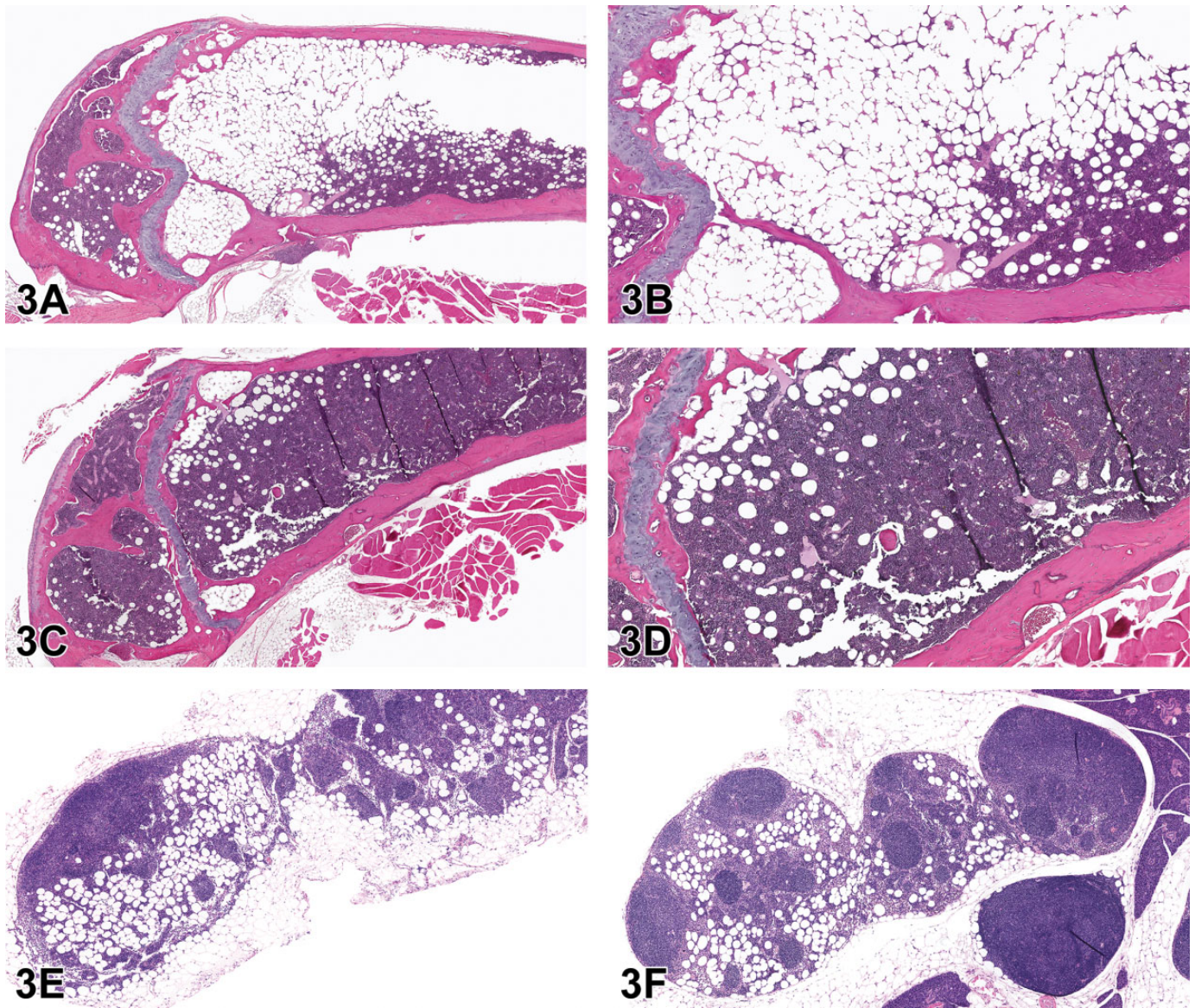


Figure 3. Bone marrow lesions (A-D) and lymph node lesions (E-F) from adult female B6C3F1/J mice from the National Toxicology Program Aging Mouse Study (case 5). Increased adipocytes in the bone marrow (A-B) were only noted in females from this particular strain of aged mouse. Note that hematopoietic elements of the bone marrow, particularly in the metaphyseal region, are almost entirely replaced by abundant numbers of adipocytes, as compared to the normal bone marrow (C-D). Infiltration of adipocytes in the medullary sinuses of the mesenteric (E) and mandibular (F) lymph nodes in adult female B6C3F1/J mice from the National Toxicology Program Aging Mouse Study. This finding occasionally accompanied incidences of increased adipocytes in the bone marrow in this strain. Chronic active inflammation of the epicardium from an adult female NZO/HILtJ mouse from the National Toxicology Program Aging Mouse Study (G-J) (case 6) and lung lesions from Cast/Eij mice (K-L) (Case 7) from the National Toxicology Program Aging Mouse Study. In the NZO/HILtJ mouse strain, inflammation was only present in females and was always associated with mediastinal lymphoma (G). In the heart (H-J), circumferential thickening of the epicardium was characterized by infiltration of lymphocytes, plasma cells, and lesser numbers of neutrophils, fibrosis, and mesothelial hyperplasia. Eosinophilic crystals (K) were a common finding in both males and females from the Cast/Eij strain of mouse and were typically not associated with any additional pathology in the lung, except for rare diagnoses of proteinosis (L).

the egg” issue with regard to increased adipocytes and decreased hematopoietic cells (ie, is there a primary increase in adipocytes with a subsequent loss or “pushing out” of hematopoietic cells or a primary decrease in hematopoietic cells with relative replacement by adipocytes?). The diagnostic criteria for both diagnoses, as described on <https://www.goreni.org>,¹

were discussed. Both can be focal, multifocal, or diffuse. With decreased hematopoietic cells, single or multiple cell lines can be affected, and peripheral blood cell counts can prove to be beneficial since reductions in affected lineages can sometimes be apparent. Dr Crabbs stated that unfortunately, blood work had not performed for this study.

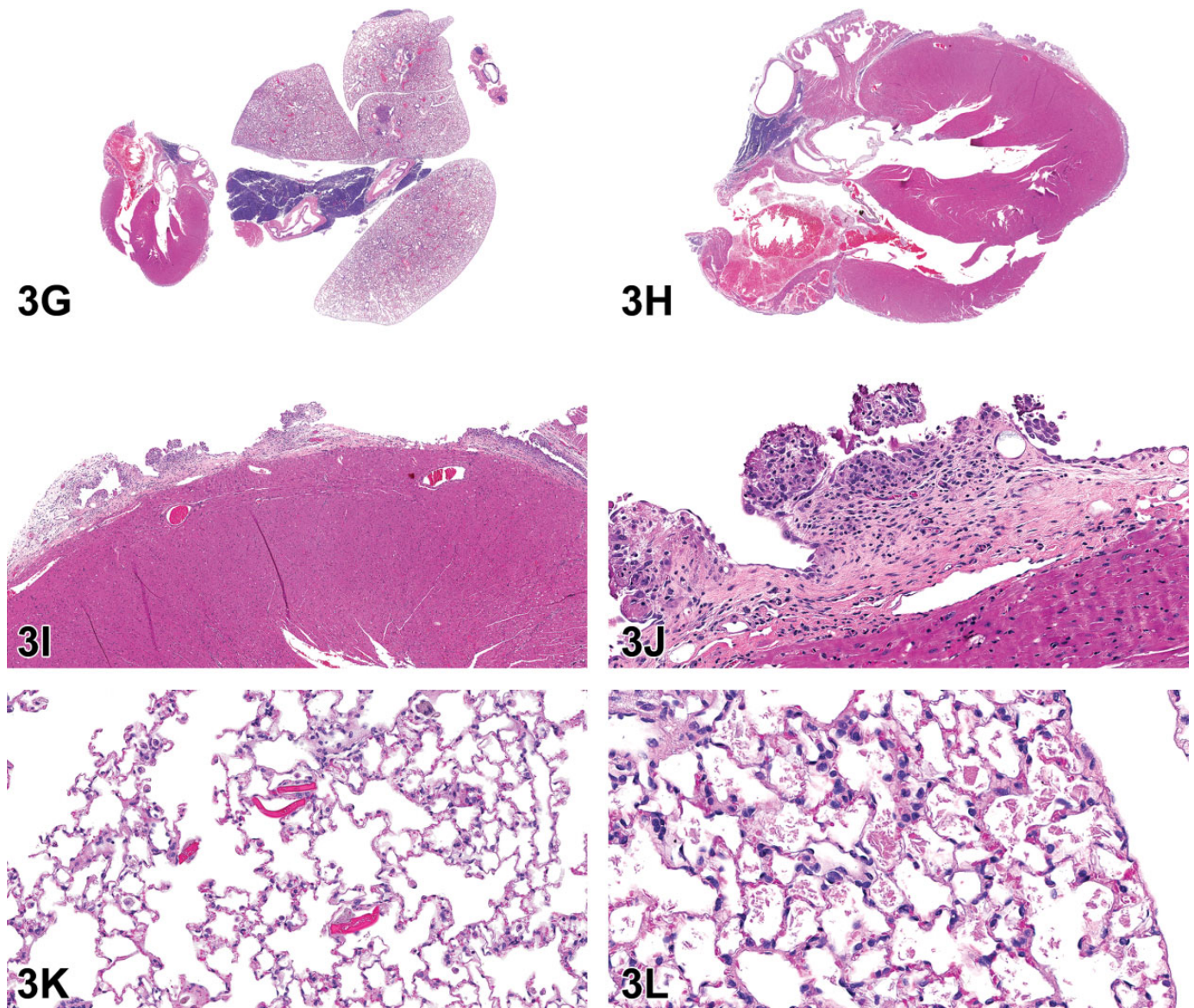


Figure 3. (continued).

Case 6 was from an adult female NZO/HILtJ mouse. Histologically, there was circumferential thickening of the epicardium of the heart due to infiltration of lymphocytes, plasma cells, and lesser numbers of neutrophils (chronic active inflammation), fibrosis, and mesothelial hyperplasia. This finding was only present in females (12%) and was always accompanied by mediastinal lymphoma (Figure 3G).

The audience was shown representative photomicrographs of the heart (Figure 3G-J). The initial voting choices and results for this case were as follows: within normal limits (1%), chronic active inflammation (3%), mesothelial hyperplasia (18%), chronic active inflammation and mesothelial hyperplasia (65%), mesothelioma (13%), and other (0%).

While Dr Crabbs agreed with the majority of the audience that both chronic active inflammation and mesothelial

hyperplasia were present in the projected images, she stated that she had failed to clarify prior to the vote that her intentions had been for the audience to vote specifically on how they would have recorded these changes had they been presented during review of one of their studies. In other words, she was seeking clarification on whether the majority would have recorded both chronic active inflammation and mesothelial hyperplasia or whether they would have recorded one or the other and then describe the accompanying finding in the narrative. Therefore, Dr Crabbs conducted an additional informal poll (via hand raise) to clarify this point; approximately 75% of the audience voted to record one (either chronic active inflammation or mesothelial hyperplasia) and describe the other in the narrative.

Following the initial poll, the audience was asked to vote for one of the following concerning addition of a subsite modifier:

no subsite (4%), epicardium (70%), pericardium (26%), myocardium (0%), and other (0%). There was general consensus between the audience and the preferred diagnosis, which was the addition of epicardium as a subsite.

The seventh case involved several photomicrographs of lung from an adult male Cast/EiJ mouse. The voting choices and results for this case were as follows: edema (2%), proteinosis (4%), eosinophilic crystals (81%), foreign body (0%), within normal limits (12%), and other (1%). There was general agreement between the audience and the reviewing pathologist's preferred diagnosis of eosinophilic crystals (Figure 3J). This finding was extremely common in this strain, affecting 90% of males and 85% of females, and typically was not associated with any accompanying inflammatory or neoplastic lesions. However, proteinosis (Figure 3K) was recorded in 12% of males and 14% of females.

An Unusual Testicular Lesion in Rats Exposed In Utero to Phthalates

Dr Mark Cesta (NIEHS/NTP, Research Triangle Park, North Carolina) presented two lesions in the rete testis of rats exposed in utero to a phthalate (unpublished study). Dr Cesta acknowledges scientific contributions from Anika Dzierlenga (NTP), Chad Blystone (NTP), Cynthia Shackelford (EPL), Gabrielle Willson (EPL), and Cynthia Willson (ILS).

The first case (Figure 4A, C, E) was from an adult male Hsd:Sprague Dawley SD rat from a 2-year NTP carcinogenicity study, which included perinatal exposure (beginning in utero on gestation day 6, then via dam's milk, then via dosed feed to study termination). At low magnification, the rete testis is expanded by a mass-like lesion consisting of eosinophilic, fibrillar material with scattered basophilic elongated structures (spermatozoa). This material is surrounded by large, foamy, or epithelioid macrophages with some multinucleated cells. Amid the eosinophilic material, there are aggregates of macrophages and cholesterol clefts. The remainder of the rete testis is expanded by fibrosis and multiple tubular profiles. Additionally, the seminiferous tubules show evidence of atrophy. The voting choices and results were as follows: sperm granuloma (24%), fibrosis (1%), fibrosis and sperm granuloma (48%), spermatocele (13%), inflammation, chronic (3%), inflammation, chronic and fibrosis (4%), hyperplasia (1%), or other (7%). The original diagnosis by the study pathologist was sperm granuloma. The PWG diagnosis for the lesion was fibrosis and sperm granuloma.

The second case was also from an Hsd:Sprague Dawley SD rat from the same study as the rat from the first case (Figure 4B, D, F). This lesion was very similar to the lesion in the first case, but without the sperm granuloma. The rete testis was expanded by eosinophilic fibrillar material (fibrosis) amid increased numbers of tubule profiles. The tubules had increased numbers of epithelial cells. Amid the fibrosis, there were occasional clusters of foamy macrophages. As in case 1, there was atrophy of the seminiferous tubules. There was also interstitial edema. The voting choices and results were as follows: sperm

granuloma (3%), fibrosis (47%), fibrosis and sperm granuloma (13%), spermatocele (4%), inflammation, chronic (3%), inflammation, chronic and fibrosis (24%), hyperplasia (5%), or other (2%). The original diagnosis by the study pathologist was fibrosis. The PWG agreed.

After the cases were presented, Dr Cesta discussed an article in which the authors described the rete testis lesion and noted that the sperm granuloma is more prevalent at earlier time points, while the fibrosis was more prevalent at later time points.⁵ Dr Cesta pointed out that in the 2-year NTP study, of which these animals were a part, there were 11 fibrotic lesions in the rete testis region, two of which also had sperm granulomas. Furthermore, the foamy macrophages seen in some of the fibrotic lesions suggested they may have been resolving sperm granulomas. So, the evidence suggests that sperm granulomas form in the rete testis as a result of phthalate exposure in utero and resolve into fibrotic lesions.

Next, Dr Cesta discussed the association of the sperm granulomas/fibrosis in the rete testis with testicular dysgenesis, another lesion that is caused by phthalate exposure in utero. In the NTP study, the incidence of sperm granuloma or fibrosis was 11 of 50 (the lesion was only seen in the highest dose group). There were 9 dysgenesis lesions in the same group, and 5 of those animals had both lesions in the same testis. Therefore, it appears that these lesions often occur together. For a review of testicular dysgenesis, please see the proceedings from the 2018 NTP Satellite Symposium,⁶ where Dr Cynthia Willson presented those lesions, or the Barlow et al article.⁵

Next, Dr Cesta discussed the advantages of obtaining multiple sections of the testis. Multiple sections ensure at least one section includes the rete testis. Multiple sections can also help better characterize the lesion. As an example, Dr Cesta showed 2 sections from the same testis. One of the sections contained a sperm granuloma, whereas the other only exhibited fibrosis. So, the diagnosis could vary depending on the area of the rete testis that is examined.

Dr Cesta then briefly discussed possible pathogeneses for the sperm granuloma/fibrosis in the rete testis. His first point was that it seems unlikely that the sperm granulomas are caused by the dysgenesis because the dysgenesis is upstream of the rete testis (in the seminiferous tubules). One of the most common causes of sperm granulomas is a blockage in the flow of seminiferous fluid with subsequent rupture of the tubule basement membrane and granuloma formation. Another possibility is that there was a blockage of some sort in the efferent tubules; these are difficult to trim in and are not routinely evaluated in NTP studies, so this possibility cannot be excluded. A third possibility is the rupture of the basement membrane of the rete testis as a direct result of phthalate exposure. In a 2017 article in *Scientific Reports*, Lara et al have shown that phthalate exposure during the masculinization programming window (E15.5-18.5) results in rupture of the basement membrane of the normally formed seminiferous tubules with subsequent formation of tubular dysgenesis.⁷ If this also occurred in the rete testis, this could result in a sperm granuloma; however,

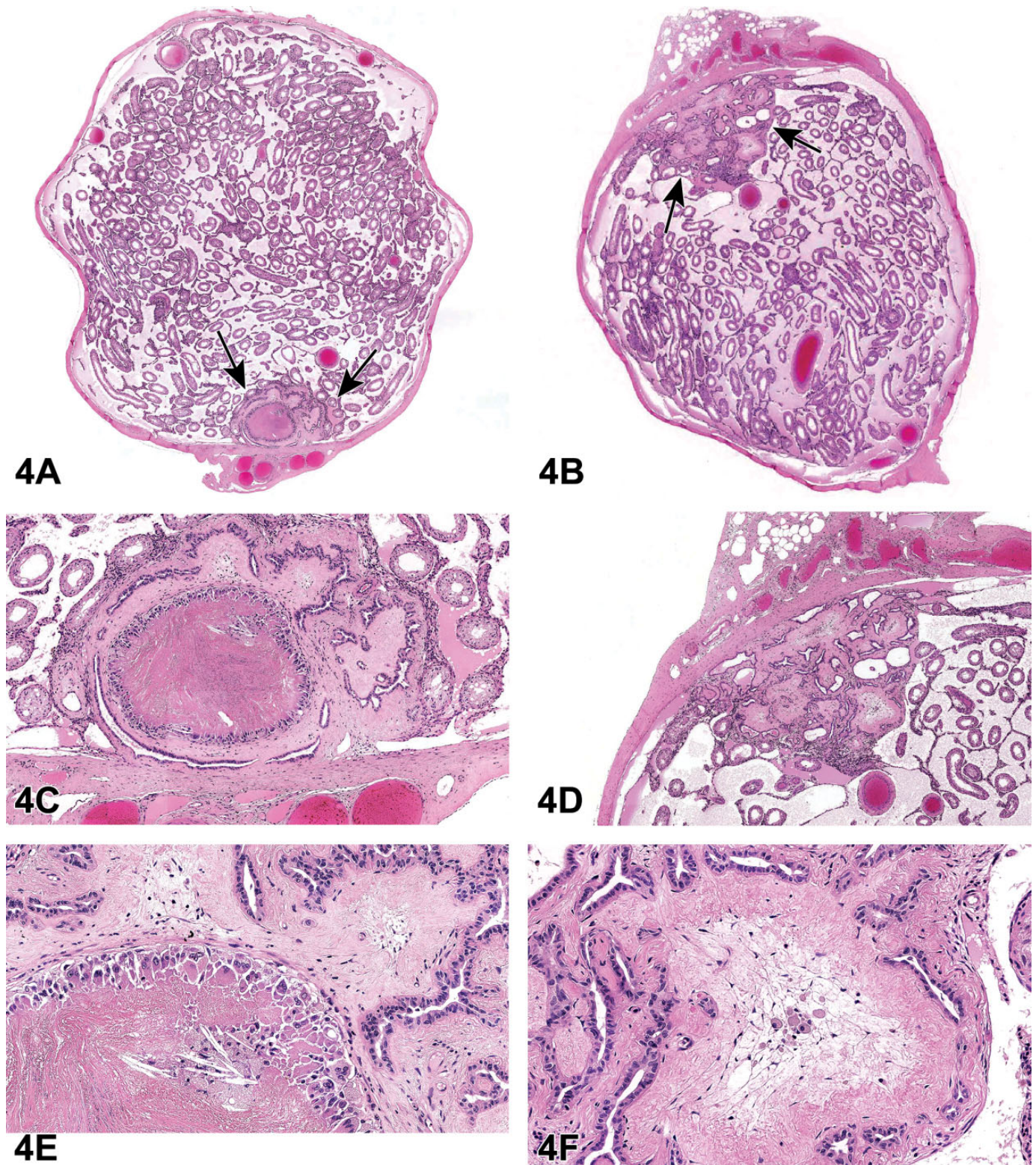


Figure 4. Rete testis lesions in Hsd:Sprague Dawley SD rats (A-F) from a National Toxicology Program perinatal chronic bioassay. All were exposed in utero to a phthalate. A, C, and E, The rete testis (arrows) is expanded by a sperm granuloma and fibrosis. E, Numerous spermatids in the rete testis are surrounded by a rim of epithelioid and multinucleated macrophages. Within the granuloma, there are smaller aggregates of macrophages and cholesterol clefts. B, D, and F, Fibrosis in the rete testis (arrows). F, The rete testis is expanded by fibrosis with smaller aggregates of foamy macrophages, suggesting progression from a sperm granuloma.

there are no data to support this hypothesis. In fact, Dr Cesta pointed out that all of these possible pathogeneses are just conjecture and the pathogenesis of the rete testis sperm granulomas is unknown.

Dr Cesta then asked the audience if anyone has seen these rete testis lesions as a treatment-related finding as a result of exposure to any chemical other than a phthalate. No one answered in the affirmative, and the only mention of this lesion in the literature is in the Barlow et al article.⁵ So, it seems that to date, the sperm granulomas and fibrosis of the rete testis are specific to phthalate exposure in rats exposed in utero.

Ovarian Lesion in a Young Sprague Dawley Rat

Dr Haoan Wang (West China-Frontier Pharma Tech Co, Ltd [WCFP] Chengdu, Sichuan, China) presented a rare neoplasm involving the ovary of a young female Crl:CD Sprague Dawley rat from a 13-week repeated dose oral gavage toxicity study. Dr Wang acknowledged Dr Fei Zhou (WCFP), who was the original study pathologist. The author also acknowledged Drs Peter C. Mann, Torrie A. Crabbs, and Tom Steinbach (EPL) for their support and help and Dr Kyathanahalli Janardhan (ILS) for his assistance with the IHC.

This case involved a terminal sacrifice control female Crl:CD Sprague Dawley rat. The animal was 6 to 7 weeks of age at the study start and survived until scheduled sacrifice (19-20 weeks of age). No abnormalities were noted during routine palpation by the clinical veterinarian. In addition, clinical signs, body weight, hematology, and blood chemistry were all unremarkable following the 13-week treatment. However, ovarian organ weight and organ weight ratios were increased in this animal compared with the remaining females in the control group. At necropsy, the ovaries were noted grossly to be normal; however, multiple smooth round nodules ranging in size from $0.1 \times 0.1 \times 0.1$ cm to $0.4 \times 0.4 \times 0.3$ cm were noted on the surface of the pancreas.

Representative photomicrographs of the ovaries were presented to the audience (Figure 5A-C). Microscopically, cauliflower-like protuberances with an exophytic growth pattern were noted on the surface of one of the ovaries. The mass was relatively well demarcated from the adjacent areas. Compression of the adjacent normal ovarian tissue was not observed. Tumors presented as solid, cystic, and papillary structures composed of pleomorphic, cuboidal to low columnar cells that were occasionally ciliated. The cells showed nuclear pleomorphism and an increased nuclear/cytoplasmic ratio. Mitotic figures were occasionally noted. Partial necrosis of tumor cells with cellular debris, neutrophilic infiltration, and neovascularization was present in some solid regions of the tumor. Metastases which were similar in appearance to the primary tumor were histologically noted in the hilus of the spleen and the adipose tissue surrounding the pancreas, which were correlated with the gross lesions noted at necropsy.

The audience was asked to vote for their preferred diagnostic term. The voting choices and results were as follows:

cystic/papillary hyperplasia (16%), tubulostromal carcinoma (31%), cystadenoma (5%), cystadenocarcinoma (21%), malignant mesothelioma (22%), and other (5%). Although the majority of the audience opted for a diagnosis of tubulostromal carcinoma, the presenter's preferred diagnosis was cystadenocarcinoma. Dr Wang proceeded to explain the rationale for this diagnosis.

Dr Wang reviewed the histologic features of the tumor from this case, as previously described, and reviewed the results of the IHC staining which had been performed in an effort to differentiate neoplasms arising from the surface epithelium of the ovary from mesothelioma. The initial hypothesis had been that mesotheliomas would stain positively for both cytokeratin (CK) and vimentin, while neoplasms arising from surface epithelium of the ovary would only stain positively for CK. To address this, IHC staining was performed by using vimentin, CK-7, and cytokeratin-wild spectrum (CK-WS) antibodies.

The IHC results showed that, in this tumor, staining for vimentin was cytoplasmic and present in $\sim 60\%$ of the neoplastic cells; staining for CK-7 was cytoplasmic and present in only $\sim 10\%$ of the neoplastic cells; and no staining was observed for CK-WS in the neoplastic cells (Figure 5D-F). Interestingly, in the current evaluation, the normal ovarian surface epithelium (OSE) also stained positively for both vimentin and CK (Figure 5G-I). Therefore, the IHC results demonstrated that distinction between mesothelioma and OSE neoplasms is not possible using vimentin and CK.

Dr Wang then gave some illustrations about this finding. Ovarian surface epithelium is characterized by keratin types 7, 8, 18, and 19, which represent the keratin complement typical for simple epithelia in humans, but OSE cells also constitutively coexpress keratin with vimentin, which is a mesenchymal intermediate filament.⁸ The IHC results of the present case demonstrated that keratin, an epithelial marker, and vimentin, a mesenchymal marker, coexist in OSE in Crl:CD Sprague Dawley rats. A literature review by Kim et al⁹ put forward the viewpoint that coelomic epithelium differentiates into mesothelium in the peritoneal cavity and into the OSE in the gonadal ridge, where the ovary forms. Because the OSE is a type of mesothelium covering the ovary, it is also known as ovarian mesothelium (OM). When the mesothelium lining the peritoneum undergoes a malignant transformation, the resulting tumor is called a (peritoneal) mesothelioma. On the other hand, transformation of the OM leads to an ovarian carcinoma. Based on this point, Dr Wang thought that the tumor in this case should be diagnosed as an ovarian carcinoma.

Dr Wang reviewed the INHAND publication on the rodent female reproductive system¹⁰ for the audience to explain why a final diagnosis of cystadenocarcinoma had been chosen for this case as opposed to another type of ovarian tumor. The INHAND describes the pathogenesis/cell of origin of a cystadenocarcinoma as the surface epithelium of the ovary and includes the following diagnostic features: solid or cystic mass lined by cuboidal or low columnar pleomorphic epithelium that may be ciliated, frequent mitotic figures, possible presence of folds or papillary projections, delicate stromal

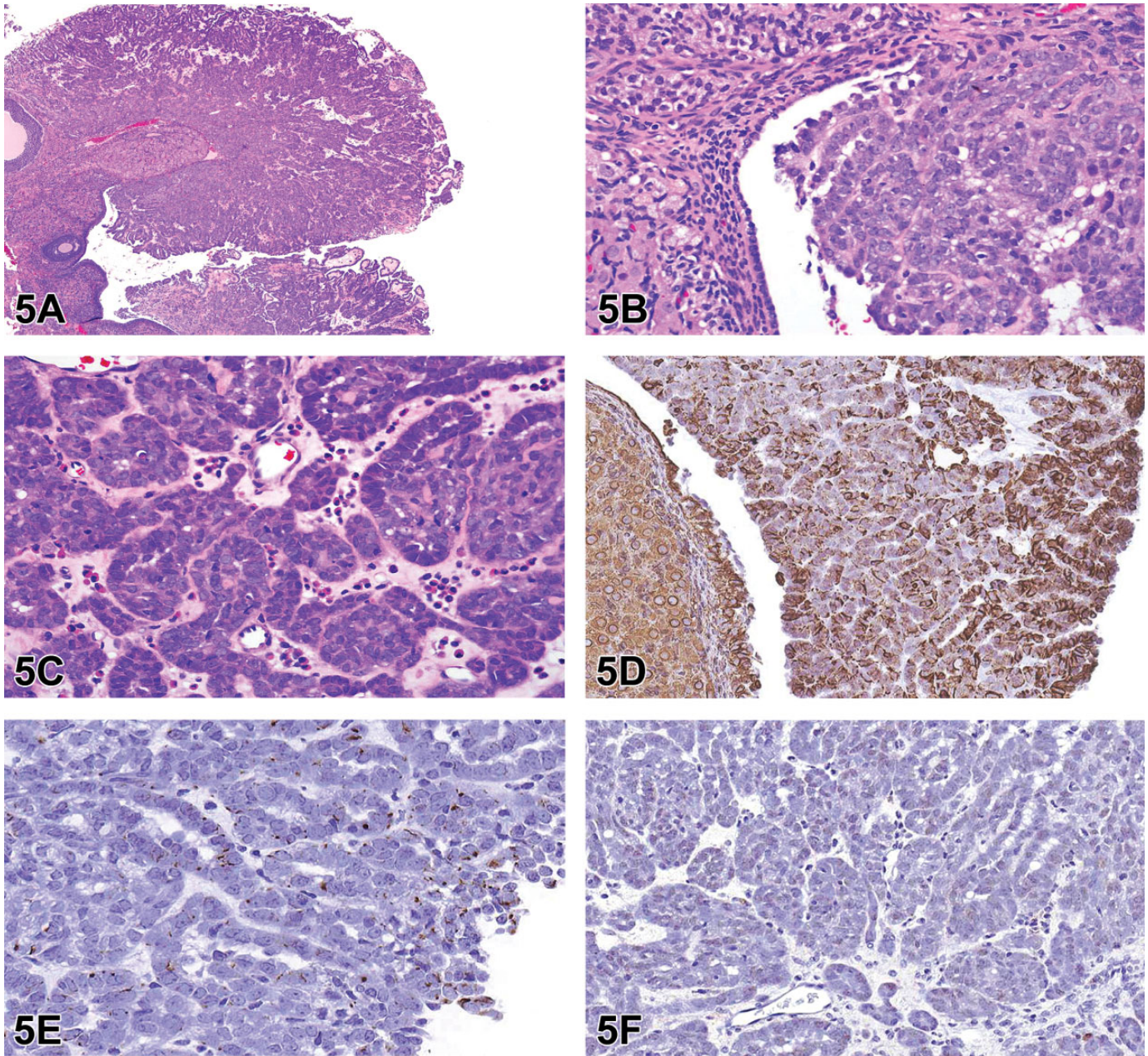


Figure 5. Ovarian tumor (A-I) from a control nearly 20-week-old CrI:CD Sprague Dawley rat. A low magnification image (A) of the cauliflower-like tumor with an exophytic growth pattern on the surface of one of the ovaries. Higher magnification (B) shows the mass is derived from the ovarian surface epithelium (OSE), which is relatively well demarcated from the adjacent areas. The mass is composed of solid or papillary structures of pleomorphic, cuboidal to low columnar cells that are occasionally ciliated. Higher magnification (C) shows the neutrophilic infiltration and neovascularization in some solid regions of the tumor with a delicate stromal compartment. D-F, Immunohistochemical characterization of the tumor. Neoplastic cells are positive for vimentin (~60%) (D) and CK-7 (~10%) (E) and negative for CK-WVS (F). G-I, Immunohistochemical characterization of the OSE in the SD rat. The normal OSE stains positively for vimentin (G), CK-7 (H), and CK-WVS (I). Immunohistochemical characterization of the ovarian surface epithelium (OSE) in the SD rat (G-I). The normal OSE stains positively for vimentin (G), CK-7 (H), and CK-WVS (I).

compartment that is not an inherent part of the tumor, and infiltration of adjacent tissue. These features are nearly identical to the morphologic features of this present case. Therefore, based on all of the above information, the ovarian tumor of this young CrI:CD Sprague Dawley rat was diagnosed as a cystadenocarcinoma.

Ovarian cystadenocarcinoma is one of the epithelial (ovarian coelomic mesothelium) origin tumors in the ovary.¹¹ In laboratory rodents, it is a common lesion in some mouse strains but uncommon in rats.¹⁰ In one report, the incidence of ovarian cystadenocarcinoma in F344 rats was 3%.¹² In CrI:CD Sprague Dawley rats, it was only recorded in 1 of 7748 females at 101 to

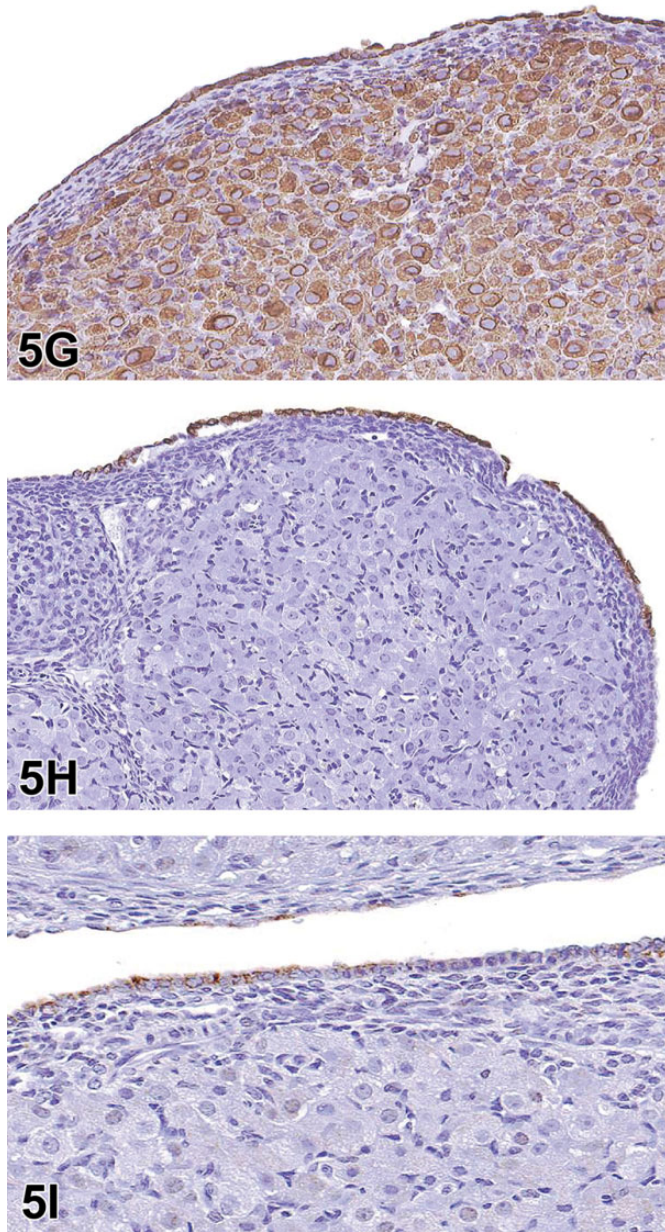


Figure 5. (continued).

110 weeks of age,¹³ suggesting that this neoplastic lesion is very rare even in older rats. In another report, there were no incidences of spontaneous cystadenocarcinomas of the ovary recorded in young Crl:CD Sprague Dawley rats aged 10 to 32 weeks.¹⁴ In this case, an ovarian cystadenocarcinoma was found in a control Crl:CD Sprague Dawley female rat nearly 20 weeks of age. To our knowledge, this is the first report of a cystadenocarcinoma in a young rat.

This case provoked continued discussion between multiple audience members with regard to origin of these tumors. Given the mesothelial origin of the OSE, it was questioned whether the most appropriate terminology is being used by the toxicologic pathology community.

Metastatic Periorcular Schwannoma in a Rat

Dr Gregory Krane (NIEHS/NTP and North Carolina State University, Research Triangle Park, North Carolina) presented a case of an F344/N rat from an NTP 2-year carcinogenicity inhalation study of 1,2-epoxybutane,¹⁵ a stabilizer in chlorinated hydrocarbon solvents. This male rat from the high dose group had a large, unencapsulated, expansile, multinodular retro-orbital mass. Bundles and streams of spindle cells dissected a fibrovascular stroma. These cells with indistinct borders had low amounts of eosinophilic, fibrillar cytoplasm and ovoid to spindle nuclei with coarsely granular chromatin and indistinct nucleoli. Cellular and nuclear pleomorphisms were low, and mitoses were not observed (Figure 6A and B).

Initial voting choices and results were as follows: hemangiopericytoma (4%), melanoma (15%), meningioma (13%), neurilemmoma (5%), neurinoma (3%), neurofibroma (25%), perineurioma (3%), sarcoma (7%), and schwannoma (26%). After voting, Dr Krane presented images detailing immunohistochemical analysis of this case. Stains presented (and associated immunoreactivity for this case) were as follows: S-100 (strong positive, nuclear; Figure 6C), SOX-10 (positive, nuclear; Figure 6D), and antiepithelial membrane antigen (EMA; negative—data not shown). There was then a second round of voting, with results as follows: hemangiopericytoma (0%), melanoma (13%), meningioma (7%), neurilemmoma (5%), neurinoma (3%), neurofibroma (21%), perineurioma (0%), sarcoma (4%), and schwannoma (48%). Based on the histologic and immunohistochemical features, schwannoma was considered the most appropriate diagnosis by the audience.

After final voting, Dr Krane presented further information about the case. In the lungs, there were numerous, multifocal to coalescing nodules of a mass with features similar to the retro-orbital schwannoma (Figure 6E and F). Immunohistochemical analysis of the mass showed robust nuclear reactivity for S-100 (Figure 6G) and lack of reactivity for EMA (Figure 6H). Immunohistochemistry of the lung samples for SOX-10 was not available to Dr Krane at the time of the symposium.

Schwannomas, previously referred to as neurinomas or neurilemmomas, represent benign and malignant variants of nerve sheath tumors.¹⁶ They are common in domestic species, with the most frequent occurrence in the canine and bovine.¹⁶ In humans, they are often lumped with neurofibroma and associated with a genetic condition known as neurofibromatosis. This is caused by mutations in the *NF1* and *NF2* genes (chromosome 22).¹⁷ This results in loss of expression of merlin, a protein that restricts cell surface expression of growth factor receptors (such as epidermal growth factor receptor [EGFR]), and in its absence, cells proliferate in response to growth factors.¹⁷ Although this rodent case was determined to be malignant due to the overwhelming pulmonary involvement, schwannomas rarely metastasize. They can however be locally invasive and recur, especially in cases of neurofibromatosis.

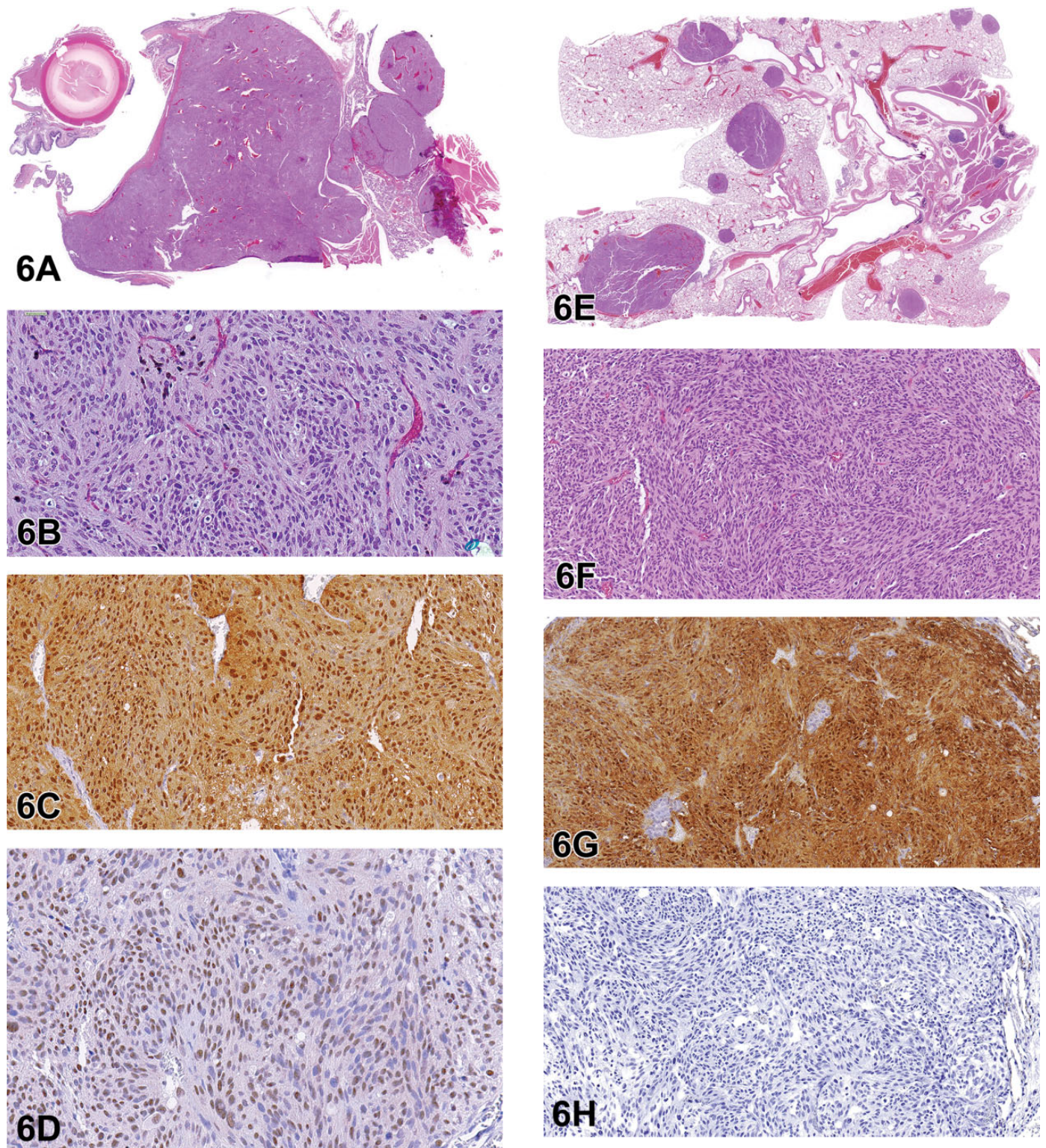


Figure 6. Retro-orbital Schwannoma (A-D) from a 2-year-old male F344/N rat from a National Toxicology Program chronic bioassay that was treated with 1,2-Epoxybutane via inhalation (high-dose group). A, The unencapsulated, multinodular mass expands the retro-orbital region. B, Bundles and streams of spindle cells with indistinct borders dissect a fibrovascular stroma. Cells have low amounts of eosinophilic, fibrillar cytoplasm, and ovoid to spindle nuclei with coarsely granular chromatin and indistinct nucleoli. Cellular and nuclear pleomorphism is low, and mitoses are not observed. There is robust diffuse nuclear immunoreactivity for S-100 (C) and diffuse nuclear immunoreactivity for Sox-10 (D). Retro-orbital schwannoma continued. E-F, There are numerous, multifocal, small to large pulmonary tumors similar to the retro-orbital mass. There is robust nuclear immunoreactivity for S-100 (G) and lack of immunoreactivity for EMA (H).

Table 3. Immunohistochemical Markers.²¹⁻²⁴

Immunohistochemistry Stain	Schwannoma	Meningioma	Neurofibroma	Perineurioma
S-100	+++	+/-	+/-	-
Sox-10	+	-	nr	nr
EMA	-	+	-	+

Abbreviation: nr, not reported.

Table 4. Expanded List of Immunohistochemical Markers.^{16,18-20,25,26}

Immunohistochemistry Stain	Schwannoma	Meningioma	Neurofibroma	Perineurioma	Leiomyoma
CNPase	+	nr	nr	nr	nr
S-100	+++	+/-	+/-	-	nr
Laminin	+	-	nr	+	nr
Sox-10	+	-	nr	nr	nr
GFAP	+/-	-	nr	+/-	-
PLP	+	nr	nr	nr	nr
PMP22	+	nr	nr	nr	nr
EMA	-	+	-	+	nr
Periaxin	+	nr	nr	nr	nr
CD56 (Leu-7)	+/-	nr	nr	nr	nr
Schwann/2E	+	-	-	-	-
Desmin	-	nr	nr	nr	+
SSTR2A	-	+	nr	nr	nr
Vimentin	+	nr	nr	+	nr
Collagen IV	+	nr	nr	+	nr
Claudin-I	-	nr	+	+	nr
GLUT-I	-	nr	nr	+	nr

Grossly, schwannomas generally consist of nodular masses or thickening of spinal, paraspinal, or cranial nerves. They have variable firmness and are white to gray, shiny, and smooth.¹⁶ They are often unilateral though, in human neurofibromatosis, can be present bilaterally in cranial nerve 8.¹⁸ Schwannomas can be either intra- or extradural when present in the central nervous system and subcutaneous or intradermal when present in the skin.¹⁶

Histologically, schwannomas consist of interwoven bundles, streams, and/or whorls of densely packed fusiform cells with scant cytoplasm and poorly defined borders. There can be Wallerian degeneration of affected nerve bundles. Classic features of schwannomas such as Antoni A and B configurations and Verocay bodies are possible, though they are more common in human cases as opposed to veterinary species.¹⁶ Reticulin special stain and/or electron microscopy can be used to highlight the continuous basal lamina, a feature of schwannoma cells.^{19,20} Histologic variants of schwannoma include cellular (primarily Antoni A configuration but lacking Verocay bodies), granular (appears similar to granular cell tumor), melanotic (has pigmented melanosomes), and plexiform (multinodular pattern in various nerve branches).¹⁹

Due to the overlapping histologic appearance of schwannomas with other mesenchymal neoplasms, IHC is a vital tool when definitive diagnosis is required. Perineuriomas can appear similar to schwannomas or neurofibromas, but in contrast, a perineurioma is not associated with a genetic mutation

and it does not recur after complete excision.^{21,22} A useful, succinct immunohistochemical panel (with associated reactivity) to differentiate schwannoma from other differential diagnoses is S-100 (strong positive), SOX-10 (positive), and EMA (negative; Table 3).²³ Perineurioma is generally immunoreactive for EMA and immunonegative for S-100.^{21,22} Neurofibroma is generally immunoreactive for both S-100 and EMA.²⁴

S-100, originally isolated in the central nervous system, is present in a wide distribution of tissues. It is a calcium flux regulator that can be useful to highlight cells of Schwann cell, melanocytic, or chondrocytic lineage.¹⁸ SOX-10 is a neural crest transcription factor that is required for Schwann cell and melanocytic differentiation and survival.²⁵ Epithelial membrane antigen is a protein thought to be involved in cell secretion that is positive in perineurioma and meningioma.²³ Table 4 summarizes additional immunohistochemical markers for schwannoma and its differential diagnoses.

In the rat, schwannoma has been induced by a variety of test articles. These include, but are not limited to, N-nitrosoethylurea (ENU),²⁷ methyl-methane sulfate, 7,12-dimethylbenz[α]anthracene, N-nitrosomethylurea,¹⁹ and nonionizing radiofrequency radiation (RFR).²⁸ N-nitrosoethylurea exposure can lead to schwannoma due to a mutation of *neu/erdb-2* at nucleotide 2012.²⁹ This is thought to be mediated by affecting acid hydrolase levels.²⁷ The most common site for ENU-induced schwannoma is the trigeminal nerve, with BDIX strains of rats being most affected and

BDIV strains being resistant.³⁰ N-nitrosomethylurea-induced schwannomas have been reported in a variety of tissues including the thoracic cavity, abdominal cavity, pancreas, prostate, thymus, and heart.³¹ Recently, a 2-year NTP carcinogenicity study found that cell phone RFR caused clear evidence of cardiac schwannomas in male rats.²⁸ There was also a nonsignificant increase in Schwann cell hyperplasia (a precursor to schwannoma) in male rats.²⁸ At the symposium, an audience member asked if schwannomas in different locations should be combined for incidence tables and statistical analysis. It was mentioned that some do not recommend combining cardiac schwannomas with schwannomas found elsewhere in a given animal, as the heart is considered to be a unique site.

The head and neck are also commonly reported sites for schwannomas in the rodent, with reports in the literature representing the brain (meninges and pituitary gland),³² trigeminal nerve and ganglion,³² eye (including retrobulbar region), mandibular salivary gland, skin/subcutis, and more.²⁰ In the presentation, Dr Krane reinforced the importance of carefully examining all regions of the head and neck if schwannoma was a concern in the study, as these tumors can extend through a variety of locations in the head and neck region. One audience member mentioned that many of these structures of the head and neck are supplied by branches of the trigeminal nerve and indicated a hypothesis that there may be a population of pluripotent stem cells at the trigeminal nerve susceptible for schwannoma induction. This hypothesis gave further support to examining head and neck structures supplied by the trigeminal nerve should there be concern regarding schwannoma in a given study.

Although schwannomas can often be presumptively diagnosed based on location and histologic appearance, definitive diagnosis often requires the use of IHC. Due to the association of schwannoma with neurofibromatosis, a recurrent condition caused by a genetic mutation, definitive diagnosis can be important, not only for human patients but also for toxicologic pathologists to accurately inform stakeholders of a given study.

Dr Krane would like to acknowledge Dr David Malarkey (NIEHS/NTP) for general mentorship and for nominating him to participate in the satellite symposium, Dr Susan Elmore (NIEHS/NTP) for her tireless efforts coordinating the satellite symposium, Dr Maggie Gruebbel (EPL) for assistance with a literature review, and the NIEHS histology, IHC, and image preparation laboratories for helping to generate high-quality slides and images. Finally, Dr Krane made a special acknowledgment to Dr Gordon Flake, who was the NTP pathologist for this case before his untimely passing in 2018. Dr Flake was a longstanding member of the NTP pathology team, and he is remembered fondly for his brilliance, kindness, and dedication.

Unusual Lesions in the Pancreas and Liver of Hsd:Sprague Dawley SD Rats

Dr Torrie A. Crabbs (EPL, Inc) presented lesions from 2 Hsd:Sprague Dawley SD rats from a recent NTP 2-year

carcinogenicity/chronic toxicity study. For each case, several representative photomicrographs were presented, and the audience members were asked to vote for their preferred diagnostic term. Dr Crabbs acknowledged Dr Margarita Gruebbel (EPL) for her assistance in data collection and interpretation and in the preparation of this manuscript and Maureen Paucini and Emily Singletary (EPL) for assistance with image acquisition. Additional collaborators on this project included Drs Jerry F. Hardisty (EPL), Cynthia C. Shackelford (EPL), Mark Cesta (NTP/NIEHS), and David E. Malarkey (NTP/NIEHS).

Case 1 was from the liver of a high-dose terminal sacrifice female (Figure 7A and B). The audience was informed that while this finding was from a high-dose animal, the PWG confirmed that this lesion was not considered a test article-related finding. The voting choices and results for this case were as follows: chronic inflammation (1%), cholangiofibrosis (21%), periductal cholangiofibrosis (32%), cholangiocarcinoma (39%), adenocarcinoma (3%), fibrosis (0%), and other (4%).

Case 2 was from the pancreas of a low-dose terminal sacrifice female (Figure 7C and D). The voting choices and results were as follows: chronic inflammation (16%), cholangiofibrosis (12%), periductal cholangiofibrosis (56%), cholangiocarcinoma (7%), adenocarcinoma (2%), fibrosis (4%), and other (4%). The preferred diagnostic term for cases 1 and 2 was periductal cholangiofibrosis of the liver and pancreas, respectively.

Hepatic cholangiofibrosis in rats has been documented as a chronic lesion ranging from small scattered parenchymal foci to large confluent areas affecting entire liver lobes.³³⁻³⁶ The lesions consist of abnormal bile ductular-like structures supported by an often dense and abundant fibrous stroma, frequently infiltrated by inflammatory cells. The bile ductule-like structures are typically dilated and/or tortuous and contain variable but often copious amounts of pale eosinophilic to basophilic, fibrillary to amorphous mucin-like material, sloughed lining cells, and/or necrotic debris. The ductule-like structures are typically lined by single to multilayered epithelium that varies from thin attenuated to columnar basophilic cells. The lining epithelium can also exhibit intestinal metaplasia, a hallmark feature of cholangiofibrosis, consisting of abundant goblet cells and occasional Paneth cells interspersed among the basophilic columnar cells.^{33,35-37}

Cholangiofibrosis in rats has long been regarded as an induced change, confined to the liver. It generally results from administration of various chemical agents including furan, dioxin and dioxin-like compounds, 2-acetylaminofluorene, and methapyrilene hydrochloride^{33-35,38} and has also been associated with experimental feeding of corn naturally contaminated with *Fusarium moniliforme*.³⁹ In at least some experimental rat models, chemically induced cholangiofibrosis has demonstrated the potential for progression to malignant neoplasia (cholangiocarcinoma).^{33,37}

Rats of several strains (including F344/N and Hsd:Sprague Dawley SD) have been affected.^{33-35,40} Spontaneously occurring hepatic cholangiofibrosis-like changes have also been

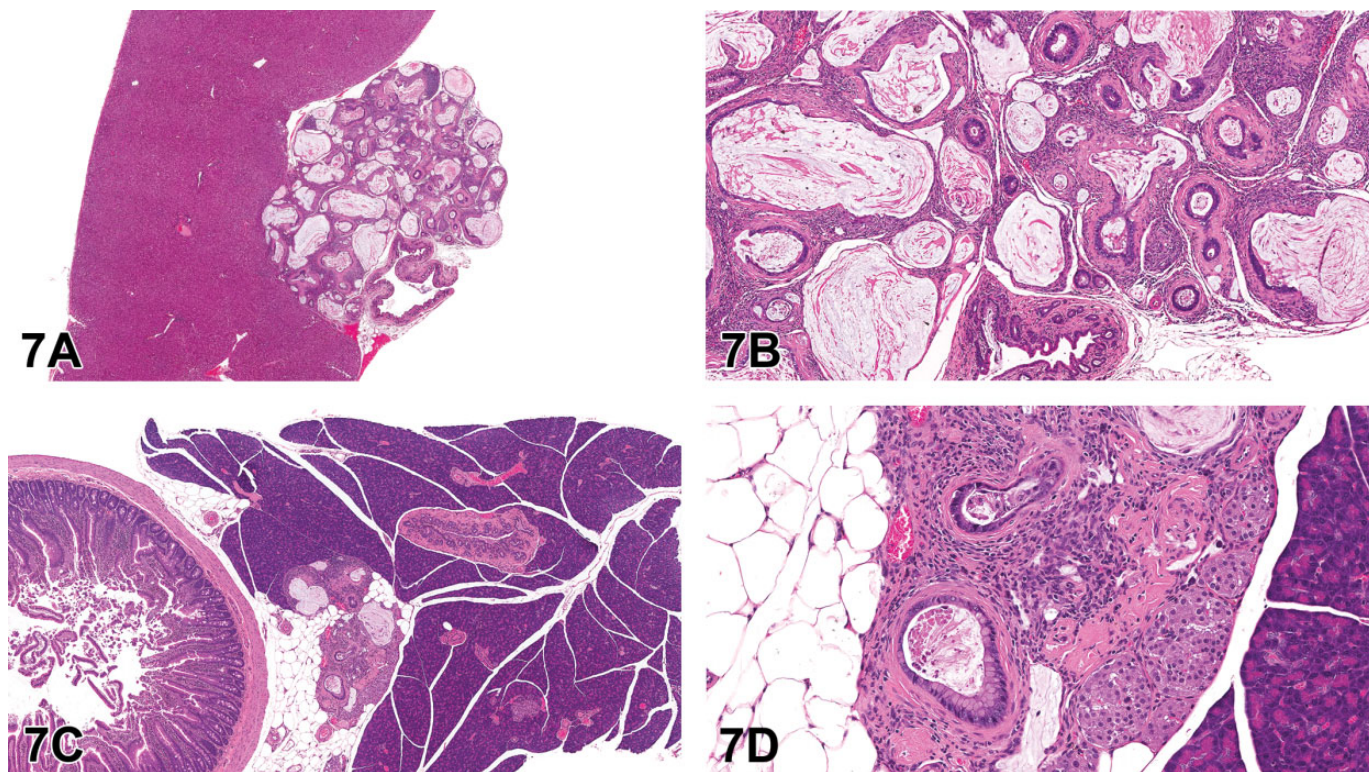


Figure 7. Examples of spontaneous periductal cholangiofibrosis (A-D) in 2-year-old Hsd:Sprague Dawley SD rats from a National Toxicology Program chronic bioassay. Spontaneous periductal cholangiofibrosis in the liver of a female rat as was presented in case 1 (A-B). Low magnification (A) shows a focal, nodular, extracapsular mass immediately adjacent to the main hepatic bile duct. At higher magnification (B), the mass is characterized by dilated and/or tortuous bile ductule-like structures with mucous-like intraluminal material, cuboidal to columnar lining epithelium with intestinal metaplasia, and abundant supporting fibrous stroma with variable inflammatory cell infiltrates. Spontaneous periductal cholangiofibrosis in the pancreas of a female rat as presented in case 2 (C-D). Low magnification (C) shows a focal finding in the parenchyma of the pancreas. Note the close approximation to the common bile duct. Higher magnification (D) shows the mass is characterized by dilated and/or tortuous bile ductule-like structures with mucous-like intraluminal material, cuboidal to columnar lining epithelium with intestinal metaplasia, and abundant supporting fibrous stroma with variable inflammatory cell infiltrates.

noted in Long-Evans Cinnamon rats (a rodent model of Wilson disease), but these lesions were components of the concurrent, genetically related hepatotoxicity and lacked the characteristic intestinal metaplasia.⁴¹

In a recent NTP 2-year study with Hsd:Sprague Dawley SD rats (90 control animals/sex and 540 treated animals/sex), focal cholangiofibrosis was noted in the liver or pancreas of 9 males and 21 females; 3 animals with liver lesions (2 males and 1 female) were unexposed controls. In this study, 100% (9/9) of lesions in males were associated with the liver, while in females, 76% (16/21) of the lesions were associated with the pancreas. Incidences in exposed groups were low, sporadic, and unrelated to dose and were, therefore, regarded as incidental and unrelated to exposure.

The findings in this first NTP study prompted a retrospective review of 9 other recent NTP 2-year carcinogenicity/chronic toxicity studies in Hsd:Sprague Dawley SD rats. Liver and pancreas (including the pancreas section typically sectioned with the duodenum) were examined in all untreated and vehicle control animals from the 9 studies (total of 260 males and 705 females). Four additional periductal cholangiofibrosis

cases were noted: 3 liver cases (2 in females and 1 in a male) and 1 pancreas case (in a male); because all cases were in control animals, they were considered spontaneous.

The light microscopic morphology of the NTP Hsd:Sprague Dawley SD rat lesions was generally consistent with previous descriptions of cholangiofibrosis: dilated and/or tortuous bile ductule-like structures with mucous-like intraluminal material, cuboidal to columnar lining epithelium with intestinal metaplasia, and abundant supporting fibrous stroma with variable inflammatory cell infiltrates. Each affected animal exhibited either a hepatic or pancreatic lesion; there were no cases in which hepatic and pancreatic cholangiofibrosis occurred simultaneously in the same animal. However, in some respects, the NTP Hsd:Sprague Dawley SD cases differed from previous descriptions. Rather than being diffuse or confluent, the NTP Hsd:Sprague Dawley SD hepatic and pancreatic lesions were singular, circumscribed, discrete, and often nodular. Some NTP Hsd:Sprague Dawley SD lesions occurred in an extrahepatic location (pancreas). The NTP Hsd:Sprague Dawley SD hepatic lesions were often extracapsular and frequently near the main hepatic bile duct. Only a few hepatic lesions were noted grossly

at necropsy as liver masses or pale foci. The NTP Hsd:Sprague Dawley SD pancreatic lesions (none of which were noted grossly) were located in the pancreatic parenchyma, adjacent to the common bile duct near its termination in the proximal duodenum.

Given their spontaneous occurrence, distinctive singular distribution, and frequent close proximity to a large bile duct in the liver or pancreas, these NTP Hsd:Sprague Dawley SD hepatic and pancreatic findings were termed “periductal cholangiofibrosis” to differentiate them from the chemically induced hepatic cholangiofibrosis and the genetically related cholangiofibrosis-like lesions documented in previous reports. While the audience generally concurred that these cases likely represented a unique presentation of cholangiofibrosis, it was proposed that the lesion may be more appropriately captured by using bile duct as the tissue of origin.

Subsequent to the initial report of these findings in NTP Hsd:Sprague Dawley SD rats,⁴² another case of focal liver cholangiofibrosis, which was very similar to those in the NTP studies, has been reported in a control male Wistar rat from a non-NTP 2-year carcinogenicity/chronic study,⁴³ demonstrating spontaneous occurrence of cholangiofibrosis in at least one other rat strain.

Polyovular Follicles in Beagle Dogs

Dr Matthias Rinke (retired Director of Pathology and Clinical Pathology at Bayer AG, Wuppertal, Germany) presented a case of polyovular follicles (POFs) seen in 2 different young (age at study start 3 to 5 months) beagle dogs from a routine 13-week toxicity study with an agrochemical. Voters could decide between malformation (0%), normal, no corpora lutea developed (6%), and different terms available in the literature. Most of the audience seemed to be familiar with the finding, yet only 15% voted for POF, which is the current INHAND term for rodents; 44% decided for the more descriptive term “multioocyte follicle” (MOF) that has been frequently used in the past; 18% voted for “increased number of follicular oocytes”; and 18% “follicle, polyoocytic.”

Polyovular follicles are observed in dogs, especially in younger animals,⁴⁴ and are characterized as multiple oocytes surrounded by granulosa cells within a common follicle (Figure 8A and B). Such follicles frequently undergo degeneration, but at pre- and peripubertal ages, POFs can be found and can persist into maturity.⁴⁵

Since the description of the follicle and oocyte by van Baer in 1827, the presence of MOFs and POFs has drawn the attention of many scientists. Nearly 100 years later, Hartman⁴⁶ stated for the opossum: “For this species the occurrence of polynuclear ova is the rule rather than the exception, and in some ovaries they occur by hundreds. Polyovular follicles are, moreover, often found in astounding numbers and of almost every variety yet reported for other mammals.” Two years later, Mainland⁴⁷ described POFs for the ferret, followed by an overview on the frequency of POFs in different mammals by Telfer and Gosden⁴⁸ in 1987. While mice, rats, sheep, and

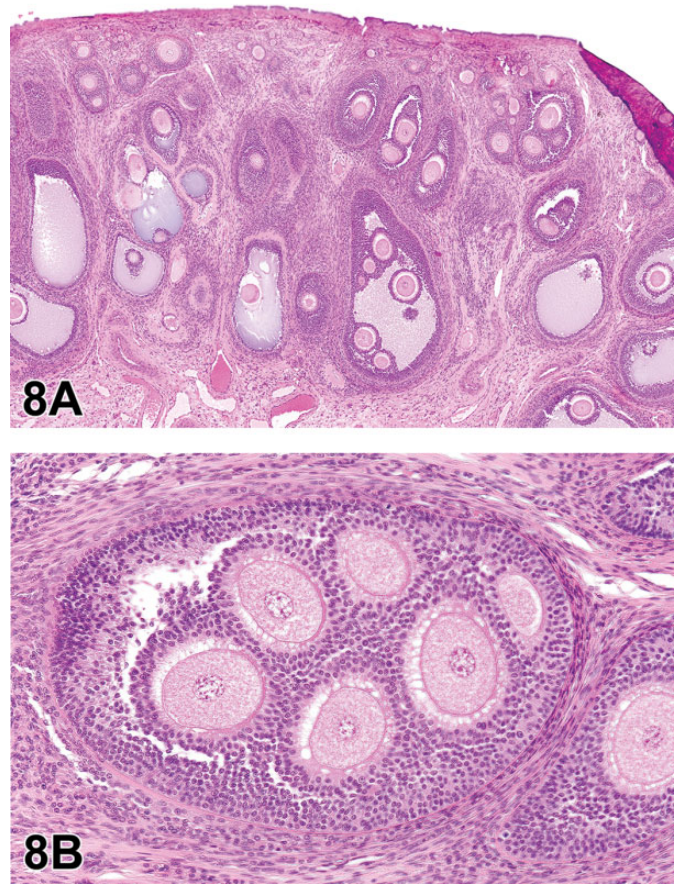


Figure 8. Polyovular follicles in beagle dogs (A-B). A, An ovary of a young untreated beagle dog with multiple polyovular follicles containing up to 6 intact ova. B, A high magnification of a polyovular follicle from a second dog showing that each ovum is surrounded by granulosa cells.

marmosets show less than 0.1% of growing follicles containing multiple oocytes, follicles with 2 oocytes are seen in 0.91% of rabbits, 1.49% of rhesus monkeys, and 2.72% of humans; follicles containing 3 oocytes are observed occasionally in humans (0.2%) and rhesus monkeys (0.3%). In the investigated cat ovaries, 3.61% had 2 and 0.45% had 3 oocytes per follicle. In the investigated collective of dogs, 8.89% showed follicles with 2 oocytes, 2.97% had 3, and 2.08% had 4 or more oocytes visible in one common follicle. More recent investigations showed that 68.4% of prepubertal and 62.2% of dogs under 1 year had POFs, but the number decreased with age as only 30.4% animals aged 7 to 8 years had such findings.⁴⁹ These authors also found that POFs are seen twice as much in mongrels than in pure breeds. Sato et al also list POFs among the spontaneous findings seen in beagles.⁵⁰ Age-related differences in POFs are also known for pigs.⁵¹

Polyovular follicles occur with a low frequency in mice and rats, though there may be some slight differences among the various strains.¹⁰ In rodents, folliculogenesis begins soon after birth and is accompanied by programmed oocyte death and

germ cell loss. In mice, neonatal exposure to the synthetic estrogen diethylstilbestrol induces POFs, which contain 2 or more oocytes per ovarian follicle. This has been attributed to estrogenic dysregulation of genes involved in the breakdown of germ cell cysts during the formation of primordial follicles.⁵² However, mouse lines selected for high fecundity also show a higher occurrence of POFs without being exposed to estrogens.⁵³

Dr Rinke then showed an example of a 13-week study in dogs in which increased numbers of POFs were observed in 1 mid- and 2 high-dose group animals and asked the audience whether a treatment effect should be assumed. Afterward, he showed results from an evaluation that his former colleague, Dr Christine Ruehl-Fehlert from Bayer AG, had done in another 13-week study in which she counted the follicles with multiple oocytes from a control and a high-dose animal. As a prerequisite, one H&E section from the both ovaries was taken. Only large primary, secondary, and tertiary follicles were counted, and at least 1 oocyte in the POFs was supposed to have a clear nucleus. Her results showed that POFs with 4 or more oocytes were quite frequent and that there was no obvious difference between the control and treated dogs. Based on these explanations, Dr Rinke requested a vote. No one had the opinion that the presence of POFs represents an adverse finding that has to be recorded and reported; 28% thought it is a recordable non-adverse finding, while 18% regarded it as a potentially adverse finding; 15% voted for a normal variance in (young) dogs that does not need to be recorded, while 36% said that this normal variance should be recorded; and only 4% still had no opinion.

As a take-home message Dr Rinke pointed out that folliculogenesis covers sequential steps in the development of a follicle, from primordial to preovulatory. Most of the time one follicle contains a single oocyte, but some follicles are polyovular in that they contain several oocytes surrounded by granulosa cells. The origin of the alteration is still unknown; failure of germ cell breakdown during early stages of folliculogenesis is proposed. The developmental rate might be faster than the differentiation of surrounding somatic cells, resulting in the inclusion of several germ cells in one follicle. Polyovular follicles are a normal feature in young dogs; they are seen less frequently in older animals but still occur. Importantly, the normal variation per species, strain, and age should be considered for each study.

Dr Rinke opened the discussion by asking the audience about their experience with this finding and if they had been asked by regulators about the significance of the finding in cases of skewed incidences. Finally, he wanted to know how to deal with the term for the INHAND nonrodent manuscripts. From the voting results and following discussions, it became clear that the finding of POFs in dogs should be recorded in any case, and the importance of having reliable historical control data was highlighted by several contributors from the audience. Moreover, representatives of the nonrodent INHAND working groups indicated that they would prepare a precise description in their manuscripts.

Hypertrophy in the Pituitary Gland Pars Distalis in 2 NTP Studies

Dr Cynthia Willson (ILS) presented 2 cases of pituitary gland lesions in the pars distalis from NTP studies. Dr Willson acknowledges scientific contributions from Drs Kyathanahalli Janardhan (ILS), Anika Dzierlenga (NTP), Chad Blystone (NTP), Cynthia Shackelford (EPL), Gabrielle Willson (EPL), Anthony Skowronek (Batelle Memorial Institute), and Mark Cesta (NTP). Heather Jensen (NIEHS) and Natasha Clayton (NIEHS) are acknowledged for their assistance with histology and IHC.

The first case was of a pituitary gland from an adult male Hsd:Sprague Dawley SD rat from a 2-year NTP carcinogenicity bioassay, which included perinatal exposure (beginning in utero on gestation day 6, then via dam's milk, then via dosed feed throughout life) to a phthalate currently in the review process (Figure 9A-F). At low magnification, the pars distalis of the treated animal in case 1 showed scattered pale cells (Figure 9B and D) when compared with the control (Figure 9A and C). At higher magnification, the pale cells were seen to be enlarged compared to surrounding endocrine cells, with abundant, pale eosinophilic cytoplasm (compare Figure 9C and D). Many of the enlarged cells also contained vacuoles—either finely vacuolated throughout, with low numbers of large vacuoles, or with a single large vacuole that peripheralized the nucleus (“signet ring” cells; Figure 9D). The voting choices and results for the pars distalis lesion were as follows: hyperplasia (0%), hypertrophy (11%), vacuolation (10%), cytoplasmic alteration (16%), cytoplasmic alteration and hyperplasia (22%), cytoplasmic alteration and vacuolation (16%), hyperplasia and vacuolation (8%), hypertrophy and vacuolation (16%), or other (2%). The original diagnosis by the study pathologist was pars distalis cytoplasmic alteration. The PWG diagnosis for the lesion was pars distalis hypertrophy.

The second case presented was of a pituitary gland from an adult male Fischer 344/N rat from a 13-week feed study of ethylene thiourea. Similar to case 1, enlarged endocrine cells were scattered throughout the pars distalis; many had finely vacuolated cytoplasm (controls Figure 9G and I compared to treated Figure 9H and J). For the second case, the voting choices and results were as follows: hyperplasia (0%), hypertrophy (9%), vacuolation (9%), cytoplasmic alteration (7%), cytoplasmic alteration and hyperplasia (13%), cytoplasmic alteration and vacuolation (25%), hyperplasia and vacuolation (6%), hypertrophy and vacuolation (31%), or other (0%). The second case was from a study reported in an NTP technical report in 1992, and the diagnosis made at that time was pars distalis cellular vacuolization.⁵⁴

After the cases were presented, Dr Willson discussed the criteria used for pars distalis hypertrophy, which were in accordance with the INHAND guidelines.² The INHAND guidelines for the endocrine system additionally include the potential diagnoses of pars distalis vacuolation as well as the combination diagnosis of pars distalis hypertrophy and vacuolation.

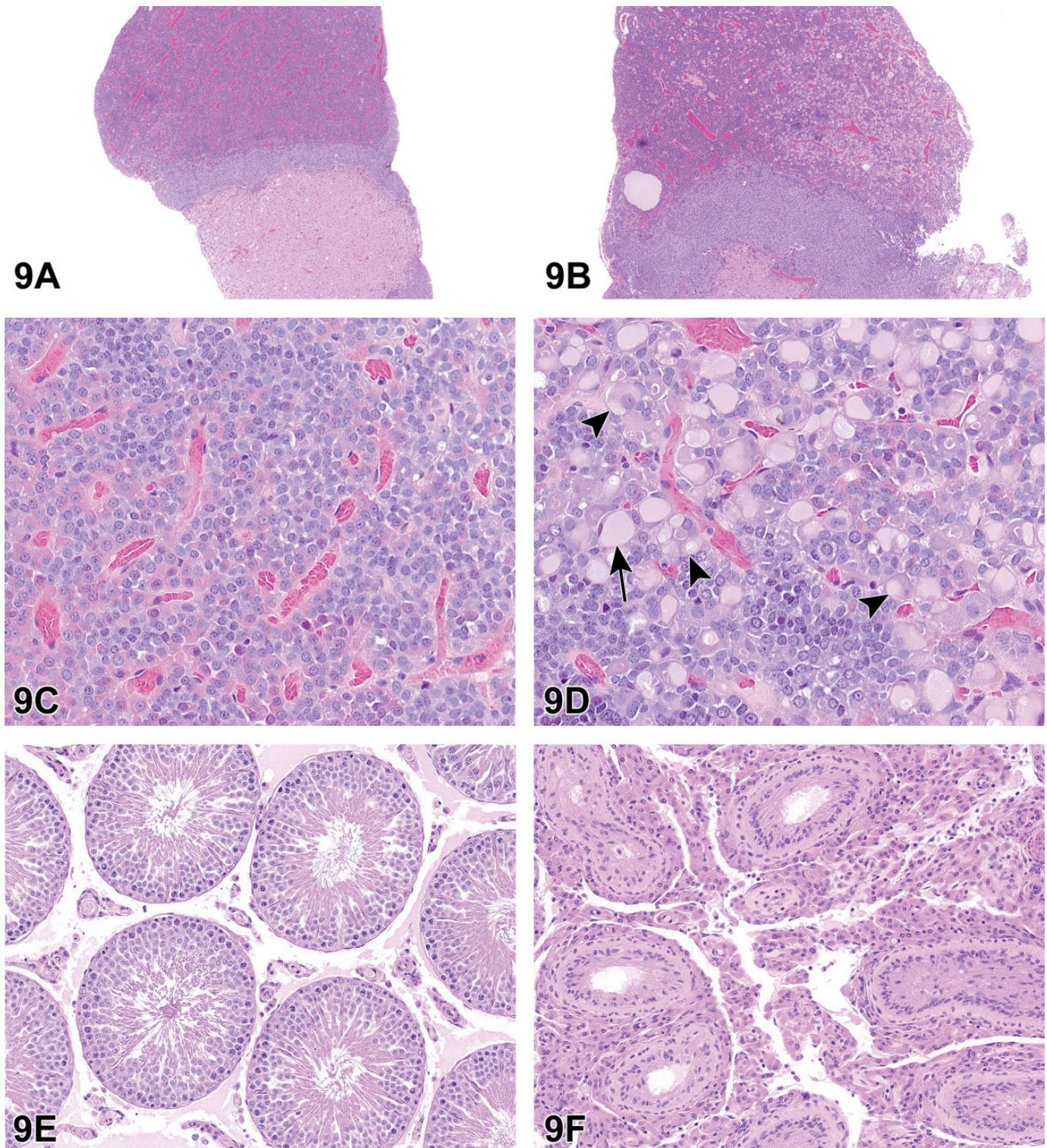


Figure 9. Hypertrophy of pars distalis endocrine cells from an adult male Hsd:Sprague Dawley SD rat from a 2-year National Toxicology Program perinatal chronic bioassay presented as case 1 (A-F). At low magnification (B, original objective $\times 4$), there are numerous pale-staining cells scattered throughout the pars distalis in the pituitary gland from a male rat exposed to the highest dose of a phthalate, when compared to a control male rat (A). At high magnification (D, original magnification $\times 40$), the pale-staining cells are enlarged with expanded cytoplasm, some are finely vacuolated, some have large vacuoles that do not peripheralize the nuclei (arrowheads), and some have a single large vacuole that peripheralizes the nucleus ("signet ring" cells; arrow), when compared to a control (C). The treated animal with pars distalis hypertrophy in (B) and (D) had testicular lesions, including atrophy and Leydig cell hyperplasia (F, compare to control rat in E). Hypertrophy of pars distalis endocrine cells from an adult male Fischer 344/N rat from a 13-week National Toxicology Program study presented as case 2 (G-L). The rat

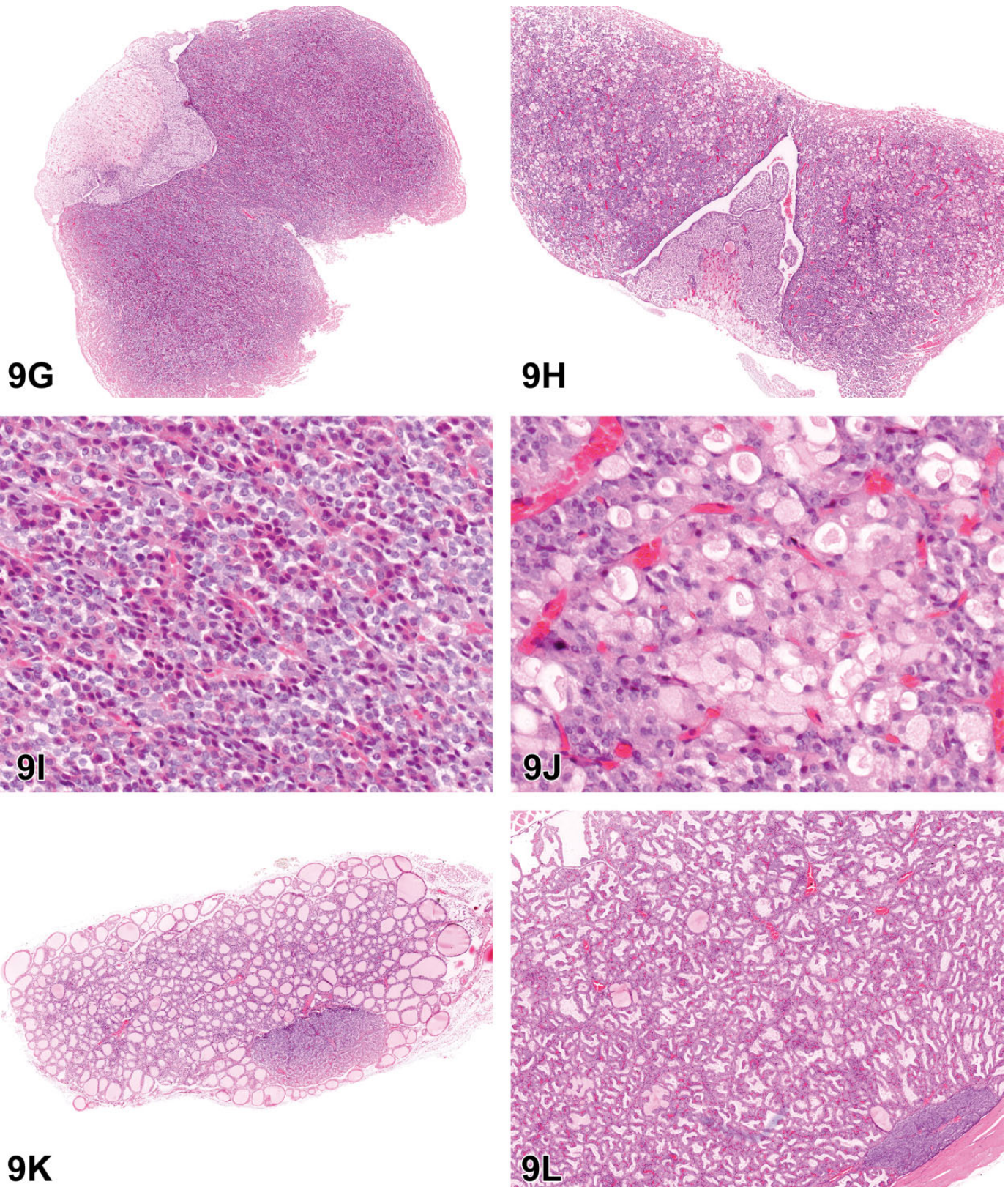


Figure 9. (continued). treated with ethylene thiourea (H, J) had enlarged endocrine cells scattered throughout the pars distalis (compared to a corresponding control rat G, I). These cells had pale cytoplasm that was frequently finely vacuolated (H, J). When compared to control animals at the same magnification, there were increased incidences of diffuse follicular cell hyperplasia in the thyroid glands of ethylene thiourea-treated rats (L, compared to control rat in K).

Although some of the enlarged endocrine cells also had finely vacuolated cytoplasm or a few to one large vacuole(s), sometimes peripheralizing the nucleus (“signet ring cells”), the NTP has elected to use the single diagnosis of “pituitary gland, pars distalis—hypertrophy” for this lesion in case 1. This would have been the contemporary preferred diagnosis for case 2. The rationale for this is that the change uniformly seen in the endocrine cells is enlargement and that not all contained vacuoles. Any associated vacuolation is to be described in the pathology narrative. Moreover, the use of a single diagnosis of “hypertrophy” aids in consistency within and across studies.

The development of enlarged “signet ring” or “gonadectomy” cells after castration in the rat has been well described.⁵⁵ Following surgical ablation, disease, or toxicity of a target organ (eg, testis, thyroid gland, or adrenal gland), there is a decrease in hormone production by that target organ. The decrease in hormone production triggers degranulation by the corresponding population of pars distalis endocrine cells, leading to the rapid release of storage granules of the trophic hormone. Soon after, the single cell population of endocrine cells undergoes cell enlargement (hypertrophy) due to cytoplasmic expansion and increased rough endoplasmic reticulum (RER). If the insult is chronic (eg, weeks to months after castration), the expanded cytoplasm of some or all cells can become vacuolated. This is seen ultrastructurally in rodents after castration as increased numbers of dilated cisternae of RER.⁵⁶ If the decrease in target organ hormone production continues in some cells, multiple vacuoles may coalesce, forming a single large vacuole that displaces the nucleus peripherally (ie, “signet ring,” “gonadectomy,” “thyroidectomy,” or “adrenalectomy” cells). This is seen ultrastructurally as the coalescence of cisternae of RER into one large dilated cisterna.⁵⁶

These changes (hypertrophy, vacuolation) may or may not be followed by increased cell numbers of the endocrine cell population (hyperplasia). Hyperplasia can be difficult to diagnose because basophils or acidophils may appear chromophobic on H&E staining when they are degranulated or actively synthesizing hormones. Moreover, endocrine cell populations of the pars distalis may have scattered distributions; there is a wide range of normal, and there is variation in numbers of different endocrine cell populations due to variation in staining, level of sectioning, age, sex, parity, and even stage of estrous cycle.

The lesion of pars distalis hypertrophy is one of the common responses of the pituitary gland in toxicity studies when there is disruption in hormone synthesis in gonads or endocrine organs. Hypertrophy of pituitary endocrine cells reflects a disruption in the hypothalamus–pituitary–end organ axis. Phthalates, the agent in case 1, have been shown to decrease testosterone production by Leydig cells. This causes a decrease in the normal negative feedback of testosterone on the hypothalamus–pituitary–gonad axis, leading to increased gonadotropin-releasing hormone release by the hypothalamus and, subsequently, increased luteinizing hormone and follicle-stimulating hormone release by gonadotrophs in the pars distalis of the pituitary gland. The population of endocrine cells

can be identified using IHC for secretory hormones or it can be inferred based on the peripheral tissues affected. In case 1, in utero phthalate exposure was also associated with lesions consistent with decreased androgen tone in the male reproductive system, suggesting that the hypertrophied endocrine cells in case 1 are gonadotrophs. Grossly, these organs were noted as small in exposed animals: testes, epididymides, prostate glands, and seminal vesicles. Histologically, pars distalis hypertrophy (Figure 9B and D) was associated with testicular atrophy (Figure 9F), testicular Leydig cell hyperplasia (Figure 9F), epididymal hypospermia, and decreased secretory fluid in the prostate glands and seminal vesicles.

In case 2 (Figure 9G-L), exposure to ethylene thiourea resulted in enlargement of endocrine cells of the pars distalis and proliferative lesions of the thyroid gland (Figure 9G-L). The hypertrophied cells of the pars distalis of the pituitary gland in case 2 (Figure 9H and J) were seen in conjunction with thyroid follicular cell hyperplasia (both diffuse [Figure 9L] and focal) and follicular cell adenomas in the 13-week study.⁵⁴ Ethylene thiourea accumulates in the thyroid gland where it interferes with thyroid peroxidase, thereby leading to decreased production of the thyroid hormones T3 and T4. Based on the lesions in the thyroid gland, the enlarged pars distalis endocrine cells in case 2 are likely thyrotrophs. Decreased thyroid hormone production causes a decrease in the normal negative feedback of thyroid hormones on the hypothalamus–pituitary–thyroid axis, leading to increased thyrotropin-releasing hormone release by the hypothalamus. This subsequently leads to thyrotroph hypertrophy and increased thyroid-stimulating hormone (TSH) release, with prolonged stimulation of the thyroid by TSH leading to thyroid follicular hyperplasia and tumors. Case 2 was from a 13-week study, but in the companion 2-year bioassay, which included thyroid hormone measurements, there were treatment-related increases in thyroid follicular cell neoplasms, follicular cell hyperplasia, decreased T3 and T4 in rats, and increased TSH in rats and mice.⁵⁴

Dr Willson finished with some epidemiological data about ethylene thiourea exposure in humans. Ethylene thiourea is found in the environment primarily as a degradation product of heavily used ethylene bis-dithiocarbamate (EBDC) fungicides. There is some evidence for potential thyroid disruption in humans who are exposed in occupational settings. For example, in the Agricultural Health Study, a large prospective study of the health of farmers and their families in North Carolina and Iowa, the spouses of farmers who apply EBDC fungicides had an increased risk of thyroid gland dysfunction. This was seen as an increased risk of either clinically diagnosed hypothyroidism or hyperthyroidism.^{57,58}

The intent of presenting these 2 cases was to highlight that a morphologically similar microscopic lesion in the pituitary gland pars distalis can have different causes. These pituitary gland endocrine cell lesions can be useful for interpretation of other histopathological or clinicopathological changes in a study.

Blood Smear Contaminant

Dr Greg Travlos (NIEHS) presented one case of a Romanowsky-stained blood smear of a mouse. For this case, the animal was a 4-month-old male C57BL/6 mouse that had been genetically modified with a double knockout of a fibroblast-specific gene. The animal had been presented as “sick” to the clinical veterinary staff of the Comparative Medicine Branch at the NIEHS, and an EDTA whole blood sample was collected for a complete blood count analysis and blood smear preparation. During evaluation of the blood smear, an object was noted and several images of various magnifications were captured. Since the majority of symposium attendees do not typically evaluate blood smears, this exercise was meant to be novel as well as to provide a brief review of artifacts that may be present on a blood film.

For this case, low-, mid- and high-magnification images were shown to the audience. Since it depicted the most distinguishing features of the structure of interest, only the high magnification image was presented for review prior to voting. The case for voting consisted of a Romanowsky-stained blood smear containing a single, thin, basophilic, coiled structure (Figure 10). The structure appeared to be enclosed in a clear capsule. The voting choices and results were as follows: hemoparasite in blood (9%), microfilarial microorganism (54%), *Borrelia* sp. microorganism (4%), *Candida* sp. microorganism (7%), Trypanosomal microorganism (9%), *Enterobacter* sp. microorganism (0%), *Plasmodium* sp. male microgamete (5%), and other (12%). The overwhelming selection (ie, microfilarial microorganism at 54%) by the voting audience was incorrect. The most appropriate selection would have been “other,” which was selected by 12% of the voters. The voting choice was subsequently expanded to describe that “other” was a contaminant that appeared as a presumptive fungal spore (ie, conidia of a helicosporous hyphomycete).

Fungal spores are an incidental contamination artifact that can occur during preparation of blood smears through air or staining solutions and have been erroneously identified as a microfilaria.⁵⁹⁻⁶² There are several genera of helicosporous hyphomycetes (eg, *Helicomycetes*, *Helicosporium*, *Helicoma*, *Helicoön*, *Moorella*, *Spirosphaera*)^{62,63}; they are saprobic fungi that survive on decaying wood, leaves, or plant material and thrive in moist places or around water. They produce various forms of coiled 2- or 3-dimensional conidia, and it is the conidia that can contaminate a blood smear, thereby resulting in a diagnostic dilemma. As noted above, fungal spores have been mistakenly identified as microfilariae, and there have been reports that described them as a new species of nematode (eg, *Sergentella* spiroides).^{64,65}

As part of the general features,⁶⁰⁻⁶² these fungal spores are less than 100 μm in length and can vary from 1 to 2 μm in thickness. These organisms are usually coiled and typically form approximately 1.5 to 3 coils; conidia presented as thread forms or atypical helical shapes, however, can occur.⁶⁰ The inner structure contains variable areas of darkly

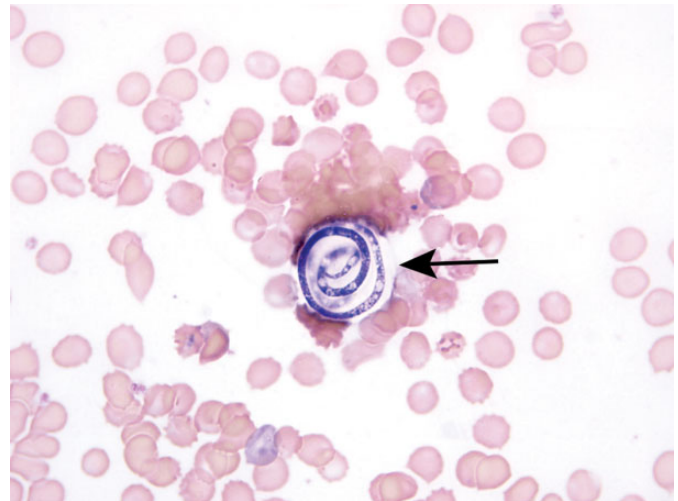


Figure 10. An example of a fungal spore that is an incidental contamination artifact of peripheral blood smears that can occur with air or staining solutions. This smear shows a single, encapsulated (arrow), coiled structure consistent with a fungal spore (ie, the conidia of a helicosporous hyphomycete).

basophilic stained and unstained material, and no organization is observed internally. In contrast, microfilariae differ from *Helicosporium*-type conidia by being larger in size (3-10 μm \times 163-315 μm) and a well-defined internal organization has been characterized.⁶⁶ In fact, size alone would preclude fungal spores from being considered as microfilariae. Since erythrocytes are wider (4-7 μm mouse; 6-8 μm human) than the thickness of a conidia, erythrocyte diameter can act as a reasonable arbiter of a width size comparison for determining a *Helicosporium*-type spore versus a microfilaria. Furthermore, individual microfilariae are typically presented on a blood smear in a serpentine-type shape versus the characteristically coiled shape of the fungal spore. While some microfilariae are sheathed, fungal spores are not, though they may be encapsulated (Figure 10). Once a fungal spore is observed on a stained blood smear, attempts to repeat the finding on subsequent blood smears routinely do not yield additional blood smears with spores.

In addition to fungal spores, a variety of other potential sources of blood smear contamination/artifact was discussed. Other potential sources presented included hairs, fibers, stain precipitate, bacteria, endothelial cells, and sporozoan microgametes. Some basic features regarding these additional sources of blood smear contamination were presented, and salient features are found in the attached references: hairs and fibers,^{67,68} stain precipitate,⁶⁹ bacteria,^{70,71} endothelial cells,⁷²⁻⁷⁴ and sporozoan microgametes.⁷⁵⁻⁷⁸ In summary, the take-home message regarding the spores of helicosporous fungi is that they are air-borne or water-based contaminants in laboratories and they may be mistaken for microfilariae in stained blood smears.

Beyond the Spectrum of Chronic Progressive Nephropathy

Dr Erin M. Quist (EPL) presented several interesting cases recently reviewed by a PWG conducted at the NTP/NIEHS. The presented cases featured lesions from 3 different male B6C3F1 mice that were part of a 2-year toxicity/carcinogenicity study in which Dr Allen W. Singer (Battelle Columbus) was the study pathologist and Dr Quist was the QA pathologist.

For cases 1 to 3, a series of photomicrographs were presented to the audience that included both low- and high-power magnifications of a spectrum of kidney lesions from the 2-year study (Figure 11A-F). Dr Quist informed the audience that there would be 2 rounds of voting for each case. The same list of voting options would be presented in both rounds, but the answers would not be revealed until the second round of voting. The voting choices and results for round 1 are presented in Table 5.

After the first round of voting was complete, Dr Quist provided a brief overview on chronic progressive nephropathy (CPN) in rodents, including a detailed summary of the spectrum of renal lesions that may present as a component of CPN or as stand-alone diagnoses independent of CPN. Chronic progressive nephropathy is a common, spontaneous lesion of aged rodents. Most of the physiological factors we attribute to development of CPN are derived from information about the rat, as CPN is not as well characterized in the mouse. Physiological factors associated with CPN include age (increased severity with increasing age), sex (more common in males), high protein diet or caloric intake, strain (most common in B6C3F1 mice, Sprague Dawley, and Fischer rats), endocrine, and immunological factors.⁷⁹⁻⁸¹

According to the INHAND criteria, 3 characteristic features should be present for the diagnosis of CPN. These include tubular basophilia, nuclear crowding with or without the presence of simple tubular hyperplasia, and thickened basement membranes.⁸¹ Additional renal lesions that may present as a component of CPN or as independent processes in the absence of thickened basement membranes are indicated in Table 6.

The audience was presented with the cases once again for the second round of voting. Case 1 (Figure 11A, C, E), provided an example of classic end-stage CPN. The kidney was markedly shrunken and fibrotic with a lumpy, undulating capsular surface (Figure 11A). Higher magnification images depicted examples of hyaline casts, interstitial fibrosis, glomerulosclerosis, thickened basement membranes, tubular hypertrophy, tubular degeneration, inflammatory infiltrates and pigment (Figure 11C and E). However, in case 2 (Figure 11B, D, F), the tubular changes appear distinct from those of the classic CPN presented in case 1. On subgross examination, the kidney is not shrunken or fibrotic, rather the cortex is diffusely highlighted by profound basophilia (Figure 11B). On higher magnification, the interstitium is scant and compressed by wall-to-wall basophilic tubules (Figure 11D). In addition, renal tubules exhibit variable hyperplasia, hypertrophy, degeneration, regeneration, karyomegaly,

and increased mitoses without the appearance of thickened basement membranes. The PWG determined that the preferred terminology to characterize the changes in case 2 was “renal tubule—regeneration.”

Results from the second vote demonstrate that Dr Quist was able to successfully convince the majority of audience members to select the preferred diagnostic term of CPN for cases 1 and 2; however, case 3 remained a diagnostic challenge for many of the voting participants (Table 7).

Dr Quist expected some dissention among the audience given that the PWG participants had experienced similar difficulties during their review. She explained that the term “renal tubule—regeneration” was ultimately selected by the PWG as the preferred terminology for the lesions in cases 2 and 3 based on several factors: (1) to distinguish a treatment-related effect from spontaneous CPN, (2) to maintain consistency across studies (this lesion had been observed in both rats and mice in the 13-week and 2-year studies), and (3) to denote progression of a lesion first identified in the 13-week studies. For this study, “renal tubule—regeneration” was characterized by increased cytoplasmic basophilia, karyomegaly, hypertrophy, hyperplasia, degeneration and increased mitoses, and as with CPN, the incidence of “renal tubule—regeneration” was much higher in males than females. Dr Quist concluded her presentation by agreeing that renal tubular lesions are often difficult to diagnose because a constellation of findings may be present with overlapping morphologies between spontaneous (CPN) and treatment-related disease. As pathologists, it's important to distinguish treatment-related lesions from spontaneous change, but it's not always possible to find terminology that can capture both the morphology of a lesion and the suspected disease process.

One audience member asked Dr Quist why the males appeared to be more affected than the females for this study. She added that upon further review, the tubular lesion had been localized to the proximal convoluted tubule and recalled that male and female mice have different transporter (eg, organic anion transporter, OAT) gene expression in the kidney; this sexual dimorphism in *OAT* gene expression may be associated with differences in the excretion or absorption of the study compound.

The author would like to thank Drs Amy Brix (EPL) and Karen Cimon (EPL) for their assistance and Emily Singletary (EPL) for photographic editing and support.

Granularity Matters for the Diagnosis of Neoplasms

Dr Kyathanahalli Janardhan (ILS) presented 3 cases to demonstrate how sometimes the diagnosis of tumors based solely on H&E-stained sections can be less accurate and how accuracy can be improved using immunohistochemical markers.

The first case was from a F344/N female rat which was part of an NTP 2-year dosed water carcinogenesis bioassay. The rat was on test for 729 days before being terminally euthanized. Grossly, there was a mass in the right kidney and a mass in the

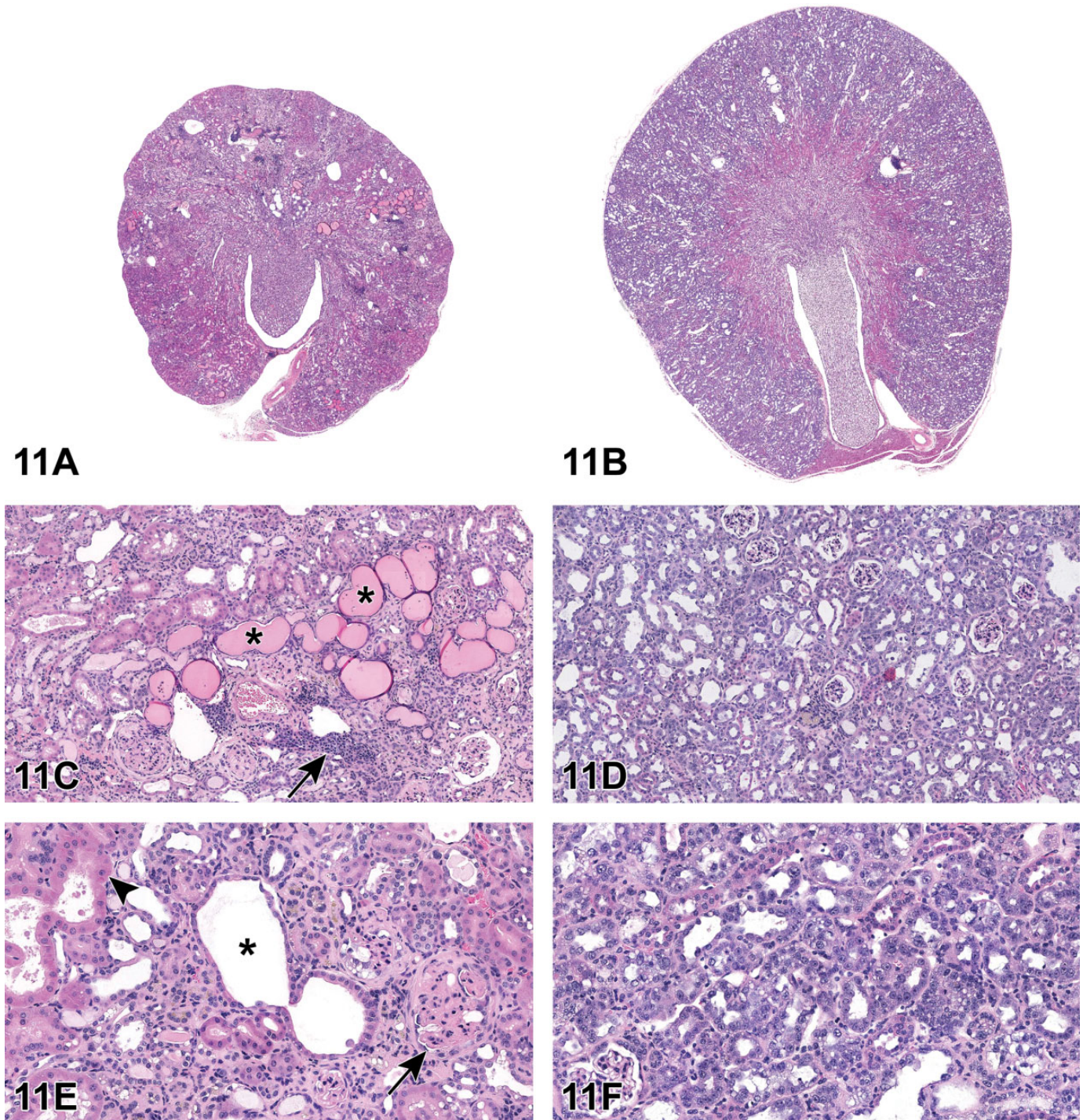


Figure 11. Selected renal lesions (A-F) from a 2-year National Toxicology Program study in B6C3F1 mice presented as cases 1 and 2. Case 1, Chronic progressive nephropathy (CPN; A, C, E). A, End-stage CPN characterized by a shrunken, fibrotic kidney with an undulating capsular surface. C, Chronic progressive nephropathy features include hyaline casts (asterisks), interstitial fibrosis, glomerulosclerosis, tubular hypertrophy, and hyperplasia, as well as inflammatory infiltrates (arrow) and pigment. E, Higher magnification of areas of interstitial fibrosis and glomerulosclerosis (arrow), tubular dilation (asterisk), tubular degeneration, and hypertrophy (arrowhead). Case 2, Renal tubule—regeneration (B, D, F). B, Renal cortex is diffusely highlighted by increased basophilia. D, Within the cortex, the interstitium is compressed by wall-to-wall basophilic tubules. F, Higher magnification reveals additional features of karyomegaly, hypertrophy, and hyperplasia as well as regeneration and increased mitoses. Fibrotic changes are notably absent as well as prominent thickened membranes.

Table 5. Voting Results for Cases 1-3: Round 1.

Voting Choice	Case 1	Case 2	Case 3
Renal tubule, cytoplasmic alteration	1%	1%	1%
Renal tubule, degeneration	7%	9%	1%
Renal tubule, regeneration	1%	25%	17%
Renal tubule, basophilia	1%	22%	57%
Renal tubule, hyperplasia	2%	7%	5%
Renal tubule, atypia cellular	1%	12%	3%
Renal tubule, hyperplasia—atypical	0%	19%	6%
Chronic progressive nephropathy (CPN)	86%	3%	10%
Other	2%	2%	0%

Table 6. Additional Renal Lesions That May Present as a Component of CPN or as Independent Processes in the Absence of Thickened Basement Membranes.^{1,81}

Renal tubule, basophilia	<ul style="list-style-type: none"> • Basophilic cytoplasm • No thickening of basement membranes • Cells may appear swollen or plump • Increased nuclear:cytoplasmic ratio • Increased mitoses
Renal tubule, regeneration	<ul style="list-style-type: none"> • Basophilic cytoplasm • No thickening of basement membranes • Flattened epithelium to low cuboidal cells • Karyomegaly • High mitotic index
Renal tubule, simple tubular hyperplasia	<ul style="list-style-type: none"> • Basophilic cytoplasm • No thickening of basement membranes • Nuclear crowding • Increased cell number • Cells do not extend into the lumen beyond a single layer
Renal tubule, vacuolation	<ul style="list-style-type: none"> • Discrete, clear cytoplasmic vacuoles (macro or micro) • No thickening of basement membranes • Pale, granular, or swollen cytoplasm
Renal tubule, degeneration	<ul style="list-style-type: none"> • Cytoplasmic vacuolation • No thickening of basement membranes • Tinctorial change (eg, basophilia) may be present • Cell blebbing or sloughing
Renal tubule, dilation	<ul style="list-style-type: none"> • Luminal expansion • No thickening of basement membranes • Normal or flattened epithelium • May contain casts, cellular debris, or inflammatory cells
Renal tubule, atypical hyperplasia	<ul style="list-style-type: none"> • Solid tubular profiles encircled by connective tissue • No thickening of basement membranes • Occurrence is solitary • No compression of adjacent parenchyma
Renal tubule, hypertrophy	<ul style="list-style-type: none"> • Increase in cell size (without increase in cell number) • No thickening of basement membranes • Brightly eosinophilic cytoplasm • Apical nuclei

Table 7. Voting Results for Cases 1-3: Round 2.

Voting Choice	Case 1	Case 2	Case 3
Renal tubule, cytoplasmic alteration	0%	0%	0%
Renal tubule, degeneration	0%	7%	2%
Renal tubule, regeneration	0%	35% ^a	4% ^a
Renal tubule, basophilia	1%	11%	68%
Renal tubule, hyperplasia	0%	22%	6%
Renal tubule, atypia cellular	0%	5%	1%
Renal tubule, hyperplasia—atypical	0%	12%	4%
Chronic progressive nephropathy (CPN)	98% ^a	6%	16%
Other	1%	2%	0%

^aPreferred terminology as determined by pathology working group.

mammary gland. Three images from the H&E-stained sections of kidney mass were shown at different magnifications. The choices and voting results were as follows: granular cell tumor (31%), histiocytic sarcoma (17%), lymphoma (2%), natural killer (NK) cell tumor (7%), mast cell tumor (39%), and other (5%). Dr Janardhan agreed with the majority of the participants that it was a mast cell tumor.

The second case was from a Wistar Han female rat which was part of an NTP 2-year carcinogenesis bioassay. It was a whole-body inhalation study and the rat was on test for 586 days before being euthanized. Multiple gross lesions were present including pale bone marrow, 2 to 3 mm masses in all lobes of the lung, enlarged mesenteric and mediastinal lymph nodes, subcutaneous mass, left kidney mass, and irregular pancreas and mesentery. Four images from H&E-stained sections of subcutaneous mass were shown at different magnifications. The choices and voting results were as follows: granular cell tumor (14%), histiocytic sarcoma (37%), lymphoma (14%), NK cell tumor (9%), mast cell tumor (24%), and other (2%). Although the majority of the participants felt that it was a histiocytic sarcoma, Dr Janardhan indicated NK cell tumor as the favored diagnosis.

The third case was from a F344/N male rat which was part of an NTP 2-year carcinogenesis bioassay. It was a gavage study and the rat was on test for 714 days before being euthanized. Grossly, pancreatic and mesenteric lymph nodes were enlarged and there was a splenic mass. Three images from the H&E-stained sections of pancreatic lymph node were shown at different magnifications. The choices and voting results were as follows: granular cell tumor (11%), histiocytic sarcoma (53%), lymphoma (24%), NK cell tumor (3%), mast cell tumor (6%), and other (3%). Dr Janardhan agreed with the majority of the participants that it was a histiocytic sarcoma.

After presenting all 3 cases, Dr Janardhan presented the results of various histochemical and immunohistochemical stains to support his favored diagnosis for each case. The first case (Figure 12A-F) was originally diagnosed as a mast cell tumor and was supported by the majority of the participants. Staining with toluidine blue (TB) demonstrated the presence of metachromatic granules in the neoplastic cells, supporting the diagnosis of mast cell tumor.⁸² Although no additional staining beyond TB staining was essential, Dr Janardhan included other

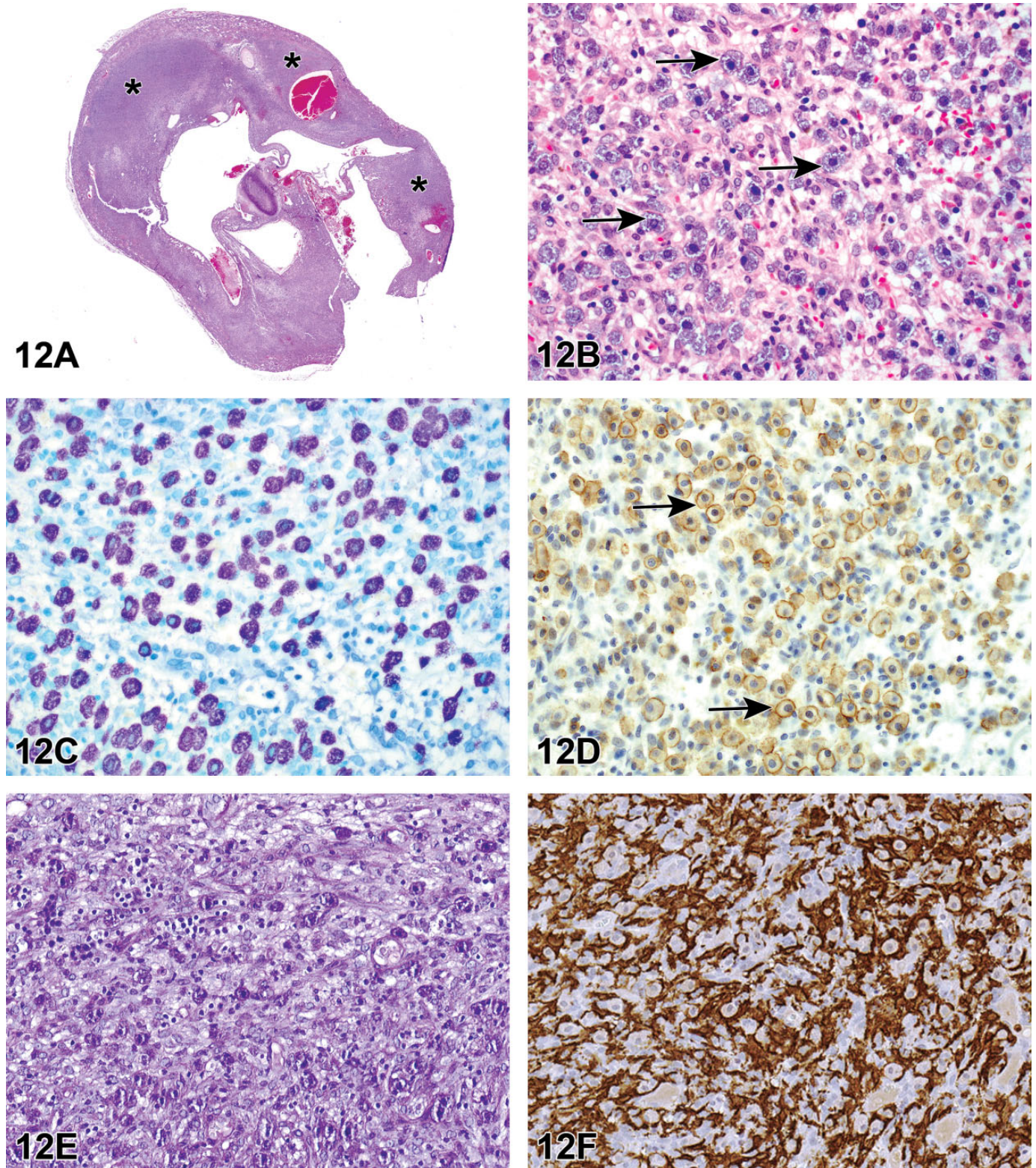


Figure 12. Mast cell tumor in a kidney of a female F344/N rat (A-F) from a National Toxicology Program 2-year carcinogenicity bioassay presented as case 1. H&E-stained section of a kidney (A) with a neoplasm (asterisks) effacing the normal architecture of the kidney. Magnified view (B) of the neoplasm shown in (A). The neoplasm has effaced the normal architecture of the kidney and is composed of round to polygonal cells containing cytoplasmic granules (arrows). Toluidine blue-stained section (C) demonstrates metachromatic granules in the neoplastic cells. Immunohistochemistry with a CKIT antibody (D) demonstrates membranous staining on the neoplastic cells (arrows). Diaminobenzidine (DAB) chromogen and hematoxylin counterstain. Periodic acid–Schiff (PAS) (E) staining shows no PAS-positive granules in the neoplastic cells. Neoplastic cells are negative for IBA1 (F), a macrophage marker. However, there are large numbers of IBA1-positive tumor-associated macrophages. DAB

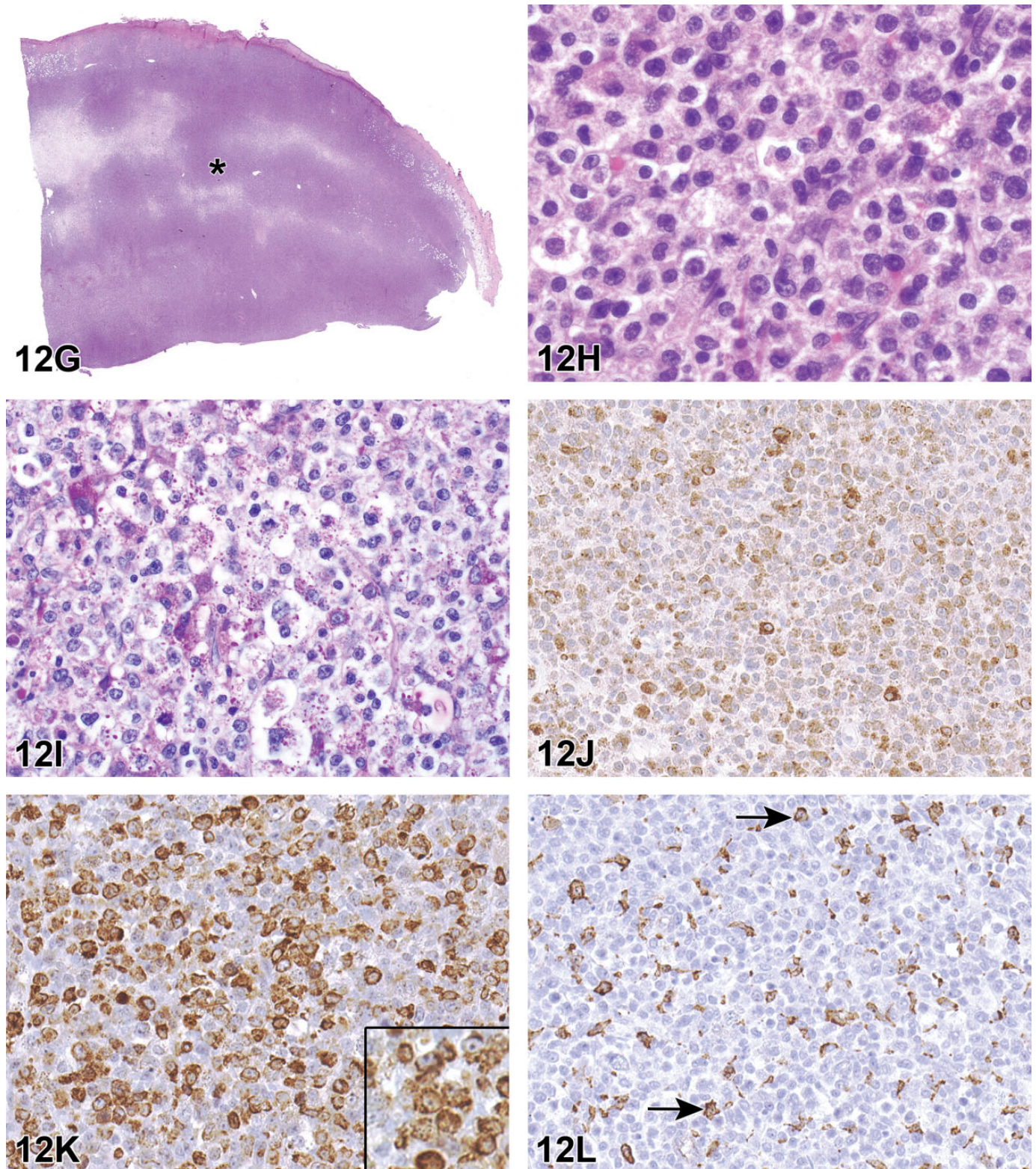


Figure 12. (continued). chromogen and hematoxylin counterstain. Natural killer (NK) cell tumor from a female Wistar Han rat (G-L) from a National Toxicology Program 2-year carcinogenesis bioassay presented as case 2. H&E-stained section (G) of a subcutaneous mass showing a very large neoplasm (asterisk). Magnified view (H) of the neoplasm shown in (G) shows large round neoplastic cells with granular cytoplasm. The PAS-stained section (I) shows PAS-positive cytoplasmic pink granules in the neoplastic cells. The neoplastic cells are diffusely positive for cytoplasmic perforin (J) and CD3 (K). Compare the cytoplasmic staining for CD3 in the inset associated with (K) to the membranous CD3 staining in the inset associated with Figure (R). The neoplastic cells in (L) are negative for IBA1 but the tumor-associated macrophages are positive (arrows). Diaminobenzidine (DAB) chromogen and hematoxylin counterstain (J, K, L). Histiocytic sarcoma from a male F344/N rat (M-R) from a National

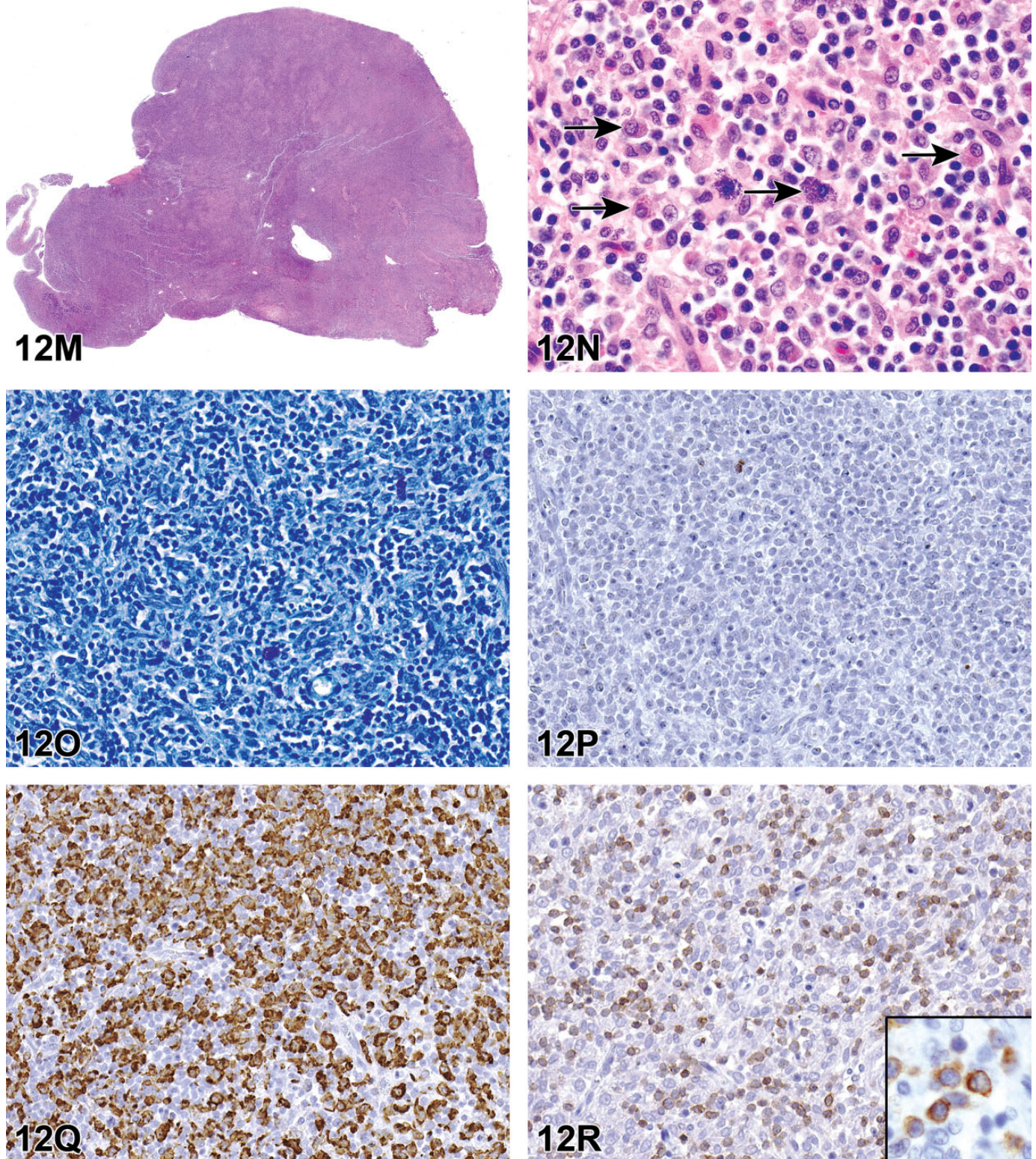


Figure 12. (continued). Toxicology Program 2-year carcinogenesis bioassay presented as case 3. Section of a pancreatic lymph node (M) which is enlarged due to the presence of a neoplasm. Magnified view (N) of the neoplasm demonstrates variably sized round to polygonal cells. Some of the cells show granules in their cytoplasm (arrows). The remnant lymphocytes are admixed with the neoplastic cells. The neoplastic cells contain no metachromatic granules in the toluidine blue–stained section (O) and are negative for perforin (P) and positive for IBA1 (Q). Most of the unstained cells in between the neoplastic cells in (Q) are remnant lymphocytes which stain for CD3 (R). The inset in (R) highlights the CD3 staining in the

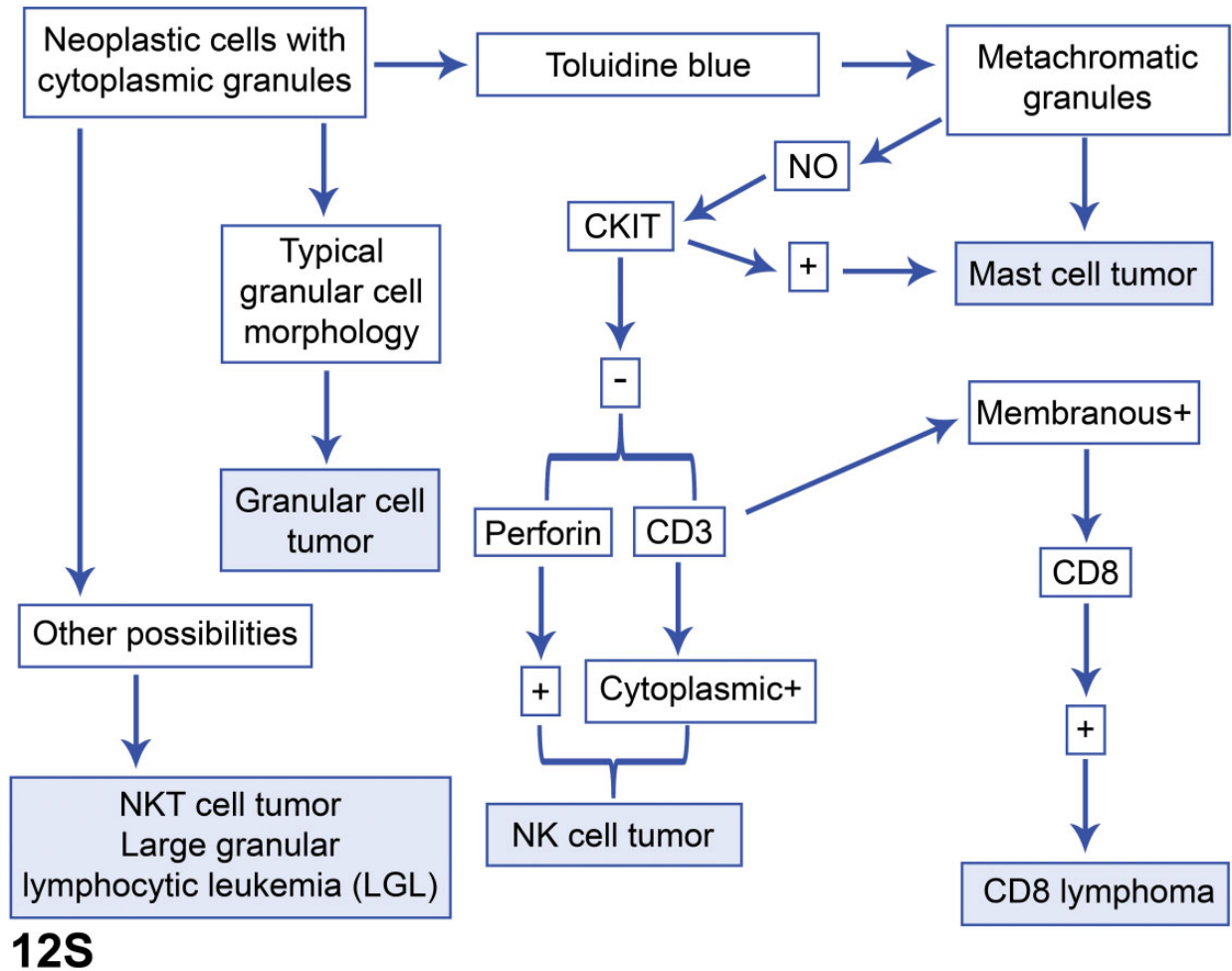


Figure 12. (continued). membrane as opposed to the cytoplasmic staining seen in the NK cell tumor (K). Diaminobenzidine chromogen and hematoxylin counterstain (Q, R). A simplified algorithm (S) for diagnosing a tumor with cytoplasmic granules in the neoplastic cells.

stains for completeness and comparison. Membranous staining for CKIT, a marker expressed by mast cells,⁸²⁻⁸⁴ was present on the neoplastic cells. The neoplastic cells did not have periodic acid-Schiff (PAS)-positive granules and no staining was observed for perforin (NK cell marker),⁸⁵ CD3 (T-cell marker),⁸⁶ and IBA1 (macrophage marker).⁸⁷ Although the neoplastic cells were not expressing IBA1, very large numbers of IBA1-positive macrophages were present in the neoplasm. Dr Janardhan highlighted the importance of being familiar with the possible presence of large numbers of macrophages in various neoplasms. He showed several images where IBA1-positive macrophages outnumbered neoplastic mast cells in some areas of the tumor.

The second case (Figure 12G-L) was originally diagnosed as “neoplasm not otherwise specified.” The majority of participants diagnosed histiocytic sarcoma. However, additional stains supported the diagnosis of NK cell tumor. The neoplasm had no metachromatic granules in TB-stained sections. Cytoplasmic granules in the neoplastic cells were PAS positive, and the cells were immunohistochemically positive for perforin and

cytoplasmic CD3 (no surface CD3 staining), and were negative for CKIT and IBA1. These features support the diagnosis of NK cell tumor.^{85,88,89} Small numbers of IBA1-positive macrophages were present between the neoplastic cells.

The third case (Figure 12M-R) was originally diagnosed as a “mast cell tumor.” The pathologist also included a tissue note indicating the presence of granules in some of the neoplastic cells; no granules were demonstrated in the TB- and PAS-stained sections. The neoplastic cells were negative for CKIT and perforin and were positive for IBA1. Remnant lymphocytes present in between the neoplastic cells had membranous staining for CD3. All these features supported the diagnosis of histiocytic sarcoma.

In the final part of the presentation, Dr Janardhan briefly discussed the individual voting choices presented for all the 3 cases, along with a few other possibilities where neoplastic cells can have cytoplasmic granules. Natural killer cells arise from common innate lymphoid progenitor cells and are one of the group 1 innate lymphoid cells. In humans, NK cells are positive for CD56 and negative for surface CD3.

Furthermore, they are classified as CD56 bright and CD56 dim cells. CD56 bright cells constitute approximately 90% of NK cells, considered to be fully mature cells, and have cytotoxic function. CD56 dim cells are considered to be immature, constitute approximately 10% of NK cells, and are involved in cytokine production and decidual angiogenesis. Cells with downregulated MHC-1 molecules are targeted by NK cells, which use their cytoplasmic cytotoxic granules containing perforin and granzyme to kill the cells.⁹⁰ Rats and mice do not express CD56.⁹¹

CD161 and Ly49s3 can be used for rats and CD27 can be used for mice as markers to understand the NK cell biology.⁹² Cells expressing features of both NK cells and T cells are referred to as NK-T cells.⁹³ These cells are recognized for their role in tumor immunity and not much information is available regarding NK-T cell neoplasms. Cytotoxic T lymphocytes are CD3⁺CD8⁺ and their cytoplasmic granules contain granzyme and perforin.⁹⁴ Numerous types of clinically relevant cytotoxic T-cell neoplasms have been described for humans.⁹⁵ The occurrence of NK cell, NK T cell, and cytotoxic T-cell neoplasms in rats are very rare. However, the true incidence rate is not known as previous studies have not attempted to subclassify the rat lymphomas in detail.

In rats, large granular lymphocytic leukemia (LGL) is another type of tumor in which cells can have cytoplasmic granules. The incidence rate in F344 rats is very high, but it is very low in other strains. The neoplasm almost always involves spleen, and the neoplastic cells are present in the vascular lumens of numerous tissues, especially the liver. Many studies have tried to understand the biology of these tumors. However, the cell of origin is not completely understood.⁹⁶⁻⁹⁸ The presentation and histological features of the NK cell tumor shown in this talk is very different from the LGL.

Mast cells arise from hematopoietic stem cells which are CD34⁺, CD117⁺, and CD13⁺.⁸⁴ Mast cells contain cytoplasmic granules which demonstrate metachromatic staining with TB staining.⁸² Mast cell neoplasms are extremely rare and only isolated cases have been reported in rats.⁹⁹ In the NTP 2-year bioassays from 1982 to the present time containing 41 238 male and 43 612 female rats, only 4 instances of mast cell tumor have been reported in males and females (2 per sex). See "Incidences of Mast Cell Tumor and Histiocytic Sarcoma in Rats in NTP Studies" for more detailed data: NTP Incidence Data.

Granular cell tumors have a typical presentation with regard to location and cell morphology. This neoplasm usually occurs in meninges or uterine/cervix tissues and contains oval, round, or polygonal neoplastic cells containing PAS-positive cytoplasmic granules. The cell of origin is not established.¹⁰

Although histiocytic sarcomas do not contain cells with granules, sometimes they can be confused for other tumors such as mast cell tumors, as in the current case (case 3). This confusion is due to the presence of some granular cells in between the neoplastic cells. Most cases involve liver, lung, spleen, subcutis, and lymph nodes. IBA1 can be used as an immunohistochemical marker to aid the diagnosis.^{87,100} The

incidence of histiocytic sarcoma is low across different strains of rats. In the NTP 2-year bioassays from 1982 to date, the incidence rate for F344/N rats is only 179 (0.4%) of 43 612 for males and 125 (0.3%) of 41 238 for females. For Hsd:Sprague Dawley SD rats, it is 4 (0.15%) of 2740 for males and 13 (0.2%) of 6758 for females, whereas for Wistar Han rats, it is 9 (0.6%) of 1500 in males and 6 (0.4%) of 1500 in females. See "Incidences of Mast Cell Tumor and Histiocytic Sarcoma in Rats in NTP Studies" for more detailed data: NTP Incidence Data .

During discussions, some of the participants wanted to know how to approach cases in which IHC highlights the presence of large numbers of macrophages or other cell types intermixed with the neoplastic cells, especially when the neoplastic cells are lower in number. Dr Janardhan opined that the histomorphology of the cells (even though they are low in number) should be relied upon to determine the cell of origin of the neoplasm. Dr Janardhan concluded the discussion by presenting an algorithm that demonstrated how to approach diagnosis of neoplasms containing cells with cytoplasmic granules (Figure 12S).

Retinal Lesions in a Rhesus Macaque (*Macaca mulatta*)

Dr George Schaaf (Wake Forest University [WFU], Winston-Salem, North Carolina) presented retinal lesions in a rhesus macaque (*Macaca mulatta*). The animal was a 10-year, 5-month-old male rhesus macaque that received a single dose of 8.05 gray whole-body irradiation at 6 years of age and was part of a cohort studying the long-term effects of radiation. Approximately 4 years prior to necropsy, the animal was diagnosed with cardiomegaly and systemic hypertension, and subsequently was diagnosed with type II diabetes mellitus, and shortly before necropsy became azotemic. The animal was euthanized due to multiple comorbidities and a poor prognosis.

The audience was shown a low-magnification photomicrograph (Figure 13A) of an H&E-stained slide of the retina highlighting diffuse edema of the inner and outer nuclear layers, as well as the presumed remains of a vessel in the nerve fiber layer, surrounded by eosinophilic debris (Figure 13B). At higher magnification, focal areas of neuronal swelling were shown in the nerve fiber layer and interpreted as cytooid bodies (Figure 13C). The audience was then shown photomicrographs of tortuous vessels in the nerve fiber layer with plump, redundant, and irregular endothelium (Figure 13D). Additionally, PAS-stained photomicrographs of damaged capillaries leaking PAS-positive material and arterioles with basement membrane splitting were shown (Figure 13E and F). The voting choices and results were as follows: degeneration of the inner and outer nuclear and plexiform layers (47%), dysplasia of the outer nuclear layer (1%), dysplasia of the inner and outer nuclear and plexiform layers (40%), atrophy of the inner and outer nuclear and plexiform layers (6%), and other (6%). The etiologic diagnosis voting choices and results were diabetic retinopathy (10%), radiation retinopathy (19%), hypertensive

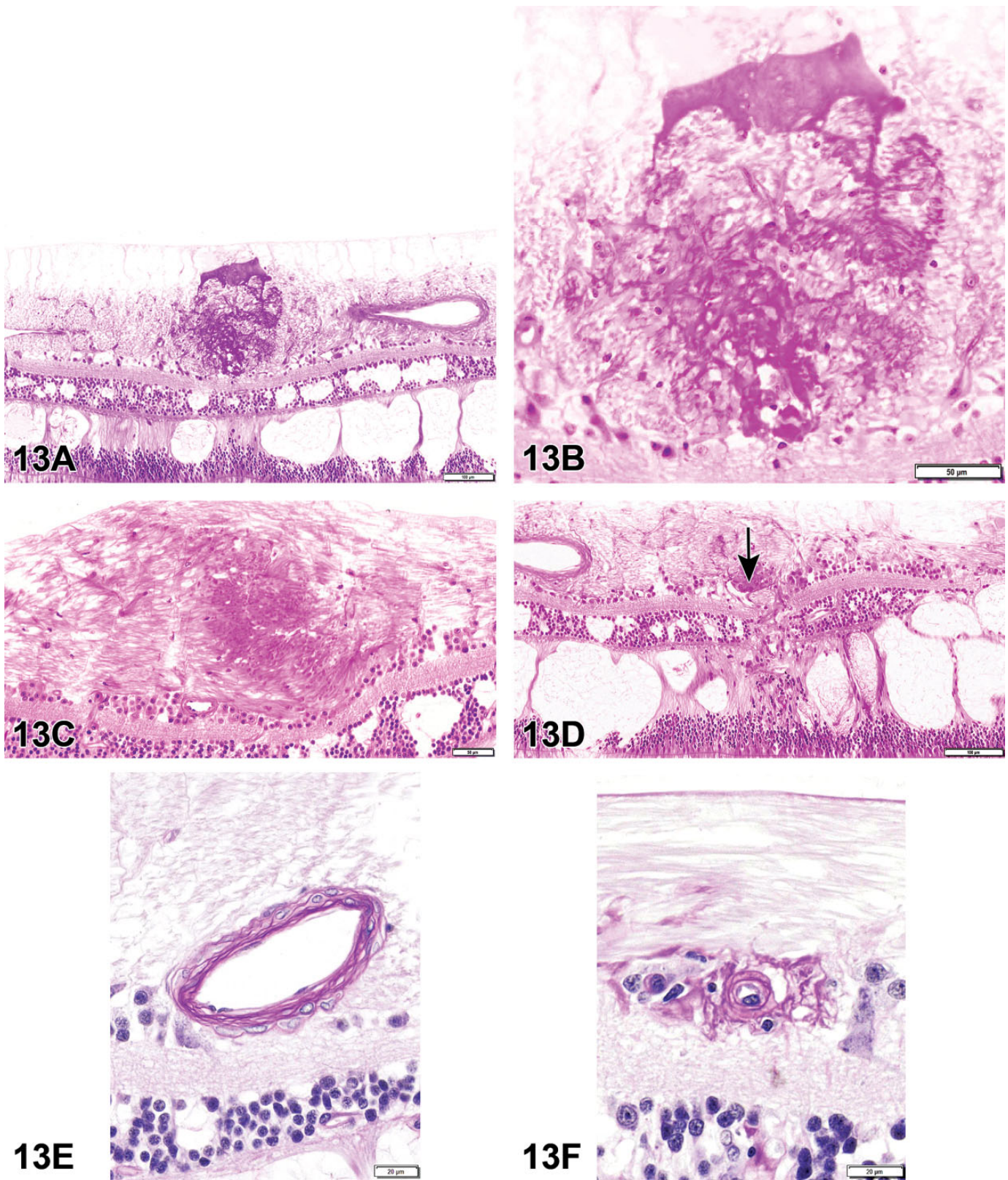


Figure 13. A-F, Retinal degeneration from a 10-year-old male rhesus macaque that received 8.05 Gy whole body irradiation and had a history of type II diabetes mellitus and systemic hypertension. The sections are stained with H&E (A-D) and periodic acid-Schiff (PAS; E and F). At low magnification stained with H&E (A), there is diffuse retinal degeneration with marked cystoid edema of the nuclear layers and the presumed remains of a damaged vessel surrounded by eosinophilic debris in the nerve fiber layer. At higher magnification (B), the destroyed vessel is seen as

retinopathy (16%), age-related macular degeneration (7%), radiation and hypertensive retinopathies (7%), diabetic, radiation, and hypertensive retinopathies (20%), all the above (17%), and other (5%).

Based on the histologic morphology, the retinal lesions were diagnosed by contributors from WFU as a diffuse retinal degeneration (inner and outer nuclear and plexiform layers) with edema, neuronal swelling (cytoid bodies), arteriolar necrosis, degeneration, and neovascularization. Based on this morphologic diagnosis and the animal's clinical history, the WFU contributors made an etiologic diagnosis of radiation and hypertensive retinopathies.

Rhesus monkeys possess a true macula and fovea and spontaneously develop type II diabetes mellitus, hypertension, and age-related macular degeneration, making them an invaluable model for the study of commonly occurring retinopathies in humans.¹⁰¹⁻¹⁰³ Radiation-induced retinopathies have been described in survivors of the Hiroshima, Nagasaki, and Chernobyl nuclear disasters, as well as patients receiving radiation therapy for head, neck, and brain tumors.¹⁰⁴

The underlying pathogenesis in diabetic, hypertensive, and radiation retinopathies remains the source of some debate but is likely related to injury of the retinal vascular endothelial cells (RVECs). Retinal vascular endothelial cells have a relatively high mitotic rate when compared to the nervous tissue of the retina, which likely predisposes them to ionizing radiation injury. The reactive oxygen species created during irradiation are also thought to play a major role in tissue injury.¹⁰⁴⁻¹⁰⁶ Prolonged hyperglycemia has been demonstrated to cause the death of pericytes, leading to a collapse of the neurovascular "support unit" that surrounds vessels in the central nervous system.^{101,107} In the cat, RVECs have been shown to be uniquely sensitive to hypertension. This is thought to be due to an exaggerated autoregulatory response that occurs in the retina as a result of systemic hypertension.¹⁰⁸ The result of all these etiologies is retinal ischemia, which leads to the development of several characteristic fundic and histopathologic lesions described below.

Cystoid macular edema has been described as a "honeycomb"-like pattern of thin pale streaks through the macula on funduscopy. It is observed as large, clear areas—generally within the outer plexiform layer—on histopathology and optical coherence tomography (OCT). It is considered a nonspecific finding, typically due to retinal ischemia.¹⁰⁹

"Cotton-wool spots" appear as fuzzy white to yellow spots on funduscopy, and histologically, they are composed of dozens of cytoid bodies, which are small circular hyper eosinophilic accumulations of intracellular constituents within the ganglion cell axons in the nerve fiber layer.¹¹⁰ On OCT, these lesions appear as dense outpouchings of the nerve fiber layer. Generally, these lesions are thought to be the result of nerve

fiber layer infarcts but can be caused by any process that disrupts axoplasmic flow (analogous to an axoplasmic "traffic jam").¹¹¹

The vascular lesions consist of plump or redundant endothelial cells that form irregular, tortuous vessels, endothelial loss of integrity and resultant leakage, basement membrane splitting, neovascularization, and eventual sclerosis. In the acute phase of injury, these are often observed both fundoscopically and histologically as focal hemorrhage which progresses to vessel dropout and subsequent regional ischemia.¹⁰⁷ Similar microvascular lesions have been observed in the brains of rhesus monkeys receiving 40 gray of fractionated whole-brain irradiation.^{112,113} Some authors have argued that vascular injury in the retina may coincide with or predict cerebrovascular injury, underlining the utility of funduscopy as a screening tool.¹¹⁴

During discussions, the use of the term "cotton-wool spot" was challenged by an audience member as a nonspecific term, since an accumulation of cytoid bodies appears identical to focal inflammatory infiltrate fundoscopically. In response, the American Academy of Ophthalmologist's definition of a cotton-wool spot was quoted, "The histological hallmark of cotton-wool spots is considered by many authors to be cytoid bodies." However, it was agreed that the description cotton-wool spot is nonspecific and likely of little value to the toxicologic pathology lexicon.

Dr Schaaf concluded his presentation by emphasizing the retina's apparent stereotypic response to vascular injury, regardless of the etiology, and the inherent difficulty when attempting to determine the etiology of any particular retinal lesion.

Select Lesions From the Non-Rodent Fish Working Group

The final presentation of the symposium, given by Dr Jeffrey Wolf, included 3 case examples of morphologic findings that might be encountered during evaluations of toxicological studies that utilize fish models. A major goal of this presentation was to highlight efforts of the INHAND Non-Rodent Fish Working Group, which is tasked with developing preferred diagnostic criteria and nomenclature for nonproliferative and proliferative microscopic lesions in fish. The initial case involved a study in which male and female tilapia *Oreochromis* sp., approximately 107 days old, had received an antibiotic administered in the feed for 20 days. Images presented to the audience consisted of low and high magnifications of H&E-stained gill tissue, in which the interlamellar spaces were nearly to completely filled by a combination of proliferating pavement cells and fewer mononuclear inflammatory cells (Figure 14A and B, with Figure 14C included for comparison).

Figure 13. (Continued). accumulations of eosinophilic debris with no discernible architecture and a mild gliosis. Another region of the nerve fiber layer (C) shows an accumulation of eosinophilic bodies, interpreted as cytoid bodies and are the result of axonal obstruction. D, A tortuous, redundant vessel with plump endothelial cells in the ganglion cell layer (arrow). When stained with PAS (E and F), basement membrane splitting of an arteriole in the nerve fiber layer can be appreciated, as well as a damaged capillary leaking PAS-positive material.

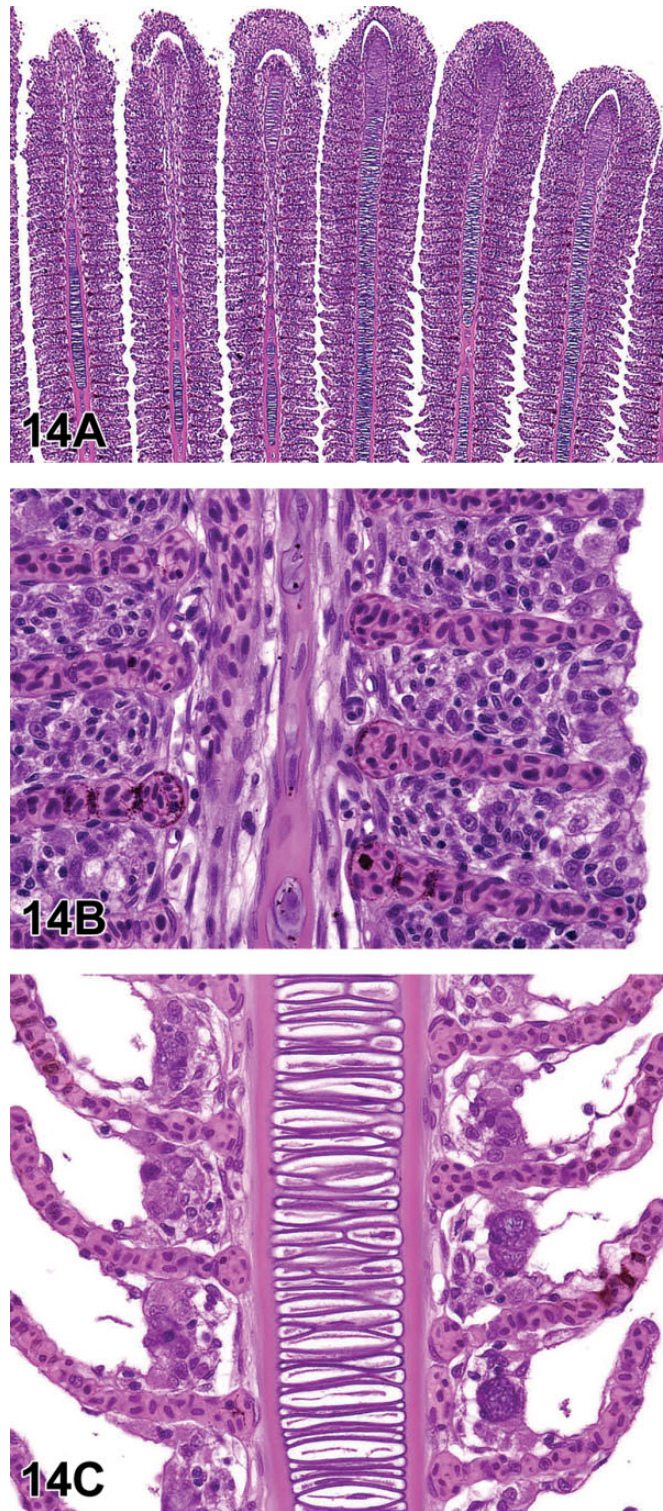


Figure 14. Examples (A-Q) of morphologic findings that might be encountered during evaluations of toxicological studies that utilize fish models. Low magnification (A) of tilapia (*Oreochromis* spp.) gills from case 1. High magnification (B) of tilapia gills to further demonstrate diagnoses of diffuse lamellar epithelial hyperplasia, diffuse lamellar fusion, and mononuclear cell infiltrates. High magnification (C) of comparatively normal (actually mildly affected) tilapia gill from the same study included for comparison. Low magnification (D) view of ovary from a female fathead minnow (*Pimephales promelas*) from case 2. High magnification (E) view of ovary to demonstrate granulomatous inflammation, characterized by sheets of epithelioid cells in this case. Granulomatous inflammation in fish can resemble dysplastic or neoplastic squamous epithelium. Another high magnification (F) of the same fathead minnow ovary. The ring of irregular dense pink material is the degenerating zona pellucida of an oocyte (compare with normal oocyte in H). The ooplasm is filled with microsporidia spores. Oil magnification (G) of microsporidia, which have the typical

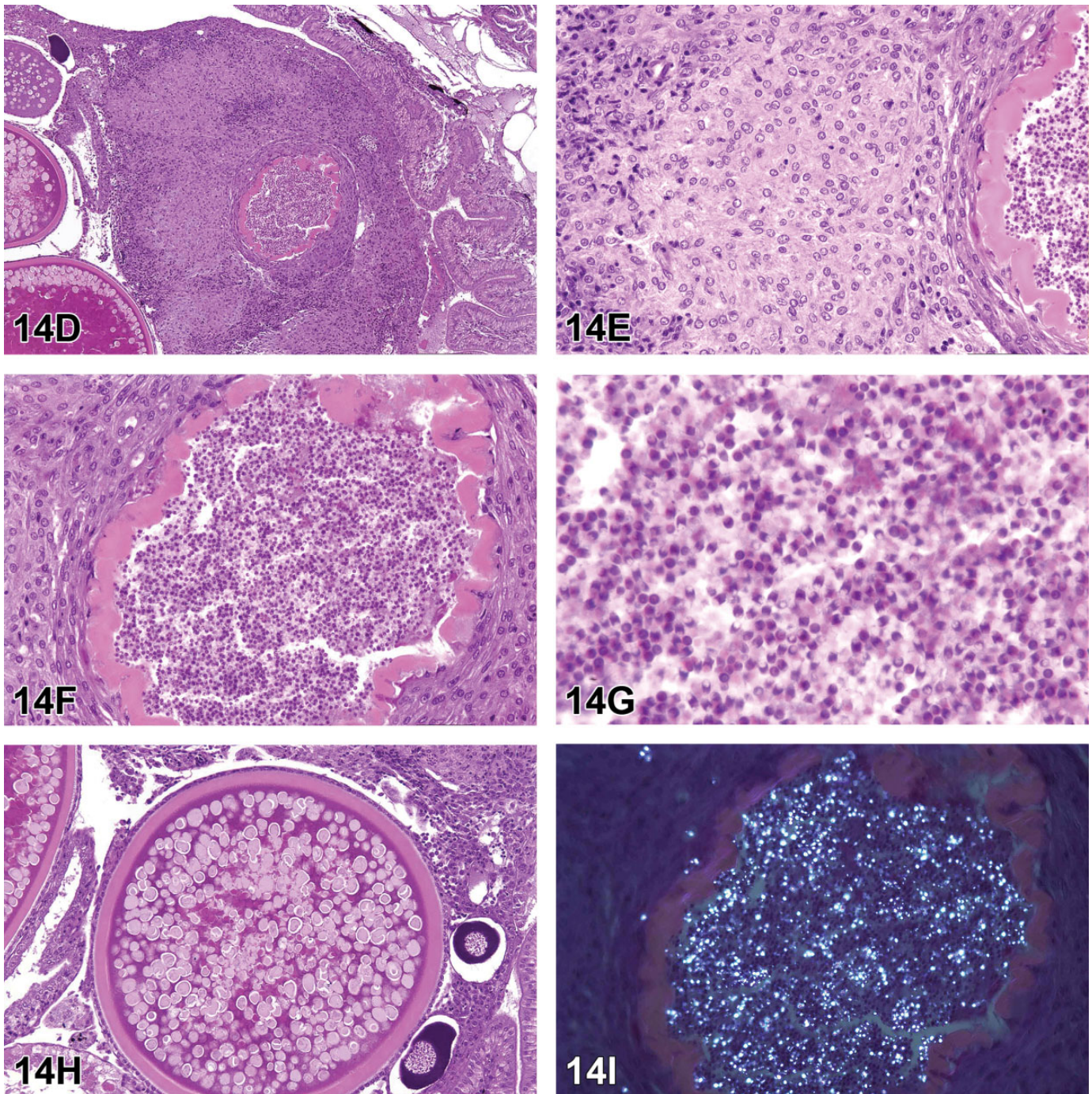


Figure 14. (continued). “bedroom slipper” appearance. Normal cortical alveolar stage oocyte (H) in the ovary of a fathead minnow included for comparison. Here, the ooplasm is filled with cortical alveoli, which are yolk precursor granules. Microsporidia spores (I) as viewed using polarized light. Not all developmental stages are refractile, thus polarized light does not always detect the organisms. H&E, polarized. Low magnification (J) of liver from an adult female white sucker (*Catostomus commersonii*) from case 3. Note the scalloped edge of the mass-like lesion and slight peripheral compression of the surrounding liver.¹¹⁵ Medium magnification (K) of white sucker liver. The lesion occupies the approximate upper half of the image, and the unaffected liver is in the lower half. In this area, finger-like projections of the lesion encircle thick cords of viable-appearing hepatocytes.¹¹⁵ Medium magnification (L) of white sucker liver. Area from the center of the lesion, which is characterized by streaming cells and whorls reminiscent of a perivascular or nerve sheath tumor.¹¹⁵ At high magnification (M), resemblance to hemangiopericytoma or nerve sheath tumor vanishes. Here it is evident that the whorls are formed by plump cells that have eccentric nuclei, marginated and clumped chromatin, and faintly granular translucent cytoplasm.¹¹⁵ Another high magnification (N) image. Here the plump cells either have eosinophilic granular cytoplasm or relatively clear cytoplasm with fine spicules. The latter type are consistent with mature rodlet cells. It is proposed that the cells with eosinophilic granular cytoplasm are rodlet cell precursors, while the cells in (M) appear to be an intermediate stage.¹¹⁵ Periodic acid–Schiff (PAS)

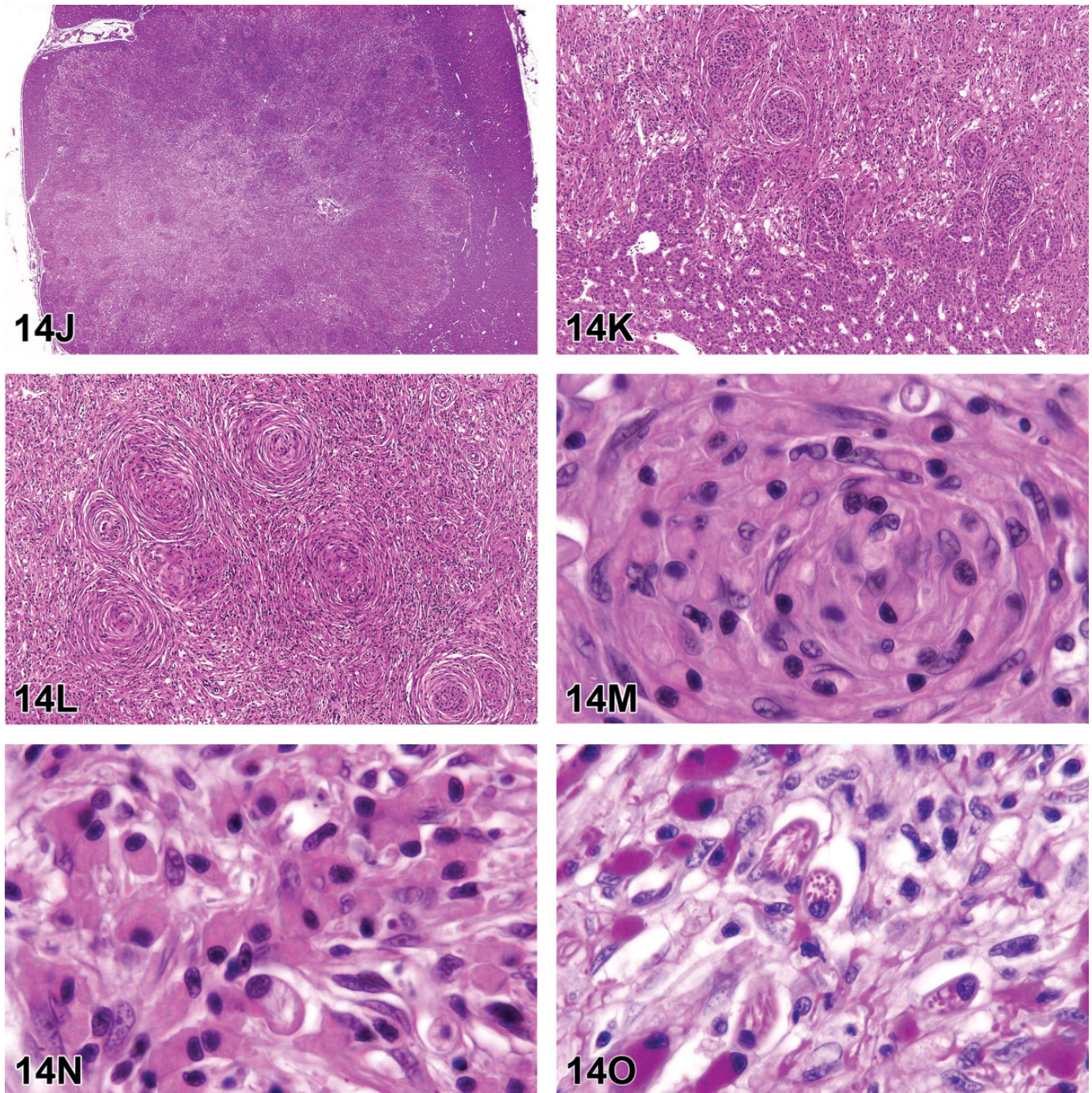


Figure 14. (continued). staining (O) highlights the rodlet cell spicules, granular cytoplasm of the precursor cells, membranous extensions of the tumor cell cytoplasm, and possibly extracellular rodlet-like material.¹¹⁵ Masson's trichrome staining (P) illustrates the relative absence of collagen within the lesion, while the wall of a blood vessel serves as an internal control. The lack of fibrosis further suggests that this is not a chronic inflammatory lesion.¹¹⁵ Transmission electron micrograph (Q) demonstrates a rodlet cell (mid-left) and a putative precursor cell with granular cytoplasm (lower right). Note the presence of extracellular rodlet-like material near the top of the image (arrows).¹¹⁵

The 9 voting choices and results were as follows: (1) hyperplasia, lamellar epithelium, diffuse (6%), (2) pseudobranch, lamellar fusion (7%), (3) branchitis, proliferative, with mucous cell hyperplasia (10%), (4) lamellar fusion, diffuse (6%), (5) filament clubbing, segmental (1%), (6) cellular infiltrate,

mononuclear cell (6%), (7) choices 1, 4, and 6 (41%), (8) choices 2, 3, 4, and 5 (17%), and (9) all of the above (6%). The preferred answer of the participants was the multiple choice #7 (41% of respondents), which was also Dr Wolf's preferred answer.

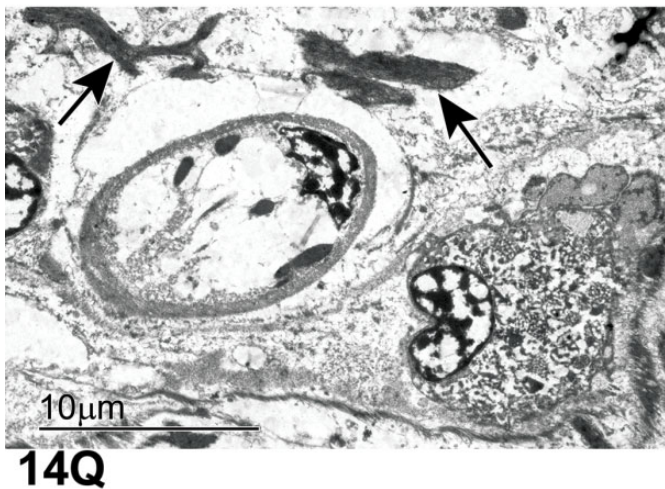
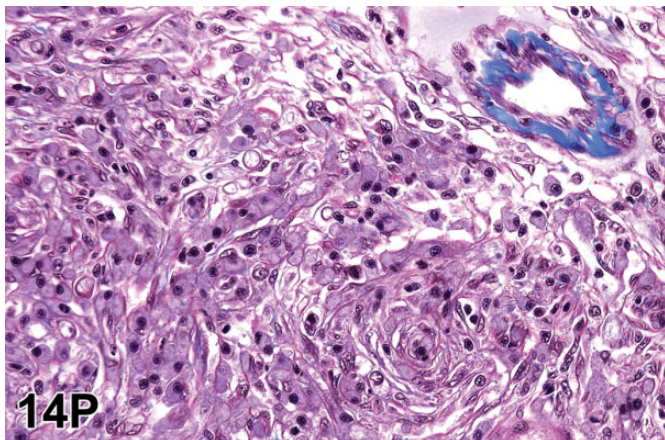


Figure 14. (continued).

Choice #2 was not considered accurate because the tissue presented was gill rather than pseudobranch. The pseudobranch is a gill-like structure that, unlike the actual gills, is not exposed directly to the aqueous environment and is thought to enhance the oxygen content of blood provided to the eyes. Choice #3 was not considered ideal because the term branchitis is a diagnostic versus descriptive term (by intent the INHAND nomenclature favors descriptive terminology) and because there were no mucous cells in the initial gill images. Finally, although filament clubbing (choice #5) could have been a valid diagnosis, the demonstrated proliferative changes were actually diffuse rather than segmental. An image of relatively normal gill tissue from the same study was presented for comparison during the discussion.

The second case of this presentation focused on tissue from an adult female fathead minnow *Pimephales promelas* that was a negative control in a 21-day bioassay. The presented images were obtained from a whole-body sagittal section, and the central feature of the initial low-magnification image was the ovary in situ. Occupying approximately one-third of the ovary was a moderately well-circumscribed, densely cellular, and heterogeneous mass-like lesion (Figure 14D). At higher

magnifications, it was evident that the lesion was comprised primarily of cells that had abundant pale pink poorly demarcated cytoplasm and open-faced nuclei, admixed with mononuclear inflammatory cells (Figure 14E). At the core of the lesion was a ring of irregular dense pink tissue (later identified as the oocyte zona pellucida), and this ring was nearly filled by myriad 1 to 2 μm eosinophilic to amphophilic punctate structures (Figure 14F-G, with normal oocyte included for comparison in Figure 14H).

The 5 voting choices and results for this ovarian lesion were as follows: teratoma (4%), rodlet cell tumor (2%), squamous cell carcinoma (2%), yolk degeneration and granulomatous inflammation with acid-fast bacilli (29%), and oocyte atresia; ovary inflammation, granulomatous; ovary, microsporidian oophoritis (63%). The preferred answer of the participants (63%) was also the correct response according to Dr Wolf.

Although background infections in laboratory fish are often incidental, disease caused by infectious agents can occasionally confound the results of toxicological studies, and parallels were drawn to examples of hepatic infections in rodent studies, including those caused by *Helicobacter* spp., murine norovirus, mouse hepatitis virus, and *Clostridium piliforme* (Tyzzer disease). Microsporidian infections occur commonly in a wide variety of freshwater and marine fish species. Piscine microsporidiosis may be relatively innocuous and well tolerated by the host or it can cause extensive inflammation. Microsporidia often target a particular organ or tissue type, but systemic infections can occur in some cases.

Examples of disease targets in laboratory fish include ovarian infections in fathead minnows caused by *Pleistophora* spp.¹¹⁶; spinal cord and nerve infections in zebra fish (*Danio rerio*) attributed to *Pseudoloma neurophilia*¹¹⁷; and zebra fish skeletal muscle infections due to *Pleistophora hypheosobryconis*,¹¹⁸ the etiologic agent of “neon tetra disease.” Microsporidia are Gram-positive obligate intracellular pathogens that are more recently classified with fungi as opposed to protists. Transmission is thought to be direct, and organisms have a typical “bedroom slipper” appearance in wet mounts and histologic preparations. Unlike most microorganisms, they frequently appear eosinophilic in H&E sections. One of the best histologic methods for detecting microsporidia is the Luna stain,¹¹⁹ and certain stages of spore formation may be highlighted by polarized light examination (Figure 14I).

The third and final presentation consisted of liver lesions in female white sucker fish (*Catostomus commersonii*) that were each gauged to be approximately 10 years old. These fish were collected along with 98 other suckers by Environment and Climate Change Canada staff from 3 sites within the St Mary’s River, which drains Lake Superior into Lake Huron and is located at the border between the twin cities Sault Ste. Marie, Ontario, and Sault Ste. Marie, Michigan.

Contaminants of particular concern that are known to occur at high concentrations in St. Mary’s River sediment include polyaromatic hydrocarbons such as benzo[a]pyrene. Such contamination is thought to be related to the historically high overall prevalence of liver tumors (5%-10%) in white suckers

Table 8. Thyroid Nomenclature.^a

Thyroid	Common	Uncommon	Not Observed, but Potentially Relevant	Not Applicable
Congenital				
Ectopic tissue, thymus			X	
Ectopic tissue, thyroid	X			
Persistent thyroglossal duct				X
Ultimobranchial cyst				X
Nonproliferative				
Amyloid			X	
Atrophy			X	
Colloid alteration		X		
Cystic follicle		X		
Follicular dilation, diffuse		X		
Hyaline degeneration, follicular cell		X		
Hypertrophy, follicular cell		X		
Hypertrophy, follicular cell, ectopic		X		
Infiltrate, inflammatory cell		X		
Inflammation		X		
Mineralization		X		
Pigment			X	
Thyroid dysplasia			X	
Proliferative				
Non-neoplastic				
Hyperplasia, C-cell				X
Hyperplasia, follicular cell		X		
Hyperplasia, follicular cell, ectopic		X		
Neoplastic				
Adenoma, C-cell				X
Adenoma, follicular cell		X		
Adenoma, follicular cell, ectopic		X		
Carcinoma, C-cell				X
Carcinoma, follicular cell		X		
Carcinoma, follicular cell, ectopic		X		

^aExample of a nomenclature table from the draft fish INHAND manuscript. Findings for each organ are divided into congenital, nonproliferative, proliferative non-neoplastic, and proliferative neoplastic categories, and further classification indicates the likelihood of encountering each finding type as a spontaneous occurrence in toxicology studies.

obtained from that stretch of river. Initially, the audience was shown a low magnification view of liver, the majority of which was occupied by a centrally located, roughly circular, heterogeneous mass with scalloped edges that demonstrated both expansile and infiltrative tendencies at different locations around the periphery (Figure 14J-K). At medium magnification, a pattern of streaming fibrous tissue with prominent whorls emerged, and as such, the lesion was reminiscent of a perivascular or nerve sheath tumor (Figure 14L). However, in subsequent high-magnification images, it became evident that the tissue was comprised of at least 2 or 3 admixed populations of plump cells, one of which had faintly granular bright eosinophilic cytoplasm, an eccentric hyperchromatic nucleus, and elongated bidirectional cytoplasmic tails (Figure 14M-N). A second population consisted of similar plump cells that also had eccentric nuclei, but the cytoplasm was instead translucent pale pink and contained spicule-like structures, while a third population shared some characteristics with each of the first 2 and therefore appeared to be an intermediate form.

The 5 voting choices and results for this liver lesion were hemangiopericytoma (31%), nerve sheath tumor (10%), neurofibrosarcoma (12%), schwannoma (6%), Schwann cell sarcoma (10%), fibrocellular hepatitis (4%), chromatophoroma (5%), rodlet cell tumor (18%), and other diagnosis (2%). The preferred answer of the participants was hemangiopericytoma, whereas Dr Wolf's preferred answer was rodlet cell tumor.

Background information on the discovery and nature of rodlet cells was presented, along with evidence which suggested that the 2 white sucker masses may be the first reported rodlet cell neoplasms. Although the existence of rodlet cells has been known since the late 19th century and their light microscopic and ultrastructural morphologies have been well characterized, the precise origin and nature of these cells remain enigmatic. Once described as parasites,¹²⁰ and later reported as secretory cells,¹²¹ rodlet cells are now widely thought to be of host origin, and many authors consider these to be nonphagocytic leukocytes that represent a component of the innate immune system. However, antipathogen activity has not been convincingly demonstrated; although increased numbers of

Table 9. An Example of Diagnostic Criteria and Other Pertinent Information for the Finding of Increased Pigmented Macrophage Aggregates.

Pigmented macrophage aggregates, increased

Other terms

- Lipofuscin deposition
- Hemosiderin deposition
- Melanin deposition
- Ceroid deposition

Pathogenesis

These constituent structures are found in a variety of tissue types, including liver. They tend to increase in size and number with age but may also increase in response to toxicant exposure or to the presence of foreign bodies or parasites. A role in antigen presentation has been proposed, and melanin may also help to scavenge free radicals.

Diagnostic features

- Discrete, periportal to randomly scattered, variably sized aggregates in liver parenchyma
- Histiocytic macrophages that contain intracytoplasmic brown, gold, or black granular to amorphous material
- May be incorporated into, or become sites of, inflammatory processes
- May be found commonly in the livers of some fish species and rarely in others

Differential diagnosis

- Pigmentation/intracytoplasmic pigment deposition within hepatocytes
- Hematoxylin or other stain precipitate
- Formalin-precipitated pigment (acid-hematin): granular yellow-brown material external to plane of section
- Hepatocellular accumulation of test compound or metabolite
- Mineralization, basophilic deposits; may be associated with calcification

Comments

In the literature, these structures are often called melanomacrophage centers. However, because a variety of pigment types may be present, the term pigmented macrophage aggregates is preferred. Increased pigmented macrophage aggregates were described after exposure to dietary methylmercury.¹²³ In tropical fish, *Astyanax fasciatus* and *Pimelodus maculatus*, organochlorines and metals also led to increases in the number of pigmented macrophages.¹²⁴ In African catfish (*Clarias gariepinus*) melanomacrophage centers were studied as immunohistological biomarkers for the toxicity of silver nanoparticles.¹²⁵ It is important to recognize that increases in pigmented macrophage aggregates may also result from nontoxic causes, like aging or infectious diseases, and the age/size of fish must be accounted for when making groupwise comparisons.

rodlet cells can be found in association with inflammation, they can also be plentiful in particular tissues for no obvious reason.

In addition to the presence of abundant rodlet cell-like cells and putative precursors (cells with eosinophilic granular cytoplasm) throughout the demonstrated lesion, evidence that the 2 liver lesions may be rodlet cell tumors included extensive PAS-positive staining (Figure 14O), near lack of collagen (ie, fibrosis) as demonstrated by Masson's trichrome staining (Figure 14P), and transmission electron micrographs that illustrated the phenotypes of both granular and maturing rodlet cells, as well as the presence of extracellular rodlet material (Figure 14Q). In a prior investigation, positivity for S100 antigen was demonstrated in 6 of 8 fish species tested¹²²; however, neither the white tumors nor rodlet cells in the non-neoplastic bile ducts were successfully immunolabeled for S100 in the current study. This lack of antigenicity may be attributed to the extended period (up to 4 weeks) in which the specimens were maintained in formaldehyde-based Davidson's fixative. Although a differential diagnosis of rodlet cell-rich sarcoma was considered initially, repeated careful study of the histologic sections did not reveal additional neoplastic tissue that was not comprised of the aforementioned cell types, and the lesions were diagnosed as putative rodlet cell tumors.¹¹⁵

One follow-up question from the audience pertained to the anatomic location of normal (ie, non-neoplastic) rodlet cells, their capacity for mobility, and whether they were present intravascularly. Dr Wolf replied that rodlet cells are typically

associated with epithelial, mesothelial, and endothelial basement membranes in a variety of tissues such as bile duct, kidney, and gills. There is little evidence that they are transported routinely via the vascular system, although some investigations suggest that rodlet cells may migrate from sub-basement membrane to more apical (luminal) locations as they mature.

Throughout the presentation, reference was made to the INHAND initiative to develop harmonized diagnostic nomenclature and criteria for nonproliferative and proliferative lesions. Some general INHAND principles were discussed, for example, the tendency to prefer descriptive rather than diagnostic terminology and attempts to adapt rodent INHAND terminology to fish findings as much as possible. Example nomenclature listings and lesion criteria were presented in publication format (Tables 8 and 9), as were challenges and considerations of special importance to the fish INHAND group. Challenges identified included the development of standardized criteria that would fairly represent a large number of fish species (>34,000), anatomical and physiological differences between fish and rodents, and problems related to background lesions and artifacts, including artifacts frequently misreported as pathological changes in the fish literature.

Acknowledgments

The authors wish to thank Eli Ney (NIEHS) for her unique and creative artwork for the symposium, Beth Mahler (EPL) for her assistance with manuscript image preparation, Brittany Scott (Charles River

Laboratories, Inc) for assistance with manuscript formatting and review, and Dr Ramesh Kovi for manuscript review. Appreciation also goes to Maureen Bayley, Tierre Miller, Matthew Price, and others at Association Innovation and Management, Inc, for their valuable help with annual advertising and meeting facilities. Also integral to the success of this meeting was the audiovisual technical expertise provided by CMI Communications. Refreshments were graciously provided by Integrated Laboratory Systems, Inc, Experimental Pathology Laboratories, Inc, and Charles River Laboratories, Inc.

Declaration of Conflicting Interests

The author(s) declared no potential, real, or perceived conflicts of interest with respect to the research, authorship, and/or publication of this article.

Funding

The author(s) disclosed receipt of the following financial support for the research, authorship, and/or publication of this article: This work was supported [in part] by the NIH, National Institute of Environmental Health Sciences.

ORCID iD

Susan A. Elmore  <https://orcid.org/0000-0002-1680-9176>

Mark F. Cesta  <https://orcid.org/0000-0002-5380-5182>

Kyathanahalli S. Janardhan  <https://orcid.org/0000-0002-5774-9317>

References

1. goRENI. <https://www.goreni.org/>. Accessed July 15, 2019.
2. Brandli-Baiocco A, Balme E, Bruder M, et al. Nonproliferative and proliferative lesions of the rat and mouse endocrine system. *J Toxicol Pathol*. 2018;31(suppl 3):1S-95S.
3. Nolte T, Brander-Weber P, Dangler C, et al. Nonproliferative and proliferative lesions of the gastrointestinal tract, pancreas and salivary glands of the rat and mouse. *J Toxicol Pathol*. 2016;29(1 suppl):1S-125S.
4. Cora M, Travlos G. Bone marrow—hypocellularity. *National Toxicology Program Nonneoplastic Lesion Atlas*. 2014; https://ntp.niehs.nih.gov/nml/hematopoietic/bone_marrow/hypocell/index.htm. Accessed July 10, 2019.
5. Barlow NJ, McIntyre BS, Foster PM. Male reproductive tract lesions at 6, 12, and 18 months of age following in utero exposure to di(n-butyl) phthalate. *Toxicol Pathol*. 2004;32(1):79-90.
6. Elmore SA, Carreira V, Labriola CS, et al. Proceedings of the 2018 National Toxicology Program Satellite Symposium. *Toxicol Pathol*. 2018;46(8):865-897.
7. Lara NLM, Driesche SVD, Macpherson S, Franca LR, Sharpe RM. Dibutyl phthalate induced testicular dysgenesis originates after seminiferous cord formation in rats. *Sci Rep*. 2017;7(1):2521.
8. Auersperg N, Wong AS, Choi KC, Kang SK, Leung PC. Ovarian surface epithelium: biology, endocrinology, and pathology. *Endocr Rev*. 2001;22(2):255-288.
9. Kim J, Park EY, Kim O, et al. Cell origins of high-grade serous ovarian cancer. *Cancers (Basel)*. 2018;10(11):E433.
10. Dixon D, Alison R, Bach U, et al. Nonproliferative and proliferative lesions of the rat and mouse female reproductive system. *J Toxicol Pathol*. 2014;27(suppl 3-4):1S-107S.
11. Gregson RL, Lewis DJ, Abbott DP. Spontaneous ovarian neoplasms of the laboratory rat. *Vet Pathol*. 1984;21(3):292-299.
12. Alison RH, Morgan KT. Ovarian neoplasms in F344 rats and B6C3F1 mice. *Environ Health Perspect*. 1987;73:91-106.
13. Lewis DJ. Ovarian neoplasia in the Sprague-Dawley rat. *Environ Health Perspect*. 1987;73:77-90.
14. Ikezaki S, Takagi M, Tamura K. Natural occurrence of neoplastic lesions in young sprague-dawley rats. *J Toxicol Pathol*. 2011;24(1):37-40.
15. National Toxicology Program. *Toxicology and Carcinogenesis Studies of 1,2-Epoxybutane (CAS No. 106-88-7) in F344/N Rats and B6C3F1 Mice (Inhalation Studies)*. Research Triangle Park, NC: National Toxicology Program; 1988. TR-329.
16. Higgins R, Bollen A, Dickinson P, Siso-Llonch S. Tumors of the nervous system. In: Meuten D, ed. *Tumors in Domestic Animals*. 5th ed. Ames, IA: John Wiley & Sons, Inc.; 2017:834-891.
17. Pytel P, Anthony D. Peripheral nerves and skeletal muscles. In: Kumar V, Abbas A, Fausto N, Aster J, eds. *Robbins and Cotran Pathologic Basis of Disease*. 8th ed. Philadelphia, PA: Saunders/Elsevier; 2010:1227-1250.
18. McKeever P. Immunohistology of the nervous system. In: Dabbs D, ed. *Diagnostic Immunohistochemistry: Theranostic and Genomic Applications*. Philadelphia, PA: Saunders Elsevier; 2010:820-889.
19. Kaufmann W, Bolon B, Bradley A, et al. Proliferative and nonproliferative lesions of the rat and mouse central and peripheral nervous systems. *Toxicol Pathol*. 2012;40(suppl 4):87S-157S.
20. Bradley A, Roulois A, McKay J, Parry N, Boorman G. The spinal cord and peripheral nervous system. In: Suttie A, ed. *Boorman's Pathology of the Rat*. 2nd ed. London, England: Elsevier; 2015:217-239.
21. Hornick JL, Fletcher CD. Soft tissue perineurioma: clinicopathologic analysis of 81 cases including those with atypical histologic features. *Am J Surg Pathol*. 2005;29(7):845-858.
22. Macareno RS, Ellinger F, Oliveira AM. Perineurioma: a distinctive and underrecognized peripheral nerve sheath neoplasm. *Arch Pathol Lab Med*. 2007;131(4):625-636.
23. Boulagnon-Rombi C, Fleury C, Fichel C, Lefour S, Marchal Bressenet A, Gauchotte G. Immunohistochemical approach to the differential diagnosis of meningiomas and their mimics. *J Neuropathol Exp Neurol*. 2017;76(4):289-298.
24. Rodriguez FJ, Folpe AL, Giannini C, Perry A. Pathology of peripheral nerve sheath tumors: diagnostic overview and update on selected diagnostic problems. *Acta Neuropathol*. 2012;123(3):295-319.
25. Elmore SA, Chen VS, Hayes-Bouknight S, et al. Proceedings of the 2016 National Toxicology Program Satellite Symposium. *Toxicol Pathol*. 2017;45(1):11-51.
26. Elmore SA, Boyle MC, Boyle MH, et al. Proceedings of the 2013 National Toxicology Program Satellite Symposium. *Toxicol Pathol*. 2014;42(1):12-44.
27. Swenberg JA, Clendenon N, Denlinger R, Gordon WA. Sequential development of ethylnitrosourea-induced neurinomas: morphology, biochemistry, and transplantability. *J Natl Cancer Inst*. 1975;55(1):147-152.
28. National Toxicology Program. *Toxicology and Carcinogenesis Studies of GSM- And CDMA-Modulated Cell Phone Radio Frequency Radiation at 900 MHz In Hsd: Sprague Dawley SD Rats*. Research Triangle Park, NC: National Toxicology Program; 2018. TR-595.
29. Nikitin A, Ballering LA, Lyons J, Rajewsky MF. Early mutation of the neu (erbB-2) gene during ethylnitrosourea-induced oncogenesis in the rat Schwann cell lineage. *Proc Natl Acad Sci U S A*. 1991;88(22):9939-9943.
30. Gering KM, Marx JA, Lennartz K, Fischer C, Rajewsky MF, Kindler-Rohrborn A. The interaction mode of premalignant Schwann and immune effector cells during chemically induced carcinogenesis in the rat peripheral nervous system is strongly influenced by genetic background. *Cancer Res*. 2006;66(9):4708-4714.
31. Yoshizawa K, Yuki M, Kinoshita Y, et al. N-methyl-N-nitrosourea-induced schwannomas in male Sprague-Dawley rats with a literature review of inducible and spontaneous lesions. *Exp Toxicol Pathol*. 2016;68(7):371-379.
32. Yoshida M. Malignant schwannoma arising from the trigeminal nerve in a rat. *J Comp Pathol*. 1992;106(3):315-318.
33. Hailey JR, Walker NJ, Sells DM, Brix AE, Jokinen MP, Nyska A. Classification of proliferative hepatocellular lesions in Harlan Sprague-Dawley rats chronically exposed to dioxin-like compounds. *Toxicol Pathol*. 2005;33(1):165-174.
34. Hickling KC, Hitchcock JM, Chipman JK, Hammond TG, Evans JG. Induction and progression of cholangiofibrosis in rat liver injured by oral administration of furan. *Toxicol Pathol*. 2010;38(2):213-229.

35. Tatematsu M, Kaku T, Medline A, Farber E. Intestinal metaplasia as a common option of oval cells in relation to cholangiofibrosis in the liver of rats exposed to 2-acetylaminofluorene. *Lab Invest.* 1985;52(4):354-362.
36. Thoolen B, Maronpot RR, Harada T, et al. Proliferative and nonproliferative lesions of the rat and mouse hepatobiliary system. *Toxicol Pathol.* 2010;38(suppl 7):5S-81S.
37. Foster J. Liver. In: Suttie A, Leininger J, Bradley A, eds. *Boorman's Pathology of the Rat.* London, England: Elsevier; 2018:81-105.
38. Ohshima M, Ward JM, Brennan LM, Creasia DA. A sequential study of methapyrilene hydrochloride-induced liver carcinogenesis in male F344 rats. *J Natl Cancer Inst.* 1984;72(3):759-768.
39. Wilson TM, Nelson PE, Knepp CR. Hepatic neoplastic nodules, adenofibrosis, and cholangiocarcinomas in male Fischer 344 rats fed corn naturally contaminated with *Fusarium moniliforme*. *Carcinogenesis.* 1985; 6(8):1155-1160.
40. Elmore LW, Sirica AE. Phenotypic characterization of metaplastic intestinal glands and ductular hepatocytes in cholangiofibrotic lesions rapidly induced in the caudate liver lobe of rats treated with furan. *Cancer Res.* 1991;51(20):5752-5759.
41. Schilsky ML, Quintana N, Vollenberg I, Kabishcher V, Sternlieb I. Spontaneous cholangiofibrosis in Long-Evans Cinnamon rats: a rodent model for Wilson's disease. *Lab Anim Sci.* 1998;48(2):156-161.
42. Crabbs TA (presenter), Gruebbel MM, Hardisty JF, Shackelford CC, Malarkey DE, Cesta M. Spontaneous Periductal Cholangiofibrosis in the Liver and Pancreas of Male and Female Harlan Sprague Dawley Rats. Paper presented at: The 15th European Congress of Toxicologic Pathology; August 30-September 02, 2017; Lyon, France.
43. Chen T, Chen K, Qiu S, Mann PC. Spontaneous cholangiofibrosis in a wistar rat. *Toxicol Pathol.* 2019;47(4):556-560.
44. McDougall K, Hay MA, Goodrowe KL, Gartley CJ, King WA. Changes in the number of follicles and of oocytes in ovaries of prepubertal, peripubertal and mature bitches. *J Reprod Fertil Suppl.* 1997;51:25-31.
45. Reynaud K, Fontbonne A, Saint-Dizier M, et al. Folliculogenesis, ovulation and endocrine control of oocytes and embryos in the dog. *Reprod Domest Anim.* 2012;47(suppl 6):66-69.
46. Hartman CG. Polynuclear ova and polyovular follicles in the opossum and other mammals, with special reference to the problem of fecundity. *Am J Anat.* 1926;37(1):1-51.
47. Mainland D. The pluriovular follicle, with reference to its occurrence in the ferret. *J Anat.* 1928;62(Pt 2):139-158.
48. Telfer E, Gosden RG. A quantitative cytological study of polyovular follicles in mammalian ovaries with particular reference to the domestic bitch (*Canis familiaris*). *J Reprod Fertil.* 1987;81(1):137-147.
49. Payan-Carreira R, Pires MA. Multiocyte follicles in domestic dogs: a survey of frequency of occurrence. *Theriogenology.* 2008;69(8):977-982.
50. Sato J, Doi T, Wako Y, et al. Histopathology of incidental findings in beagles used in toxicity studies. *J Toxicol Pathol.* 2012;25(1):103-134.
51. Stankiewicz T, Blaszczyk B, Udala J. A study on the occurrence of polyovular follicles in porcine ovaries with particular reference to intra-follicular hormone concentrations, quality of oocytes and their in vitro fertilization. *Anat Histol Embryol.* 2009;38(3):233-239.
52. Kim H, Nakajima T, Hayashi S, et al. Effects of diethylstilbestrol on programmed oocyte death and induction of polyovular follicles in neonatal mouse ovaries. *Biol Reprod.* 2009;81(5):1002-1009.
53. Alm H, Kuhlmann S, Langhammer M, Tuchscherer A, Torner H, Reinsch N. Occurrence of polyovular follicles in mouse lines selected for high fecundity. *J Reprod Dev.* 2010;56(4):449-453.
54. Toxicology and carcinogenesis studies of ethylene thiourea (Cas No. 96-45-7) in F344/N rats and B6C3F1 mice (Feed Studies). In: Research Triangle Park, NC: Public Health Services, National Institutes of Health, U. S. Department of Health; 1992. TR-388. https://ntp.niehs.nih.gov/ntp/htdocs/lt_rpts/tr388.pdf.
55. Capen CC. Functional and pathologic interrelationships of the pituitary gland and the hypothalamus. In: Jones TC, Mohr U, Hunt R.D, eds. *Monographs on Pathology of Laboratory Animals: Endocrine System.* Berlin, Germany: Springer-Verlag; 1983:101-120.
56. Koga D, Kusumi S, Bochimoto H, Watanabe T, Ushiki T. Correlative light and scanning electron microscopy for observing the three-dimensional ultrastructure of membranous cell organelles in relation to their molecular components. *J Histochem Cytochem.* 2015;63(12): 968-979.
57. Goldner WS, Sandler DP, Yu F, Hoppin JA, Kamel F, Levan TD. Pesticide use and thyroid disease among women in the Agricultural Health Study. *Am J Epidemiol.* 2010;171(4):455-464.
58. Shrestha S, Parks CG, Goldner WS, et al. Incident thyroid disease in female spouses of private pesticide applicators. *Environ Int.* 2018;118: 282-292.
59. Case #20—September. *DPDx—Laboratory Identification of Parasitic Diseases of Public Health Concern, Monthly Case Studies—1999.* 1999. <https://www.cdc.gov/dpdx/monthlyCaseStudies/1999/case20.html>. Accessed July 9, 2019.
60. Yoon KH. Peripheral blood smear contamination with helicosporium fungi resembling microfilaria. *Ann Lab Med.* 2015;35(1):169-171.
61. Olariu TR, Nicola ED, Petrescu C, Koreck A. Helical microorganisms in blood smears. *Clin Infect Dis.* 2011;53(5):468; 497-468.
62. Norman L, Donaldson AW. Spores of helicosporous fungi resembling microfilariae in blood films. *Am J Trop Med Hyg.* 1955;4(5): 889-893.
63. Singh P, Singh S. Additions to helicooid fungi from India. *Curr Res Environ Appl Mycol.* 2016;6(4):248-255.
64. Jirovec O. *Sergentella spiroides*, a new parasite of humans [in French]. *Rev Bras Malariol Doencas Trop.* 1956;8(1):203-205.
65. Galliard H, Ho Thi S, Gentilini M. *Sergentella spiroides* and conidia of helicospora in blood smears [in French]. *Bull Soc Pathol Exot Filiales.* 1961;54:203-207.
66. Orihel TC, Organization WH, Ash LR, Ramachandran CP. *Bench Aids for the Diagnosis of Filarial Infections.* Geneva, Switzerland: World Health Organization; 1997.
67. Bhatia M, Mishra B, Thakur A, Loomba P, Dogra V. Microscopic artefacts in clinical practice- a diagnostic dilemma. *JCDR.* 2018;12(7): DR01-DR04.
68. Worm Mimic. http://eclinpath.com/ngg_tag/artifact/nggallery/page/4. Accessed July 9, 2019.
69. Stain precipitate & echinocytes. http://eclinpath.com/ngg_tag/stain-precipitate/. Accessed July 9, 2019.
70. Bacteria. http://eclinpath.com/ngg_tag/artifact/nggallery/page/4. Accessed July 9, 2019.
71. Manzoni D, Sujobert P. Diagnosis of bacteremia on a blood smear. *Blood.* 2015;125(13):2173.
72. Cha CH, Kim JU. Endothelial cells in peripheral blood smear: an artifact? *Korean J Hematol.* 2010;45(3):150.
73. Strijbos MH, Gratama JW, Kraan J, Lamers CH, den Bakker MA, Sleijfer S. Circulating endothelial cells in oncology: pitfalls and promises. *Br J Cancer.* 2008;98(11):1731-1735.
74. Attia FM, Maaty A, Kalil FA. Circulating endothelial cells as a marker of vascular dysfunction in patients with systemic lupus erythematosus by real-time polymerase chain reaction. *Arch Pathol Lab Med.* 2011; 135(11):1482-1485.
75. Balestra B, Carnino L. In vitro exflagellation of *Plasmodium vivax*. *N Engl J Med.* 2016;375(12):e27.
76. Armeth B, Keller C, Schaefer S. Malaria exflagellation in a human peripheral blood smear. *IDCases.* 2017;10:51-52.
77. Karplus R, Johnston SP. Images in clinical medicine. *Plasmodium vivax* microgametes. *N Engl J Med.* 2006;354(10):1064.
78. Kuehn A, Pradel G. The coming-out of malaria gametocytes. *J Biomed Biotechnol.* 2010;2010:976827.
79. Barthold S, Griffey S, Percy D. Mouse. In: *Pathology of Laboratory Rodents and Rabbits.* 4th ed. Ames, IA: John Wiley & Sons; 2016:1-118.
80. Barthold S, Griffey S, Percy D. Rat. In: *Pathology of Laboratory Rodents and Rabbits.* 4th ed. Ames, IA: John Wiley & Sons; 2016:119-172.
81. Frazier KS, Seely JC, Hard GC, et al. Proliferative and nonproliferative lesions of the rat and mouse urinary system. *Toxicol Pathol.* 2012; 40(suppl 4):14S-86S.

82. Ribatti D. The staining of mast cells: a historical overview. *Int Arch Allergy Immunol.* 2018;176(1):55-60.
83. Jamur MC, Grodzki ACG, Moreno AN, et al. Identification and isolation of rat bone marrow-derived mast cells using the mast cell-specific monoclonal antibody AA4. *J Histochem Cytochem.* 2001;49(2):219-228.
84. Moon TC, St Laurent CD, Morris KE, et al. Advances in mast cell biology: new understanding of heterogeneity and function. *Mucosal Immunol.* 2009;3(2):111-128.
85. Hasserjian RP, Harris NL. NK-cell lymphomas and leukemias spectrum of tumors with variable manifestations and immunophenotype. *Am J Clin Pathol.* 2007;127(6):860-868.
86. Rehg JE, Bush D, Ward JM. The utility of immunohistochemistry for the identification of hematopoietic and lymphoid cells in normal tissues and interpretation of proliferative and inflammatory lesions of mice and rats. *Toxicol Pathol.* 2012;40(2):345-374.
87. Imai Y, Ibata I, Ito D, Ohsawa K, Kohsaka S. A novel gene *iba1* in the major histocompatibility complex class III region encoding an EF hand protein expressed in a monocytic lineage. *Biochem Biophys Res Commun.* 1996;224(3):855-862.
88. Gill H, Liang RHS, Tse E. Extranodal Natural-Killer/T-Cell Lymphoma, Nasal Type. *Adv Hematol.* 2010;2010:627401.
89. Picut CA, Swanson CL, Parker RF, Scully KL, Parker GA. The metrial gland in the rat and its similarities to granular cell tumors. *Toxicol Pathol.* 2009;37(4):474-480.
90. Campbell KS, Hasegawa J. Natural killer cell biology: an update and future directions. *J Allergy Clin Immunol.* 2013;132(3):536-544.
91. Van Acker HH, Capsomidis A, Smits EL, Van Tendeloo VF. CD56 in the immune system: more than a marker for cytotoxicity? *Front Immunol.* 2017;8:892.
92. Inngjerdingen M, Kveberg L, Naper C, Vaage JT. Natural killer cell subsets in man and rodents. *Tissue Antigens.* 2011;78(2):81-88.
93. Bae EA, Seo H, Kim IK, Jeon I, Kang CY. Roles of NKT cells in cancer immunotherapy. *Arch Pharm Res.* 2019;42(7):543-548.
94. Andersen MH, Schrama D, Thor Straten P, Becker JC. Cytotoxic T cells. *J Invest Dermatol.* 2006;126(1):32-41.
95. Swerdlow SH, Campo E, Pileri SA, et al. The 2016 revision of the World Health Organization classification of lymphoid neoplasms. *Blood.* 2016;127(20):2375-2390.
96. Rebelatto MC. Spleen, lymph nodes, and thymus. In: Suttie AW, ed. *Boorman's Pathology of the Rat.* 2nd ed. Boston, MA: Academic Press; 2018:469-491. Chapter 24.
97. Thomas J, Haseman JK, Goodman JI, Ward JM, Loughran JTP, Spencer PJ. A review of large granular lymphocytic leukemia in fischer 344 rats as an initial step toward evaluating the implication of the endpoint to human cancer risk assessment. *Toxicol Sci.* 2007;99(1):3-19.
98. Stromberg PC. Large granular lymphocyte leukemia, rat. In: Jones TC, Ward JM, Mohr U, Hunt RD, eds. *Hemopoietic System.* Berlin, Germany: Springer Berlin Heidelberg; 1990:194-198.
99. Terayama Y, Matsuura T, Ozaki K. Malignant mast cell tumor of the thymus in an Royal College of Surgeons (RCS) rat. *J Toxicol Pathol.* 2017;30(1):63-67.
100. Squire RA. Histiocytic sarcoma, Rat. In: Jones TC, Ward JM, Mohr U, Hunt RD, eds. *Hemopoietic System.* Berlin, Germany: Springer Berlin Heidelberg; 1990:54-58.
101. Jo DH, Cho CS, Kim JH, Jun HO, Kim JH. Animal models of diabetic retinopathy: doors to investigate pathogenesis and potential therapeutics. *J Biomed Sci.* 2013;20:38.
102. Kim SY, Johnson MA, McLeod DS, et al. Retinopathy in monkeys with spontaneous type 2 diabetes. *Invest Ophthalmol Vis Sci.* 2004;45(12):4543-4553.
103. Zeiss CJ. Animals as models of age-related macular degeneration: an imperfect measure of the truth. *Vet Pathol.* 2010;47(3):396-413.
104. Archer DB, Gardiner TA. Ionizing radiation and the retina. *Curr Opin Ophthalmol.* 1994;5(3):59-65.
105. Bonney CH, Beckman FN, Hunter DM. Retinal change induced in the primate (*Macaca mulatta*) by oxygen nuclei radiation. *Life Sci Space Res.* 1974;12:31-42.
106. Zamber RW, Kinyoun JL. Radiation retinopathy. *West J Med.* 1992;157(5):530-533.
107. Stitt AW, Gardiner TA, Archer DB. Histological and ultrastructural investigation of retinal microaneurysm development in diabetic patients. *Br J Ophthalmol.* 1995;79(4):362-367.
108. Crispin SM, Mould JR. Systemic hypertensive disease and the feline fundus. *Vet Ophthalmol.* 2001;4(2):131-140.
109. Scholl S, Kirchhof J, Augustin AJ. Pathophysiology of macular edema. *Ophthalmologica.* 2010;224(suppl 10):8-15.
110. Brown GC, Brown MM, Hiller T, Fischer D, Benson WE, Magargal LE. Cotton-wool spots. *Retina.* 1985;5(4):206-214.
111. Schmidt D. The mystery of cotton-wool spots—a review of recent and historical descriptions. *Eur J Med Res.* 2008;13(6):231-266.
112. Andrews RN, Dugan GO, Peiffer AM, et al. White matter is the predilection site of late-delayed radiation-induced brain injury in non-human primates. *Radiat Res.* 2019;191(3):217-231.
113. Andrews RN, Metheny-Barlow LJ, Peiffer AM, et al. Cerebrovascular remodeling and neuroinflammation is a late effect of radiation-induced brain injury in non-human primates. *Radiat Res.* 2017;187(5):599-611.
114. Patton N, Aslam T, Macgillivray T, Pattie A, Deary IJ, Dhillon B. Retinal vascular image analysis as a potential screening tool for cerebrovascular disease: a rationale based on homology between cerebral and retinal microvasculatures. *J Anat.* 2005;206(4):319-348.
115. Wolf JC, Smith SA, Jortner BS, McMaster ME. Putative rodlet cell neoplasms in the livers of two white suckers (*Catostomus commersonii*). *J Comp Pathol.* 2018;164:1-16.
116. Ruehl-Fehlert C, Bomke C, Dorgerloh M, Palazzi X, Rosenbruch M. Pleistophora infestation in fathead minnows, *Pimephales promelas* (Rafinesque). *J Fish Dis.* 2005;28(11):629-637.
117. Matthews JL, Brown AM, Larison K, Bishop-Stewart JK, Rogers P, Kent ML. *Pseudoloma neurophilia* n. g., n. sp., a new microsporidium from the central nervous system of the zebrafish (*Danio rerio*). *J Eukaryot Microbiol.* 2001;48(2):227-233.
118. Sanders JL, Lawrence C, Nichols DK, et al. Pleistophora hypnembryonidis (Microsporidia) infecting zebrafish *Danio rerio* in research facilities. *Dis Aquat Organ.* 2010;91(1):47-56.
119. Peterson TS, Spitsbergen JM, Feist SW, Kent ML. Luna stain, an improved selective stain for detection of microsporidian spores in histologic sections. *Dis Aquat Organ.* 2011;95(2):175-180.
120. Thélohan P. Observations sur les myxosporidies et essai de classification de ces organismes. *Bulletin de la Société Philomatique de Paris.* 1892;4:165-178.
121. Leino RL. Ultrastructure of immature, developing, and secretory rodlet cells in fish. *Cell Tissue Res.* 1974;155(3):367-381.
122. Vigliano FA, Bermudez R, Nieto JM, Quiroga MI. Development of rodlet cells in the gut of turbot (*Psetta maxima* L.): relationship between their morphology and S100 protein immunoreactivity. *Fish Shellfish Immunol.* 2009;26(1):146-153.
123. Mela M, Randi MA, Ventura DF, Carvalho CE, Pelletier E, Oliveira Ribeiro CA. Effects of dietary methylmercury on liver and kidney histology in the neotropical fish *Hoplias malabaricus*. *Ecotoxicol Environ Saf.* 2007;68(3):426-435.
124. Paulino MG, Benze TP, Sadauskas-Henrique H, Sakuragui MM, Fernandes JB, Fernandes MN. The impact of organochlorines and metals on wild fish living in a tropical hydroelectric reservoir: bioaccumulation and histopathological biomarkers. *Sci Total Environ.* 2014;497-498:293-306.
125. Sayed AH, Younes HAM. Melanomacrophage centers in *Clarias gariepinus* as an immunological biomarker for toxicity of silver nanoparticles. *J Microsc Ultrastruct.* 2017;5(2):97-104.